CLASS 3 SECRETED SEMAPHORIN REGULATION OF NEURONAL MORPHOLOGY DURING CENTRAL NERVOUS SYSTEM DEVELOPMENT

by
Eleftheria Koropouli

A dissertation submitted to Johns Hopkins University in conformity with the requirements for the degree of Doctor of Philosophy

Baltimore, Maryland
March, 2016

Abstract

Cortical pyramidal neurons have exquisite morphology and electrophysiological properties, and elucidating how these features develop and are maintained is essential to understanding the physiological development of the central nervous system (CNS). The secreted semaphorins Sema3A and Sema3F have remarkably distinct effects on the development of deep layer cortical pyramidal neurons. Specifically, Sema3A promotes the elaboration of basal dendrites whereas Sema3F constrains spine density. This remarkable functional divergence implicates Sema3A and Sema3F, and their distinct holoreceptor complexes, in the establishment of neuronal architecture. However, the molecular mechanisms by which neuropilins, the secreted semaphorin ligand binding subunits of the Sema3A and Sema3F holoreceptors, exert their effects are largely unknown. Here, I demonstrate that the two Npns, Npn-1 and Npn-2, are S-palmitoylated in cortical neurons and in the mouse brain. Interestingly, Npn-1, which binds Sema3A, and Npn-2, which binds Sema3F, exhibit distinct cell surface distribution patterns; Npn-2 is clustered whereas Npn-1 is diffusely distributed. Importantly, inhibition of Npn-2 palmitoylation abolishes Npn-2 clustering whereas it does not affect Npn-1 localization. These data suggest that palmitoylation conveys to Npn-2, but not Npn-1, a distinct localization pattern and, possibly, function. I therefore investigated the role of palmitoylation in Npn-2 localization and function. I demonstrate that mutation of the membrane-proximal Npn-2 cysteines abolishes the ability of Npn-2 to mediate spine constraint in response to Sema3F and causes profound defects in Npn-2 distribution and trafficking in cortical neurons. On the contrary, C-terminal Npn-2 cysteine residues are dispensable for these effects. Thus, there is a strong functional segregation within the

Npn-2 structure regarding cysteine residue functions. Interestingly, Npn-1 and Npn-2 serve as substrates for distinct palmitoyl acyltransferases. The palmitoyltransferase DHHC15 is involved in Sema3F/Npn-2–induced spine constraint, whereas it is not required for Sema3A/Npn-1–mediated dendritic elaboration of deep layer cortical neurons. On the other hand, the palmitoyltransferase DHHC8 is apparently indispensable for Sema3A/Npn-1–mediated dendritic elaboration but not for Sema3F/Npn-2–induced spine constraint. These observations are in accordance with biochemical and genetic experiments showing that DHHC15 and DHHC8 have distinct substrates. Palmitoyltransferase substrate specificity, therefore, plays critical roles in establishing neuronal cue signaling specificity in the CNS.

Thesis Advisor: Dr. Alex L. Kolodkin, Ph.D.

Thesis Reader: Dr. Paul Worley, M.D.

DEDICATION

I dedicate my dissertation to

My Lord Jesus Christ, Who keeps me alive, healthy and capable of thinking,
and
Virgin Mary the Life-Giving Spring for the miracles She has done in my life
and
St. John the Baptist.

Eleftheria Koropouli

ACKNOWLEDGEMENTS

I feel very privileged that I became admitted by the Department of Neuroscience of Johns Hopkins University to perform my PhD. The Johns Hopkins University and in particular its Department of Neuroscience is a very friendly environment to work. Moreover, Johns Hopkins Neuroscience researchers are very open-minded and kind, which is essential for the performance of good science.

I express my thanks and gratitude to my thesis advisor Professor Alex L. Kolodkin for allowing me to pursue my dissertation work in his lab. He has been a great scientific mentor willing to teach how to perform rigorous science. Moreover, he has been supportive and patient over the years, given the unexpected fluctuations of the scientific experimental results.

Furthermore, I have had the luck to have in my Thesis Committee successful scientists and nice people, including Dr Richard Huganir, Dr Paul Worley, Dr Seth Blackshaw, Dr Dwight Bergles and Dr David Ginty. Despite the fact that at several of my thesis meetings I didn't have conclusive and comprehensive experimental results, they very well understood the challenges of the project and kindly waited until I had more interesting and definitive experimental findings.

My work has been benefited from contributions of Qiang Wang and Sarah Mitchell, who are both members of the Kolodkin lab and loved colleagues. Besides routine discussions about the project, we have been having a productive and peaceful collaboration throughout the years in the lab.

I thank Ms Rita Ragan and Ms Beth Wood-Roig for their endless assistance and guidance with the courses, the requirements and the guidelines of the Neuroscience graduate program and all the administrative arrangements that had to take place all these years.

I gratefully thank the State Scholarships Foundation of Greece (IKY) who provided me with funding during the academic years 2008-2009, 2009-2010 and 2010-2011, following my success in the Foundation's exams in Physiology, Internal Medicine and Surgery. I also express my thanks and gratitude to the Fulbright Foundation in Greece who awarded me a Fulbright grant for the academic year 2008-2009 and the Leventis Foundation (Greece), who gave me funding during the academic year 2011-2012.

Finally but not lastly, I thank my family, who had to tolerate the fact that they wouldn't see me for very long periods of time, for their continuous help and support during all the years of my Ph.D. Especially, I thank my twin sister Vicky who called me every day to make sure I do well and we talked about the various problems I encountered in my life, and my mother who accompanied me at my first trip to the United States and visited me for help and support several times during the seven and a half years of my PhD studies.

TABLE OF CONTENTS

LIST OF FIGURES

CHAPTER 1

CHAPTER 2

CHAPTER 3

CHAPTER 4

CHAPTER 1

INTRODUCTION

Neurons are polarized cells, facilitating the performance of specialized functions by different regions of the same cell. Unique combinations of dendritic and axonal morphologies regulate synaptic properties and coordinate neural transmission within circuits. Factors that affect complexity of dendritic arbors have a profound influence on the number and type of synaptic inputs a neuron receives (Spruston, 2008). Dendrites of many neurons exhibit small protuberances called spines; these are the sites of excitatory synaptic transmission. A growing number of molecules are now known to affect excitatory synapse formation in the mammalian central nervous system (CNS), including transmembrane proteins and also secreted proteins that can be derived from neurons or astrocytes (Dalva et al., 2007; Eroglu and Barres; Mcallister, 2007). Recent work shows that members of the semaphorin protein family, too, play critical roles in establishing neural connectivity and regulating synaptic development and function.

We consider here recent work showing how semaphorins regulate neuronal polarization, multiple aspects of dendritic morphology, excitatory and inhibitory synaptogenesis, and the establishment of precise connectivity among disparate neuronal classes. Following these initial stages of synapse formation, many axonal and dendritic circuit components are refined, or pruned, to generate mature circuits, and some of these events involve semaphorin signaling. Modulation of synaptic transmission provides neural circuits with the potential for experience-dependent plasticity, and recent work suggests that semaphorin signaling functions throughout life to sculpt circuits in response

to experience. Together, all of these observations expand our view of the molecular landscape that influences neural circuit elaboration, uncovering novel influences on synapse development, function, and plasticity.

Semaphorins regulate neuronal polarity, dendritic arborization, and synapse distribution

The complexity of dendritic arbors greatly influences neuronal electrical properties. Ample evidence shows that semaphorin signaling affects the development of dendrites belonging to multiple and diverse neuronal classes. The Class 3 secreted semaphorin Sema3A promotes dendrite development with a concomitant inhibition of axon growth *in vitro* (Nishiyama et al., 2011; Shelly et al., 2011). Further, Sema3A promotes the elaboration of cortical layer 5 pyramidal neuron basal dendrites during postnatal mouse development (Gu et al., 2003; Tran et al., 2009) and also dendritic development in newly born adult dentate gyrus (DG) granule cell (GC) (Ng et al., 2013). Therefore, molecular programs that regulate dendritic development are likely conserved from embryogenesis to the adult.

In highly stratified regions of the nervous system, where synaptic specificity is achieved through neurite arborization of select neuronal populations in precisely defined layers, semaphorins function to constrain dendritic arbors within laminae. In the *Xenopus* retina, class 3 semaphorins regulate asymmetric growth of retinal ganglion cell (RGC) dendritic arbors (Kita et al., 2013). In the mouse retina, the transmembrane semaphorins Sema6A, Sema5A and Sema5B direct precise neurite patterning of select retinal cell types (Matsuoka et al., 2011a, 2011b; Sun et al., 2013). In the *Drosophila* visual system,

transmembrane Sema-1a guides growing L3 neuron axons to their laminar target in the M3 layer of the medulla (Pecot et al., 2013). Sema-1a also acts in the *Drosophila* olfactory system to pattern the dendrites of olfactory projection neurons within the antennal lobe (Komiyama et al., 2007), responding to a gradient of the secreted semaphorins Sema-2a and Sema-2b in the dorsolateral antennal lobe (Sweeney et al., 2011).

Semaphorins also influence synapse formation and subcellular synaptic localization. In *C. elegans* two transmembrane semaphorins, Sema-1 and Sema-2, which signal through the plexin-1 receptor, act to restrict *en passant* synapse formation between complementary axonal regions of two adjacent motor neurons in the same muscle field (Mizumoto and Shen, 2013). Further, in the mouse cerebral cortex the secreted semaphorin Sema3F regulates subcellular synapse specificity by constraining dendritic spine density selectively along apical dendrites of deep layer pyramidal neurons (Tran et al., 2009) (**Figure 1a**).

Pathway-specific connectivity: semaphorins and the CNS circuit development

During neural circuit assembly, growing axons recognize their postsynaptic partners and make appropriate synaptic contacts. The circuits that define spinal reflex arcs mediate spinal motor responses to specific sensory input and exhibit remarkable synapse specificity within the spinal cord. In the sensory-motor reflex arc of the cutaneous maximus (Cm) muscle, chemorepulsive signaling mediated by Sema3E-plexin-D1 is critical for preventing the formation of monosynaptic inputs between Cm proprioceptor

sensory neurons and Cm motor neurons; numerous aberrant monosynaptic inputs occur in the absence of this signaling pathway (Pecho-Vrieseling et al., 2009). However, even in the absence of Sema3E, Cm motor neurons still receive input only from Cm afferents and not triceps (Tri) muscle afferents (another spinal reflex circuit), and Cm afferents do not form ectopic contacts with Tri motor neurons. At lumbar spinal cord levels, Sema3E-plexinD1 signaling also acts to prevent the formation of aberrant monosynaptic connections between specific sensory afferents and motor neurons of functionally non-related muscles, thereby controlling monosynaptic sensory-motor innervation of appropriate motor neuron pools (Fukuhara et al., 2013).

Sema3E-PlexinD1 signaling is also a critical determinant of specific connectivity in the thalamostriatal "direct" basal ganglia pathway. Sema3E, which is expressed and secreted by the axons of thalamostriatal neurons, binds its receptor plexinD1, which is selectively expressed by the direct pathway medium spiny neurons in the striatum. Sema3E-plexinD1 repulsive signaling acts to constrain synapse formation between the thalamostriatal neurons and the striatal medium spiny neurons of the direct pathway (Ding et al., 2012). Taken together, Sema3E-plexinD1 signaling in the CNS mediates several critical aspects of cell type- and pathway-specific connectivity.

Semaphorins regulate excitatory and inhibitory synaptogenesis

Semaphorins function as regulators of synapse formation, independent from their roles in guiding axonal and dendritic projections. This was initially suggested in *Drosophila* by work showing that the transmembrane semaphorin Sema-1a is critical for the formation

of the giant fiber central synapse in developing pupae (Godenschwege et al., 2002). In mammals, Sema3F–neuropilin-2 signaling apparently alters the balance between excitation and inhibition in the mouse cerebral cortex (Tran et al., 2009) and in the hippocampus (Sahay et al., 2005) by selectively constraining excitatory synapse formation. A similar role in hippocampal synaptic transmission has also been demonstrated for Sema3A (Bouzioukh et al., 2006). The transmembrane semaphorin Sema5B reduces synapse number in cultured hippocampal neurons (O'Connor et al., 2009), whereas Sema5A constrains glutamatergic synapse development on dentate gyrus granule cells (Duan et al., 2014; O'Connor et al., 2009). Other semaphorins facilitate excitatory synapse formation in cultured hippocampal neurons. The class 4 transmembrane semaphorin Sema4B promotes the formation of excitatory synapses in cultured hippocampal neurons (Paradis et al., 2007) (**Figure 1a**). Interestingly, class 4 semaphorins, including Sema4B, can interact with PDZ domain-containing proteins such as PSD-95 when co-expressed *in vitro* (Burkhardt et al., 2005; Inagaki et al., 2001; Schultze et al., 2001), however the relevance of this interaction to synapse formation has not been determined.

Unlike excitatory synaptogenesis, the formation and maintenance of inhibitory synapses is much less well understood. Certain class 4 semaphorins are important regulators of inhibitory synaptogenesis. Sema4B promotes inhibitory synapse formation through effects on the maturation of postsynaptic specializations, similar to its role at excitatory synapses (Paradis et al., 2007) (**Figure 1b**). Furthermore, the closely related Sema4D is enriched at synapses and exclusively promotes the assembly of inhibitory synapses in hippocampal neurons, requiring the plexin-B1 receptor (Kuzirian et al., 2013;

Paradis et al., 2007; Raissi et al., 2013) (**Figure 1b**). Interestingly, exogenously supplied Sema4D *in vitro* suppresses epileptiform activity observed in organotypic hippocampal slices following TTX withdrawal. Taken together, these results show that Sema4D induces the formation of functional GABAergic synapses (Kuzirian et al., 2013).

Semaphorin-mediated synapse elimination

Though numerous signaling pathways regulate neural circuit assembly (Winberg et al., 1998), these are not sufficient to prevent the formation of ectopic synapses (Innocenti and Price, 2005). To achieve precise nervous system wiring aberrant axonal tracts must be withdrawn, a process known as pruning, and excess synapses eliminated (Riccomagno and Kolodkin, 2015). Removal of aberrant synaptic specializations can occur along with, or independent of, axon pruning. Axonal trajectories destined to be pruned often are associated with pre- and postsynaptic specializations (Liu et al., 2005; Low et al., 2008; Riccomagno et al., 2012). For example, during the pruning of the mouse hippocampal infrapyramidal tract (IPT), a mossy fiber projection normally pruned postnatally by Sema3F (Bagri et al., 2003), the Rac GTPase-activating protein (GAP) β2-chimaerin inactivates Rac1 to induce pruning (Riccomagno et al., 2012). IPT pruning is accompanied by the loss of presynaptic specializations formed earlier between the IPT axons and CA3 pyramidal dendrites. Interestingly, β2-chimaerin–mediated signaling is not required for Sema3F-mediated dendritic spine constraint or repulsive axon guidance, demonstrating that different Sema3F/Nrp-2–PlexA3 signaling modalities are engaged to regulate distinct aspects of neural wiring.

Regulation of semaphorin signaling by neuronal activity

During early stages of neural circuit maturation, neurons can simultaneously respond to guidance cues and patterns of activity (Shen et al., 2010; Greer et al., 2008). Therefore, electrical and guidance cue stimuli might converge to regulate synaptogenesis. This idea was addressed *in vitro* by showing that electrical activity modulates neuronal responses to chemotropic molecules (Ming et al., 2001; Nicol et al., 2007). A fairly recent study demonstrates an *in vivo* role for such modulation at the *Drosophila* neuromuscular junction (NMJ) (Carrillo et al., 2010). Embryonic and larval body wall muscles secrete Sema-2a, a chemorepellent that signals through the Plexin B receptor to regulate motor axon guidance and neuromuscular connectivity (Ayoob et al., 2006). Electrical activity in PlexB-expressing motor neurons enhances motor neuron responses to the muscle-derived Sema-2a, and this modulation of Sema-2a signaling requires an increase in calcium entry at the presynaptic terminal. Calcium entry in turn activates CaMKII, likely leading to the phosphorylation of downstream targets and subsequent increased sensitivity to Sema-2a. Genetic interaction experiments reveal numerous ectopic motor axon-muscle contacts in the context of reduced presynaptic activity and Sema-2a levels, showing that activity-induced enhancement of Sema-2a signaling in motor neurons is required for synaptic target selection (Carrillo et al., 2010) (**Figure 2**). These results define a regulatory mechanism that exerts spatial and temporal control over chemorepulsion, demonstrating how molecular and electrical stimuli can be integrated to precisely coordinate synapse refinement *in vivo*.

The expression patterns and functions of several semaphorins in the adult hippocampus (Sahay et al., 2005) raise the possibility that these cues signal later in

development, and even in the adult, to regulate synaptic strength in response to experience. This idea is supported by the demonstration that expression of neuropilin-2 (Nrp-2), a secreted semaphorin co-receptor, is influenced by the activity-regulated microRNA-188 (miR-188). In response to long-term potentiation (LTP), miR-188 expression increases, resulting in the downregulation of Nrp-2 expression and subsequent abolition of Nrp-2–mediated inhibition of excitatory synapse formation and synaptic transmission (Lee et al., 2012). It will be important to assess this mode of activity-dependent regulation of semaphorin signaling *in vivo*. These results suggest that Sema3F–Nrp-2 signaling, and possibly other semaphorin signaling pathways, are also regulated similarly in response to external stimuli (Baudet et al., 2013).

Conclusions

Semaphorins join an ever-growing list of synaptogenic and synapse-limiting molecules, and they have emerged as important regulators of excitatory and inhibitory synaptogenesis and function. This is of particular interest since the molecular mechanisms underlying inhibitory synapse formation are poorly defined, and it suggests semaphorins participate in regulating network properties by modulating the balance between excitatory and inhibitory synaptic functions.

Semaphorin influences on synapse formation and function raise the possibility that these molecular cues are involved in the pathogenesis of disorders characterized by profound defects in synaptic transmission, including epilepsy and various cognitive disorders. Indeed, Sema3F and Sema4D influence neuronal activity in mouse epilepsy

models (Kuzirian et al., 2013; Sahay et al., 2005), suggesting potential targets for the development of novel therapeutic approaches directed toward ameliorating epilepsy symptoms. Since electrical activity can modulate semaphorin signaling *in vivo*, integration of semaphorin signaling and neuronal activity may provide for precise control of neuronal morphology, synaptogenesis, and plasticity throughout life.

Despite that numerous studies have provided insight into the role semaphorins play in dendritic elaboration and dendritic spine development, the molecular mechanisms by which they regulate these aspects of CNS development have not been elucidated. Herein, we identify a post-translational modification of neuropilins that regulates neuropilin function and subsequently class 3 secreted semaphorin signaling in cortical neurons. We show that this modification critically controls proper dendritic spine density and distribution mediated by Sema3F/Npn-2 signaling and is also required for cortical neuron dendritic elaboration mediated by Sema3A/Npn-1 signaling. The specificity of these effects is dependent on palmitoyltransferase-substrate specificity.

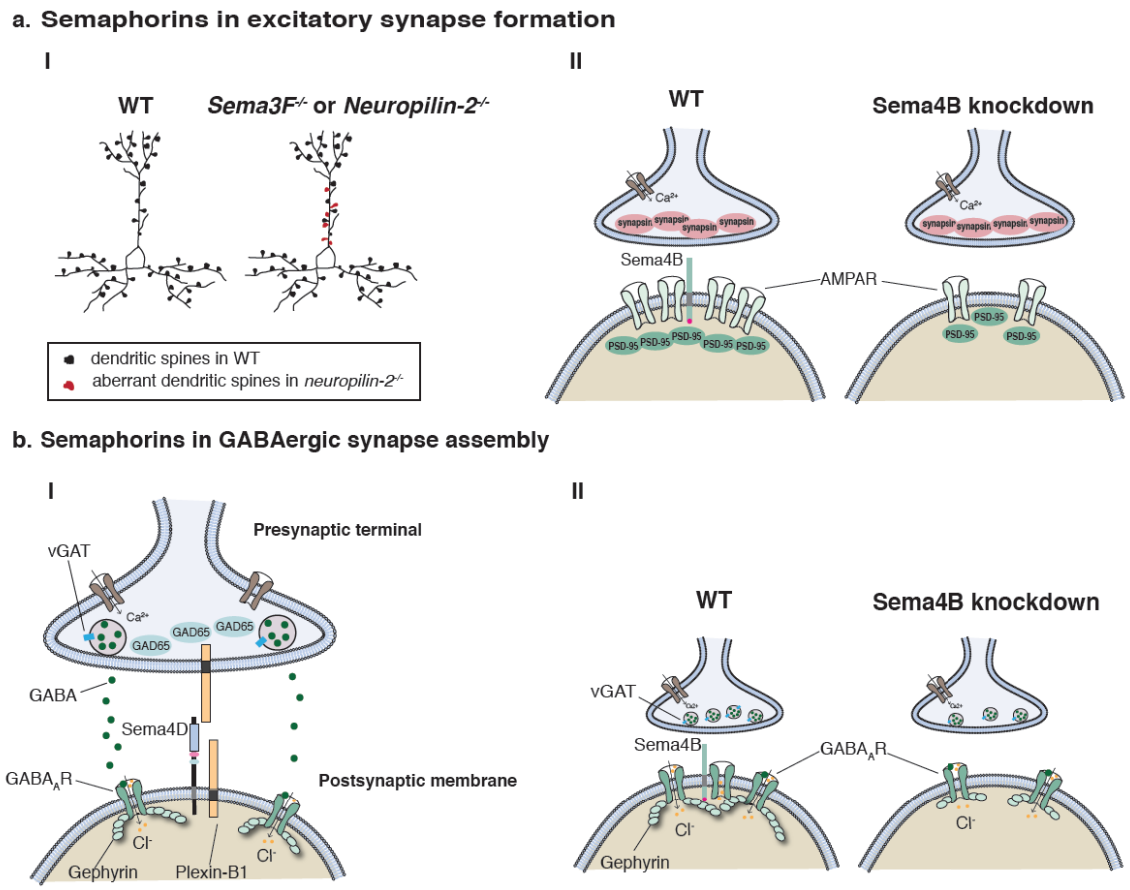

Figure 1. **Semaphorins directly affect synapse formation, altering the balance between excitation and inhibition.**

(a) Semaphorins and excitatory synaptogenesis. (I) Sema3F inhibits excitatory synapse formation by constraining the density of dendritic spines along apical dendrites of deep layer cortical pyramidal neurons. (II) Sema4B promotes the assembly of glutamatergic synapses in cultured hippocampal neurons. The Sema4B cytoplasmic domain includes a PDZ-binding motif that can associate with PSD-95, possibly mediating assembly of postsynaptic specializations (though this has yet to be demonstrated).

(b) Semaphorins and the assembly of inhibitory synapses. (I) Sema4D promotes GABAergic inhibitory synaptogenesis in hippocampal neurons *in vitro* and *in vivo*. Sema4D is required in postsynaptic neurons, where it is mainly localized to synapses, both *in vitro* and *in vivo*. However, plexin-B1 could act *in cis* (in the postsynaptic neuron) or *in trans* (in the presynaptic terminal) to mediate the assembly of inhibitory synapses. Posttranslational proteolytic Sema4D processing occurs *in vitro* and *in vivo* but apparently is not required for Sema4D regulation of GABAergic synapse assembly. (II) Sema4B promotes the assembly of inhibitory synapses by affecting postsynaptic specializations.

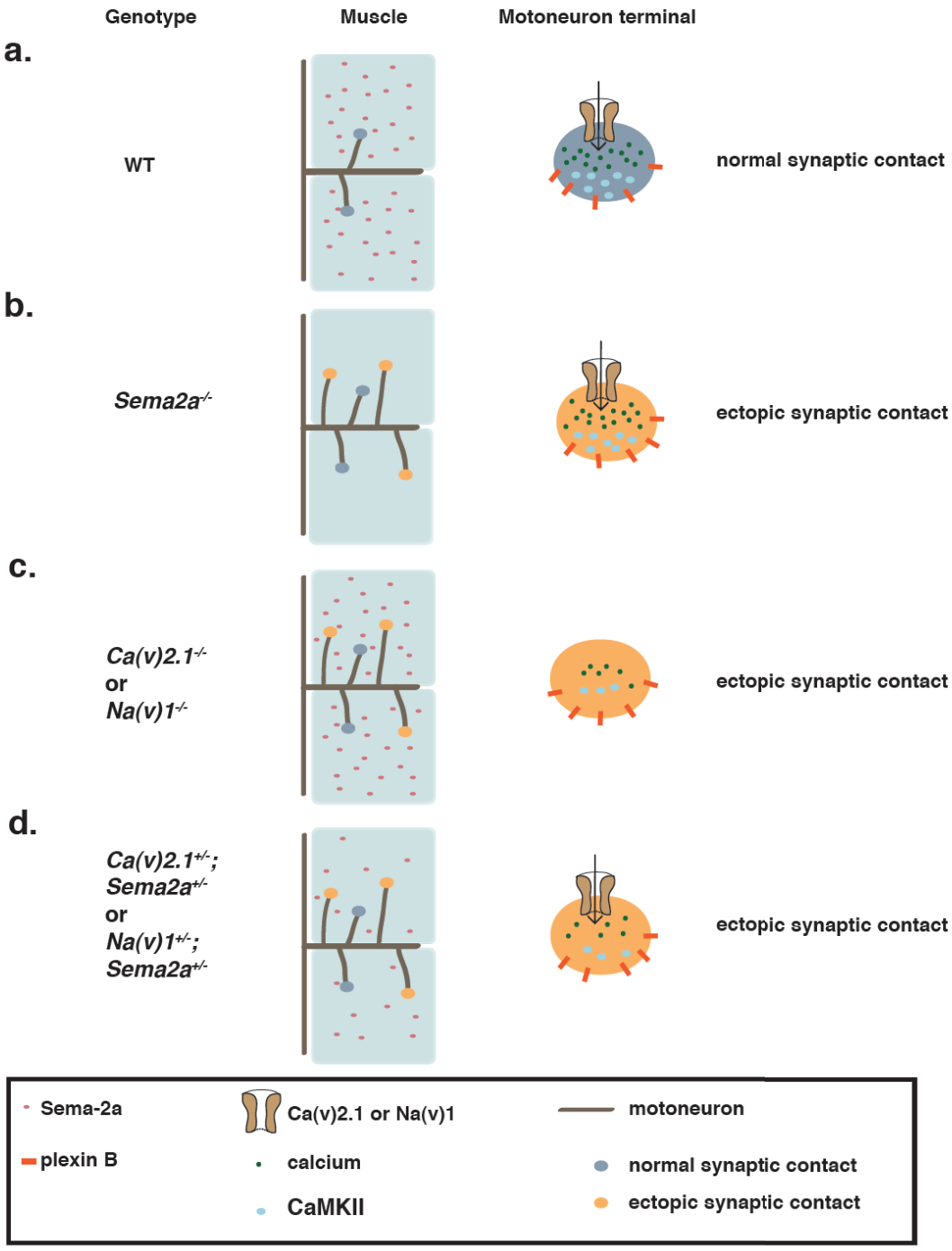

Figure 2. **Electrical activity and chemotropism in synapse refinement *in vivo*.**

(a) In *Drosophila* embryos and larvae, electrical activity in motor neurons renders them

more sensitive to the muscle-derived chemorepellent Sema-2a, causing exuberant motor neuron terminals to withdraw and preventing aberrant synapse formation at the *Drosophila* neuromuscular junction.

(b) Null mutations in *Sema-2a* or (c) ion channels, allow motor neurons to establish ectopic synaptic contacts on somatic muscles that mature into functional synapses.

(d) Electrical activity in motor neurons synergizes with the response to Sema2a, mediated by the plexin B receptor (expressed in motor neurons), and regulates formation of neuromuscular junctions. A partial loss of presynaptic activity accompanied by a partial loss of chemorepulsion leads to the formation of ectopic synaptic contacts on muscles. Therefore, electrical activity interacts with Sema-2a–Plexin-B chemorepulsive signaling to increase motor neuron responses to Sema-2a.

Intended to be blank

CHAPTER 2

NEUROPILIN PALMITOYLATION REGULATES DISTRIBUTION AND FUNCTION OF THE SECRETED SEMAPHORIN RECEPTORS

Introduction

The central nervous system consists of numerous disparate neuronal classes that exhibit remarkably different morphologies, including their dendritic arborization and the distribution of synapses formed onto them by their presynaptic partners. This is particularly prominent in layered structures such as the cerebral cortex and the retina. Cortical neurons are highly polarized and their morphology dictates to a major extent their computational properties (Spruston, 2008). However, the molecular codes that underlie such an outstanding degree of specificity are not well understood. There is an ever-growing list of proteins that regulate spine formation, synapse assembly and dendritic arborization, but the downstream effectors that make these proteins affect one or the other aspect of neuronal morphology are in most cases poorly defined. The elucidation of the molecular mechanisms that underlie proper spine formation is of critical importance given the association of dendritic spine defects with a number of CNS illnesses (Penzes et al., 2011). One class of protein that has been shown to regulate neuronal dendrites, spines and synapses is the semaphorins (Koropouli and Kolodkin, 2014). Class 3 secreted semaphorins play critical roles in the development of neuronal morphology by regulating axon guidance (Giger et al., 2000), basal dendritic arborization (Gu et al., 2003) or spine distribution and synaptic transmission (Sahay et al., 2005; Tran et al., 2009). Additional semaphorins, and specifically Sema4B and Sema4D, have been

implicated in the regulation of inhibitory synapses (Kuzirian et al., 2013; Paradis et al., 2007; Raissi et al., 2013). The molecular mechanisms that implicate different semaphorin signaling pathways in distinct aspects of cortical neuron morphogenesis are not known. Sema3A and Sema3F act through distinct holoreceptor complexes consisting of a neuropilin and a plexin; specifically, Sema3A acts through Npn-1/plexin-A4 (Kolodkin AL et al., 1997), whereas Sema3F exerts its effect via Npn-2/plexin-A3 (Chen et al., 1997; Giger et al., 1998). The molecular mechanisms that regulate the trafficking and function of these receptors, conveying functional diversification and specificity in cortical neuron morphogenesis, remain to be elucidated.

Recent work on post-translational modifications of proteins within the nervous system reveals that the reversible post-translational modification S-palmitoylation critically and dynamically regulates the distribution and function of an increasing roster of neuronal proteins implicated in CNS development (Salaun et al., 2010). These include cues that influence dendritic arborization (Takemoto-Kimura et al., 2007), spine formation such as paralemmin (Arstikaitis et al., 2008; Kutzleb et al., 1998), CDC-42 (Kang et al., 2008) and LIM1-kinase (George et al., 2015), and axon outgrowth. Besides neural development, palmitoylation also occurs on numerous other proteins, including neurotransmitter receptors (Hayashi et al., 2005, 2009), gluatamate receptor-interacting proteins (Thomas et al., 2012) and cell adhesion molecules (Brigidi et al., 2014a). It is not surprising, therefore, that palmitoylation plays critical roles in synapse assembly and synaptic transmission (Fukata and Fukata, 2010). Importantly, palmitoylation can have slow or very fast turnover, and therefore it has the potential to dynamically regulate protein trafficking and function (Martin et al., 2011). In this study, we demonstrate that

neuropilins are S-palmitoylated both in vitro and in vivo, and we show that this modification critically regulates neuropilin distribution and function in cortical morphogenesis.

Results

Npn-1 and Npn-2 exhibit distinct cell surface distribution patterns

To identify potential differences between Npn-1 and Npn-2, we first used a simple in vitro system, expression of proteins in transfected COS7 cells, to express and visualize the distributions of Npn-1 and Npn-2 on the cell surface. To this end, COS7 cells were transfected with amino-terminally (extracellular) flag-tagged Npn-1 or flag-tagged Npn-2, and a few days later neuropilin protein was visualized with live staining using a flag antibody. Strikingly, Npn-1 is diffusely distributed (**Figure 3, panel A**), whereas Npn-2 is clustered, appearing as numerous discrete puncta (**Figure 3, panel D**). This difference likely reflects a distinct tethering and partitioning of the two neuropilins into distinct domains in the cell membrane, although the identity of these domains has not been determined.

Inhibition of palmitoylation abolishes Npn-2 clustering

Our observations point toward some selective modification on Npn-2, which dictates its cell surface clustering. There is compelling evidence that palmitoylation conveys to proteins the capability to be strongly tethered on cell membranes (Shahinian and Silvius,

1995), leading to clustering on the surface of cell lines and neurons (El-Husseini et al., 2002; Webb et al., 2000). To test the possibility that Npn-2 is clustered as a result of palmitoylation, we took a pharmacological approach by using 2-bromopalmitate, a global inhibitor of palmitoylation (Jennings et al., 2009; Resh, 2006). In collaboration with Sarah Mitchell (a research technician in the Kolodkin laboratory), we treated COS7 cells expressing amino-terminally flag-tagged wild type (WT) Npn-2 with 10 μM or 50 μM 2-bromopalmitate for 6 hours, or overnight, and then visualized cell surface Npn-2 using live staining and the flag antibody (FLAG M2).

With the control treatment (DMSO, used here to dissolve 2-bromopalmitate), Npn-2 is clustered in the form of discrete puncta, suggesting that Npn-2 is localized in particular plasma membrane domains. Strikingly, in the presence of 2-bromopalmitate Npn-2 is distributed diffusely over the entire cell surface. Treatment with 10 μM 2-bromopalmitate for 6 hours caused a switch from Npn-2 being clustered to being diffuse in most cells, leaving only a few COS cells exhibiting clustered Npn-2 distribution. However, overnight treatment with 10 μM 2-bromopalmitate or treatment with 50 μM 2-bromopalmitate, either for 6 hours or overnight, caused a complete shift from Npn-2 clustering to diffuse cell surface distribution (**Figure 3, panels E, F**). Npn-2 distribution patterns obtained with live staining were quantified using a range of defined qualitative scoring parameters; these are: (1), rather diffuse (2), rather punctate (3) and punctate (4) distribution.

This finding is consistent with reports showing that 2-bromopalmitate treatment of cells causes a dispersion and/or diffusion of highly clustered proteins in cell lines (Webb et al., 2000) and neurons (El-Husseini et al., 2002). On the other hand, Npn-1 is diffusely

localized on the surface of COS7 cells in either the control treatment or any of the 2-bromopalmitate treatments applied (**Figure 3, panels A-C**). These data suggest that proteins are diffusely localized in the absence of specific determinants, and that protein clustering requires additional and/or specific molecular events such as protein-protein interactions or other modifications to be selectively localized along the cell surface. Furthermore, the inhibition of Npn-2 clustering with a palmitoylation inhibitor suggested that Npn-2 is palmitoylated and that this lipid modification is required for Npn-2 insertion into specific membrane domains along the cell surface. This prompted us to look more closely at the amino acid sequence of neuropilins and investigate whether neuropilins are indeed palmitoylated.

Npn-1 and Npn-2 are S-palmitoylated *in vitro* and *in vivo*

Both neuropilins, Npn-2 and Npn-1, harbor conserved cysteine residues in their transmembrane, juxtamembane and cytoplasmic domains. Npn-2 has three transmembrane/membrane-proximal cysteine residues (C878, C885 and C887) and also a cytoplasmic cysteine residue (C897) and a pair of C-terminal cysteines (C922 and C923; a C-terminal cysteine is defined here as being four positions from the stop codon), whereas Npn-1 has only three transmembrane/membrane-proximal cysteine residues (C875, C881 and C883) and no others (**Figure 4, panel A**). The numeration of the cysteine residues is done according to the position of these cysteines in the amino acid sequence of the *Mus musculus* Npn-2 isoform 002 (PubMed: ENSMUST00000063594)

for Npn-2, and the amino acid sequence of *Mus musculus* Npn-1 (PubMed: ENSMUST00000026917) for Npn-1.

Cysteines that lie in the membrane-proximal (or juxtamembrane) and cytoplasmic domains of transmembrane receptors are candidate palmitate acceptor sites. The position and the conservation of cysteine residues in the neuropilin coding sequence prompted us to investigate whether neuropilins are S-palmitoylated. To test this hypothesis, we utilized the **A**cyl-**B**iotin **E**xchange (**ABE**) method, a widely used biochemical assay that detects S-palmitoylation (Drisdel and Green, 2004; Drisdel et al., 2006; Kang et al., 2008; Wan et al., 2007), with which we assessed neuropilin palmitoylation in brain lysates, primary cortical neurons and cell lines. To perform the ABE method, free cysteine thiols are blocked with S-methyl methanethiosulfonate (MMTS) and then samples are incubated with hydroxylamine (HA, NH_2OH), which cleaves thioester bonds, including those formed on thioesterified S-palmitoylated cysteines, or Tris buffer (-Hydroxylamine or –HA) as a control. The newly exposed cysteines (that were previously S-palmitoylated) are biotinylated with a cysteine-specific biotin known as biotin-HPDP. Finally, the samples are incubated with streptavidin agarose resin to pull down the biotinylated proteins, which here represent the palmitoyl proteome. The detection of palmitoylated proteins is achieved by immunoblotting with an antibody directed against a protein of interest. If a protein is S-palmitoylated, there is a detectable signal in the +HA sample that is not present in the –HA sample and so -HA serves as an internal negative control.

We performed a large number of ABE experiments in different tissues, including cell lines (293T, N2A), deep layer cortical neurons derived from E14.5 WT embryos, and

brain lysates from various developmental time points (E14.5 cortical lysate, P21 forebrain, P28 forebrain and adult mouse brain). These experiments revealed that both Npn-1 and Npn-2 are S-palmitoylated in primary cortical neurons and in the mouse brain (**Figure 4, panels B and C**). Notably, neuropilin palmitoylation is already strong at early embryonic stages (E14.5) and invariably persists in adulthood, suggesting that neuropilin palmitoylation is required throughout an animal's life to regulate critical aspects of protein trafficking and function. In these assays, we also blotted against PSD-95, a known palmitoyl substrate, and SAP-102, which is not (Kang et al., 2008).

The existence of a pair of C-terminal cysteines in the Npn-2 coding sequence raises the possibility that Npn-2 is also prenylated. Two proteins that have the same C-terminal cysteine cluster as does Npn-2, RhoB and paralemmin, are prenylated on the C-terminal side of the two cysteines (fourth from the stop codon) and palmitoylated upstream of the two cysteine residues (fifth from the stop codon) (Adamson et al., 1992; Fukata and Fukata, 2010; Kutzleb et al., 1998). The possibility that Npn-2 is prenylated was not tested in this current study. However, this possibility is interesting to investigate because prenylated proteins are subjected to a proteolytic maturation cleavage of their last three amino acids, and the newly exposed prenylated cysteine is methylated on its carboxyl group (Zhang and Casey, 1996). Given that the last three amino acids of Npn-2 make up a putative PDZ-binding motif, prenylation could regulate the fraction of Npn-2 that is engaged in protein interactions mediated by this motif.

Npn-1 and Npn-2 are enriched in lipid rafts in the mouse brain

Protein palmitoylation is known to direct palmitoylated proteins into specialized domains of the plasma membrane that have a distinct composition of lipids and are known as detergent-resistant membranes, or lipid rafts (Levental I. et al., 2010). Lipid rafts play important roles in synaptic transmission acting as signaling platforms (Allen et al., 2007). Because neuropilins are robustly modified by palmitate, we wanted to test for enrichment of neuropilins in these domains. To this end, I fractionated brain lysates and isolated lipid rafts using a sucrose gradient. Twelve fractions were collected during this experiment. Samples from all collected fractions were immunoblotted with Npn-1 and Npn-2–specific antibodies. This experiment revealed that both Npn-1 and Npn-2 are enriched in the lipid raft fraction. The lipid raft fraction was identified during the experiment as an opaque white layer and by immunoblotting as the flottillin-1–rich fraction (**Figure 5**). As stated earlier, palmitoylation drives proteins into lipid rafts and promotes clustering. However, though both Npn-2 and Npn-1 are palmitoylated and lipid raft-enriched, only Npn-2 appears clustered. Given these data, the most likely explanation is that Npn-2 is enriched in specialized plasma membrane domains different from lipid rafts by means of its distinct protein-protein interactions (including interactions with palmitoylation machinery), as compared to Npn-1. Furthermore, these results suggest that palmitoylation on Npn-1 residues is functionally distinct from palmitoylation on Npn-2 amino acid residues.

A structure/distribution analysis to identify determinants of Npn-2 clustering

To better understand how Npn-1 and Npn-2 are differentially distributed on the cell surface, we sought to discover structural differences between Npn-1 and Npn-2 that are likely determinants of this distinctive distribution, since they are both palmitoylated. Qiang Wang, a post-doctoral fellow in the Kolodkin laboratory, started by using a cell line to look at the surface distribution of Npn-1 and Npn-2 in COS7 cells, which have a large surface area and allow for robust visualization of precise protein distribution. COS7 cells were transfected with N-terminally flag-tagged Npn-1– and Npn-2–expressing plasmids. Following the expression of these Npns, live staining was performed with a flag antibody to visualize cell surface neuropilin protein. Npn-1 exhibits a diffuse distribution over all membranes, whereas Npn-2 is highly clustered in the form of numerous discrete puncta (**Figure 6**). It has been shown that soluble proteins carrying one lipid group tend to be diffusely distributed, whereas proteins harboring additional lipid modifications are kinetically trapped and segregated in specific membrane domains (Rocks et al., 2010; Shahinian and Silvius, 1995). Diffuse distribution therefore seems to be a default distribution pattern, which is modified by the occurrence of additional molecular modifications. Provided that this is a prominent and invariable difference between Npn-1 and Npn-2, we sought to identify the structural domains of each neuropilin that dictate these patterns and account for this difference. Qiang Wang, in collaboration with our laboratory research technician Sarah Mitchell, generated a number of Npn-1/Npn-2 chimeric proteins, including receptors that have both their cytoplasmic and transmembrane domains swapped, or just their transmembrane domains (**Figure 6, panel A**). Hereafter, the mutant plasmids will be

referred to as Npn-a/b/c, with “a” denoting the ectodomain, “b” denoting the transmembrane domain with a few membrane-proximal amino acids and “c” denoting the cytoplasmic domain. Surprisingly, the Npn-2/1/1 and Npn-2/1/2 mutant proteins exhibit diffuse distribution, showing that the Npn-2 transmembrane domain along with a few membrane-proximal cytoplasmic amino acids is the principal determinant of the Npn-2 clustered distribution. Correspondingly, the mutants Npn-1/2/2 and Npn-1/2/1 are, for the most part, clustered, showing that the Npn-1 transmembrane/membrane-proximal domain regulates Npn-1 diffusion in the plasma membrane (**Figure 6**).

We then focused on the amino acid sequence of the neuropilin transmembrane domains and noted a few differences between Npn-1 and Npn-2. We assumed that some of these amino acids distinguish Npn-2 from Npn-1 with respect to their cell surface distribution. Qiang Wang and Sarah Mitchell generated and assessed a number of Npn-1 and Npn-2 “swap” plasmids carrying complementary small motif changes. However, none of these smaller- Npn-1 and Npn-2-motif swap receptors showed a marked shift from the original distribution pattern of the parental WT protein (data not shown).

Taken together, these data show that single amino acids or very small sequences consisting of a few amino acids, do not dictate Npn-2 clustering. However, they do show that the entire transmembrane/juxtamembrane region of 28 amino acids of Npn-2 is likely required for Npn-2 clustering. This finding, in combination with a requirement for Npn-2 palmitoylation for clustering, suggests there exists special palmitoylation events occurring on the Npn-2 transmembrane/juxtamembrne domain cysteines (membrane-proximal cysteines) that lead to specific protein-protein interactions, and that those in turn drive Npn-2 clustering.

Palmitoylation on select Npn-2 cysteines is required for cell surface Npn-2 clustering *in vitro*

Palmitoylation conveys certain neuronal proteins with the ability to become tethered to specific sites on the plasma membrane, and as a result they appear clustered (a punctate distribution). Thus far, we have shown that treatment of COS-7 cells expressing WT Npn-2 with 2-bromopalmitate abolishes the punctate distribution of Npn-2. This raises the question as to which Npn-2 cysteines are required for Npn-2 clustering via their palmitoylation. To address this issue, we assessed the surface distribution of various Npn-2 mutant proteins in COS7 cells (in collaboration with Sarah Mitchell). COS7 cells were transfected with WT, C878S/C8885S/C887S (juxtamembrane cysteins; Figure 4, panel A), C922S/C923S (C-terminal cysteines) or full CS (all TM and cytoplasmic domain cysteines missing) Npn-2 proteins. Following one or two days of expression, cells were processed for live staining with an antibody directed against the extracellular (amino-terminal) epitope tag of Npn-2. Several different experiments were performed with either pHluorin-tagged Npn-2 or flag-tagged Npn-2 expression plasmids. Experiments with both Flag-tagged and pHluorin-tagged Npn-2 proteins revealed that the WT and the C922S/C923S mutant Npn-2 both exhibit robust clustering on the cell surface. In marked contrast, the C878S/C885S/C887S Npn-2, or the full CS Npn-2, mutants lost their clustering and were distributed in a diffuse and non-selective manner over the entire cell surface membrane (**Figure 7**), reminiscent of the Npn-1 distribution. This finding, along with the loss of clustering following treatment with the palmitoylation inhibitor 2-bromopalmitate (**Figure 3**), suggest that palmitoylation of Npn-2 on cysteines C878, C885 and C887 provides Npn-2 with the ability to cluster on the cell surface.

Neuropilin-1 and neuropilin-2 exhibit overlapping, but distinct, palmitoylation patterns

We then sought to identify palmitoylated cysteine residues in the Npn-2 and Npn-1 coding sequences. We generated various cysteine-to-serine (CS) point mutants in flag-tagged Npn-2 (C878S, C885S, C887S, C878S/C885S/C887S (TCS mutant), C897S, C922S/C923S (C-terminal CS mutant), C878S/C885S/C887S/ C897S/ C922S/ C923S (full CS mutant)) and flag-tagged Npn-1 (C875S, C881S, C883S, C875S/C881S/C883S (full CS mutant)). For Npn-2, we also generated pHluorin-tagged Npn-2 CS point mutants (described later in this Chapter). We transfected neuroblastoma (N2A) cells with these plasmids and performed ABE to assess their palmitoylation levels as compared to the WT Npn-2 protein. This analysis showed that Npn-2 has a broad palmitoylation pattern and can be palmitoylated on almost all cysteine residues located in the transmembrane/ juxtamembrane and cytoplasmic domains, although to a variable extent. Specifically, C878 and C887 are robustly palmitoylated, C897 and the C-terminal cysteines are palmitoylated to a lesser extent, and C885 exhibits very little palmitoylation in this assay (**Figure 8, panels A and B**). The analysis of pHluorin-tagged Npn-2 showed similar results with flag-tagged Npn-2 (data not shown). On the other hand, Npn-1 is palmitoylated on C875 and C883, but not on C881, as shown by the reduced Npn-1 palmitoylation levels in the absence of C875 or C883 compared to the WT protein (**Figure 8, panels C and D**).

Taken together, Npn-1 and Npn-2 exhibit distinct but overlapping palmitoylation patterns, however, in their transmembrane/membrane-proximal domains they are palmitoylated in a similar pattern. This in vitro palmitoylation analysis allowed us to

implicate certain cysteine residues as being major contributors to neuropilin palmitoylation. However, the identification of the specific cysteines that are palmitoylated in vivo requires the performance of mass-spectrometry. This experiment has technical challenges and requires expertise that precludes its prosecution at the present time.

Select Npn-2 cysteines are required for Npn-2 association with the Golgi apparatus in cortical neurons

The molecular and cellular mechanisms that mediate Npn-2 trafficking and distribution, and that could also explain the cell surface localization defects of certain Npn-2 cysteine point mutants, are largely unknown. Neuropilins are transmembrane receptors and so their passage through the secretory pathway, including the Golgi apparatus, must be an essential step in their posttranslational anterograde trafficking in order to be inserted into the plasma membrane and function as transmembrane receptors. Moreover, a potential association of a protein with the Golgi apparatus is interesting for three reasons that apply to our study: 1) the Golgi is the main subcellular compartment where palmitoylation occurs (Rocks et al., 2010); 2) the Golgi provides for polarized anterograde trafficking of secretory cargo and therefore it profoundly impacts the establishment of neuronal polarity (Horton et al., 2005); and 3) a potential Golgi-associated protein pool could dynamically respond to external stimuli such as Sema3F and also neural activity, therefore regulating the amount of the protein shuttled between the endomembrane system and the cell surface.

To ask whether or not neuropilins are associated with the Golgi apparatus, we

performed Golgi isolation from WT CD1 mouse brain lysates (see "Experimental Procedures"). This experiment showed that both Npn-1 and Npn-2 are enriched in the GM130-positive *cis*-Golgi fraction, as revealed by immunoblotting with protein-specific antibodies **(Figure 9, panel A)**. To provide further evidence for neuropilin-Golgi association, we stained primary cortical neurons with antibodies directed against endogenous Npn-1 (goat), Npn-2 (goat) and GM130 (rabbit). This showed that endogenous neuropilins are associated with the somatic Golgi (a stack of interconnected cisternae localized in the perinuclear area) and also with Golgi outposts (longitudinal GM130-positive cisternae distributed along the main dendritic shafts) **(Figure 9, panels B and C)** detected in a subset of dendritic processes (consistent with (Horton et al., 2005)). The enrichment of neuropilins in the Golgi apparatus suggests that bulk palmitoylation of neuropilins occurs on Golgi membranes, which is true for most known palmitoylated proteins (Rocks et al., 2010).

Because the palmitoylation status of a protein has been associated with its Golgi localization (Hayashi et al., 2005; Huang et al., 2004; Rocks et al., 2010), we hypothesized that Npn-2 cysteines are required for Npn-2–Golgi association. To test this hypothesis, we cultured E14.5 *Npn2*$^{-/-}$ primary cortical neurons and transfected them with either WT or the indicated cysteine-to-serine (C→S) point mutants of pHluorin-tagged Npn-2 (C878S/C885S/C887S, C922S/C923S, and full CS). Several days after transfection, neurons were subjected to triple immunofluorescence with a GFP antibody (chicken) to visualize Npn-2, GM130 (rabbit) to detect the cis-Golgi and the somatodendritic marker MAP2 (mouse). Single images were acquired with using confocal microscopy and were subjected to analysis with Image J. A detailed description

of this Npn2-Golgi association analysis can be found in the "Experimental Procedures" section of this Chapter. Briefly, channels were split, images were thresholded and the area of the GM130 (A_{Golgi}), Npn-2 (A_{Npn2}) or the colocalization area ($A_{Npn2\text{-}Golgi}$) were measured. These data are expressed as a fraction of Golgi associated with Npn-2 ($A_{Npn2\text{-}Golgi}/A_{Golgi}$).

WT Npn-2 associates with the cis-Golgi to a great extent. This is consistent with the enrichment of endogenous Npn-2 in the Golgi apparatus. This shows that the basic Npn-2 trafficking properties are maintained by the exogenously expressed Npn-2, and that ectopic Npn-2 expression can be used to study Npn-2 trafficking. Similar to WT Npn-2, the C-terminal Npn-2 cysteine mutant C922S/C923S protein is associated with the somatic Golgi and Golgi outposts to a great extent, with no difference compared to the WT. On the contrary, the full CS Npn-2 exhibits a markedly reduced association with the cis-Golgi apparatus (**Figure 9, panels D and E**). Taken together, these findings point toward a role for the membrane-proximal cysteines in the Npn-2–Golgi association. The Npn-2 C878S/C885S/C887S mutant exhibits a reduced association with the Golgi marker GM130, but this defect is milder compared to the full CS. One plausible explanation for this observation is that the C897 also plays a role in Golgi localization, and/or when the three membrane-proximal cysteines are mutated (C878S/C885S/C887S) there is partial compensation mediated by C897. These findings suggest that the cysteine residues located in the membrane-proximal region are indispensable for proper Npn-2 localization on Golgi membranes. Given the reduced palmitoylation displayed by these mutants, and also the possible interaction between Npn-2 and select palmitoyl acyltransferases in the Golgi, it is likely that this defect results from the reduced palmitoylation of these Npn-2

mutant proteins.

Effects of cysteines on Npn-2 distribution and trafficking in cortical neurons

Given the punctate distribution of Npn-2 on the surface of COS7 cells and the requirement of the membrane-proximal Npn-2 cysteines for this clustering, we next wanted to assess the surface distribution of WT and CS Npn-2 in cortical neurons. To this aim, we cultured E14.5 WT primary cortical neurons on glass-bottom dishes and transfected them with pHluorin-tagged *Npn2-IRES-dsRED* expression plasmids. pHluorin is a pH-dependent variant of EGFP which fluoresces only at a basic pH; it therefore serves as a reporter of proteins expressed on the cell surface and exposed to the extracellular environment (Nl, 1998; Sankaranarayanan et al., 2000). Moreover, pHluorin is quite bright and suitable for a robust visualization of cell surface protein with live imaging. Neurons were imaged live using an inverted LSM700 microscope, and transfected neurons were identified by pHluorin and dsRed expression. Strikingly, Npn-2 WT and the C878S/C885S/C887S Npn-2 mutant had a dramatically different distribution on the surface of cortical neurons, as assessed by the pHluorin signal. Specifically, WT Npn-2 is quite punctate, in accordance with its clustered pattern in cell lines; however, the C878S/C885S/C887S protein exhibits a very diffuse distribution along cortical neuron processes (**Figure 10, panels C and D**), with an almost complete loss of puncta. We also performed this experiment in *Npn2*$^{-/-}$ cortical neurons with the same results (data not shown).

The importance of the membrane-proximal Npn-2 cysteines for Npn-2 cell surface

clustering prompted us to investigate a potential role for these cysteines in Npn-2 trafficking. To investigate this, we performed **F**luorescence **R**ecovery **A**fter **P**hotobleaching (FRAP) experiments in collaboration with the Kolodkin laboratory post-doctoral fellow Randal Hand. WT E14.5 cortical neurons (in a CD1 genetic background) were cultured on glass-bottom dishes that allow for live imaging. A few days later, neurons were transfected with either WT or C878S/C885S/C887S pHluorin-tagged Npn2−ires-dsRED expression plasmids and were incubated for several days after transfection in order to express the exogenous proteins at adequate levels. After their incubation for a total of at least 10 days in vitro, that allowed them to develop elaborate dendritic processes, neurons were subjected to FRAP analysis. For a detailed description of the experiment see the "FRAP" section in the Experimental Procedures below. Neurons included in this analysis had strong Npn-2 expression, based on the pHluorin signal, and a healthy morphology with elaborate dendritic processes. A **R**egion **O**f **I**nterest (ROI) was selected for subsequent bleaching. Time-lapse imaging was performed by the acquisition of an image every 30 seconds. Five images were acquired before bleaching (prebleach total time: 2.5 min.), one image right after bleaching (bleach), and 30 images after bleaching (postbleach total time: 15 min.) in order to monitor fluorescence recovery over time. The laser-induced bleaching was very efficient, causing a reduction in fluorescence of at least 50% of the starting fluorescence levels in the ROI (a greater decrease was observed in most cases). Time-lapse image sequences were analyzed by measuring fluorescence in the ROI and correcting for the fluorescence decay that occured in a non-bleached area of the same neuron and also for background fluorescence. Representative images for each plasmid are shown, and pooled data are

presented for each plasmid as relative (normalized) fluorescence over time. Interestingly, WT Npn-2 exhibits a significantly lower fluorescence recovery as compared to the mutant C878S/C885S/C887S protein (**Figure 10, panels A and B**). This shows that WT Npn-2, most likely due to its palmitoylation, displays very tight membrane tethering and slow trafficking across the plasma membrane. This could result from its being trapped in specialized membrane domains, which is manifested as clustering and punctate distribution on the surface of cortical neurons. In marked contrast, the C878S/C885S/C887S mutant Npn-2 protein recovers to a much greater extent, suggesting that this protein exhibits less tight association with the plasma membrane, which is also reflected in its cell surface distribution characterized by a diffuse pattern.

Our observations are consistent with the kinetic characteristics of other palmitoylated proteins; specifically, the CS mutants of known palmitoylated proteins exhibit a stronger FRAP recovery compared to the WT protein (Rocks, 2005; Rocks et al., 2010). Therefore, work from others combined with our experimental results demonstrates that tight and spatially restricted protein trafficking is a general property of palmitoylated proteins, regardless of whether they are transmembrane or cytoplasmic. Furthermore, this property apparently results from protein palmitoylation, a modification that conveys to proteins specificity in trafficking not provided by the sole presence of a transmembrane domain.

Select Npn-2 cysteines are required for Sema3F/Npn-2–mediated dendritic spine constraint in cortical neurons

Sema3F binds Npn-2 and constrains dendritic spine density along the main dendritic shaft in primary cortical pyramidal neurons in culture, and also on the apical dendrites of layer

V pyramidal neurons of the cerebral cortex in vivo in the postnatal and adult mouse brain (Tran et al., 2009). More specifically, *Sema3F* and *Npn-2* null mice exhibit significantly higher dendritic spine density compared to their WT littermates. Furthermore, bath application of Sema3F on WT cortical neurons in culture constrains spine density, as compared to control treatment. These loss-of-function and gain-of-function experiments demonstrate that Sema3F/Npn-2 signaling acts to regulate the density of dendritic spines in deep layer cortical pyramidal neurons and, subsequently, the number of excitatory synapses formed onto these neurons. Here, we provide experimental evidence that the membrane-proximal Npn-2 cysteines, but not the C-terminal cysteine residues, are required for Npn-2 to serve as a negative regulator of dendritic spines in cortical neurons.

As I have already shown, the membrane-proximal Npn-2 cysteines C878, C885 and C887 play critical roles in Npn-2 trafficking and distribution, most likely via their palmitoylation (**Figures 3 and 7**). To test whether the various transmembrane and cytoplasmic Npn-2 cyseine residues are important for Sema3F/Npn-2–mediated spine constraint in cortical neurons, we performed rescue experiments in *Npn-2*$^{-/-}$ primary cortical neurons treated with alkaline phosphatase conjugated Sema3F (Sema3F-AP) or AP control. We cultured E14.5 *Npn-2*$^{-/-}$ cortical neurons for a total of 21 days-in-vitro (DIV) so that the neurons were fully developed and had mature spines. At DIV8, neurons were transfected (using Lipofectamine) with various *pCIG2-IRES-EGFP* expression plasmids, including a flag-tagged WT Npn-2 and also flag-tagged Npn-2 cysteine-to-serine (CS) point mutants. At DIV21, neurons were treated with 5nM Sema3F-AP or AP for 6 hours. Following this treatment, neurons were fixed and processed for immunofluorescence, which included a GFP antibody (chicken) to visualize neuronal

morphology with high resolution and a Npn-2 antibody (rabbit) to detect and confirm Npn-2 protein expression from the various plasmids. Neurons were imaged with the acquisition of stacks using a 63X oil lens (upright LSM700) and the 3D projection of each stack was generated (Image J). These 3D projections of cortical neurons in culture were used for dendritic spine analysis. All dendritic spines (mushroom, stubby, filopodia-like spines) were counted along the proximal 50 μm of the main dendritic shaft emerging from the pyramidal neuron cell body. Representative images of neurons expressing each of the tested plasmids are shown, and pooled data are quantified and presented as a number of spines per μm, following either Sema3F-AP or AP treatment (**Figure 11**).

Neurons transfected with EGFP only (with no Npn-2 expression) did not respond to Sema3F (no significant difference between Sema3F-AP and AP treatment) and also had significantly more spines as compared to the neurons expressing WT Npn-2 and treated with Sema3F-AP. This shows that WT Npn-2 rescues the Npn-2–associated dendritic spine phenotype, as observed previously (Tran et al, 2019). Importantly, there is also a significant difference between EGFP only-expressing neurons and neurons expressing WT Npn-2, both treated with AP; this suggests that in the absence of exogenous Sema3F, Npn-2 WT partially rescues the dendritic spine phenotype. This raises the possibility that Sema3F itself is expressed in these deep layer primary cortical neuron cultures. In fact, we have confirmed that Sema3F is secreted by primary E14.5 cortical neuron cultures by immunoblotting concentrated culture medium derived from E14.5 primary cortical neurons harvested from a 6xMyc-tagged *Sema3F* knock-in mouse we generated (*Sema3F*^{Myc}; see Chapter 4, **Figure 26**). This likely explains why WT Npn-2 is able to constrain spine density without the application of exogenous Sema3F ligand in our

cortical neuron cultures.

Npn2$^{-/-}$ cortical neurons expressing the Npn2 C-terminal cysteine mutant C922S/C923S also responded to Sema3F and had fewer spines compared to *Npn2*$^{-/-}$ neurons that expressed only EGFP; there was no significant difference from the WT Npn2-expressing neurons. Therefore, the C-terminal Npn-2 cysteines (C922, C923) are not required for spine constraint. On the other hand, neurons expressing the Npn-2 point mutants C878S or C887S had spines that were as numerous as the spines observed in the negative control (EGFP only). Furthermore, these neurons displayed no response to Sema3F, as compared to the AP control, and they were also significantly different from WT Npn-2 expressing neurons. These data demonstrate that cysteines C878 and C887 are indispensable for Npn-2 to serve as a negative regulator of dendritic spines through the action of Sema3F. Lastly, C885 and C897 residues play a less important, but significant, role in spine constraint, since they partially rescued the spine phenotype (showing a significant difference from neurons expressing only EGFP and also from neurons expressing WT Npn-2). Of note, we also performed immunofluorescence against Npn-2 to confirm protein expression and rule out the possibility that some plasmids do not rescue because of differences in expression levels—we find that indeed all Npn-2 constructs are expressed at comparable levels at the cell surface (qualitative assessment thus far – data not shown).

In summary, there is a requirement for select Npn-2 cysteine residues for the regulation of dendritic spine number by Sema3F/Npn-2 signaling in cortical neurons. These data (**Figure 11**), along with our data on the palmitoylation of various Npn-2 cysteine point mutants (**Figure 8, panels A and B**), show a strong correlation between

the extent to which certain cyteines are palmitoylated and their contribution to the rescue of dendritic constraint following treatment with Sema3F. In greater detail, cysteines that are strongly palmitoylated (C878, C887) are necessary for rescuing the Sema3F-induced spine phenotype, whereas cysteines that are palmitoylated to a lesser extent have either intact (C922/C923) or partially compromised (C885, C897) rescue ability. This suggests a role for palmitoylation rather than the cysteine residues themselves in Npn-2 function. In subsequent chapters below we address this issue in more experimental detail.

Finally, it is intriguing the fact that the Npn-2 C922S/C923S mutant protein completely rescues the *Npn2*$^{-/-}$-associated spine constraint phenotype and raises the possibility that this cysteine motif has a different Npn-2–associated function. As I discuss below in the "Conclusions-Discussion" section of this chapter, preliminary experimental evidence suggests a different function for the Npn-2 C-terminal cysteines, which supports the notion that there is functional segregation within the Npn-2 transmembrane/cytoplasmic domains that involves these cysteine residues. On the other hand, the C-terminal SEA motif that Npn-2 harbors, which lies C-terminal to the C-terminal cysteines (CCSEA∗), has been shown to be essential for spine constraint in response to Sema3F (Tran et al., 2009). Our current model suggests that this motif is a PDZ-binding motif, and therefore, it might mediate interactions of Npn-2 with PDZ-domain–containing proteins.

Sema3F enhances Npn-2 palmitoylation in cortical neurons

Palmitoylation is a reversible post-translational modification that dynamically modifies a

protein properties, and external stimuli such as glutamate may alter baseline protein palmitoylation (Hayashi et al., 2009; Kang et al., 2008). Thus, we speculated that steady-state Npn-2 palmitoylation is altered in response to its physiologically relevant secreted ligand Sema3F. To investigate this, we treated WT CD1 E14.5 primary cortical neurons with 5nM Sema3F-AP, Sema3A-AP or AP control ligands for various periods of time including one hour-, two hour- and 6 hour-treatments and then performed ABE to assess endogenous Npn-2 palmitoylation. These experiments revealed that exogenous Sema3F robustly enhanced palmitoylation of endogenous Npn-2 in primary cortical neurons, whereas Sema3A-AP treatment left Npn-2 palmitoylation unaltered (**Figure 12, panes A and B**). This finding is important for two reasons: 1) it shows that Sema3F can be a regulator of Npn-2 palmitoylation and, more importantly, 2) it provides a link between Sema3F signaling and Npn-2 palmitoylation. A direct effect of Sema3F on the palmitoylation of specific Npn-2 cysteines could not be investigated because cell lines (neuroblastoma N2A cells) expressing exogenous Npn-2 did not show a similar effect: no response in cell lines was detected following several experiments (data not shown). The lack of response of Npn-2 palmitoylation to Sema3F in N2A cells might be due to the lack of the highly specialized machinery expressed in cortical neurons (synaptic partners, scaffolding and signaling proteins, palmitoyl acyltransferases).

The enhancement of Npn-2 palmitoylation by exogenously applied Sema3F suggests that baseline Npn-2 palmitoylation is regulated by external stimuli, and that Npn-2 palmitoylation is required for Npn-2 response to Sema3F. Moreover, provided that Npn-2 palmitoylation causes changes in Npn-2 distribution and trafficking, we could speculate that response to Sema3F requires a redistribution of Npn-2, mediated by the recruitment

of certain palmitoyltransferases that catalyze specific palmitoylation events on Npn-2.

Neuronal activity alters Npn-2 palmitoylation

Alterations in neural activity in vitro or in vivo modulate palmitoylation of numerous neuronal palmitoyl substrates (Hayashi et al., 2009; Kang et al., 2008). We therefore tested the hypothesis that activity alters steady-state Npn-2 palmitoylation, in collaboration with Qiang Wang. WT CD1 E14.5 primary cortical neurons grown for at least two weeks in vitro were treated with TTX or bicuculline for two hours, or for two days; following treatment, neurons were harvested and subjected to the ABE assay to assess palmitoylation of endogenous neuronal proteins. All treatments (TTX and bicuculline, two-hour and two-day) caused a dramatic reduction in Npn-2 palmitoylation. The same was observed for PSD-95 (**Figure 12, panels D and E**). These data suggest that proper activity levels and balanced neuronal activity is required for appropriate Npn-2 palmitoylation. However, these data obtained here are partially inconsistent with previous work, which shows that a decrease in activity (induced by TTX) causes a compensatory upregulation of palmitoylation of NR2A and NR2B (Hayashi et al., 2009). This discrepancy could be explained by variability in the type of neurons cultured and/or the treatment conditions. However, regardless of the polarity of the palmitoylation response (increase or decrease), these findings show that activity significantly alters Npn-2 palmitoylation, as has been shown for other neuronal proteins (Brigidi et al., 2014b; Hayashi et al., 2009; Kang et al., 2008). A rigorous assessment of activity-induced Npn-2 palmitoylation changes will require very carefully designed experiments with respect to

the neurons used (cortical versus hippocampal, CD1 versus other backgrounds, deep cortical layer (E14.5) versus upper cortical layer (E15.5)), days of in vitro incubation and the applied treatment. The latter should include a very short bath application of the compounds on neurons, including a 5-minute time point. Moreover, the above-described discrepancy could be due to reciprocal changes in excitatory and inhibitory synapses, which could be separated with biochemical fractionation.

In vivo rescue of the *Npn2*$^{-/-}$–associated dendritic spine phenotype

The requirement for select Npn-2 cysteines in Sema3F-mediated spine collapse in vitro prompted us to investigate whether these residues are also required for Npn-2 spine constraint in the mouse cerebral cortex. To this aim, we performed rescue experiments of the *Npn2*$^{-/-}$-associated increased dendritic spine phenotype in *Npn-2*$^{-/-}$ deep layer cortical neurons using an *in utero* electroporation protocol in collaboration with both Qiang Wang and Randal Hand. To circumvent the lethality and low breeding efficiency associated with the *Npn2*$^{-/-}$ mouse line, I crossed *Npn2*$^{-/-}$ with *Npn2*$^{F/F}$ so that all embryos of the litter are *Npn2*$^{F/-}$. *In utero* electroporation was performed at E13.5 in order to target deep layer cortical neurons with the goal to assess their spine density. This scheme for electroporations (**Figure 13, panel A**) includes two controls: 1) *pCIG2-ires-EGFP* to visualize neuronal morphology in *Npn2*$^{F/-}$ neurons; and 2) *pCIG2-ires-EGFP* + *pCAG-Cre* + *LSL-tdTomato* to excise the floxed *Npn-2* allele and render deep layer neurons *Npn2*$^{-/-}$. *LSL-tdTomato* (*LoxP-STOP-LoxP-tdTomato*) is co-electroporated to serve as a reporter of Cre activity. If this strategy works, neurons with excision of the floxed *Npn2*

allele (control 2) should have more spines compared to the neurons expressing only EGFP (control 1), recapitulating the *Npn2*$^{-/-}$ spine phenotype. Importantly, this analysis revealed that, indeed, neurons expressing both Cre and EGFP (and thus *Npn2*$^{-/-}$) have a higher spine density compared to neurons expressing only EGFP (**Figure 13, panels B and C)**.

Next, we electroporated another litter with *Flag-Npn2 WT-ires-EGFP + Cre + LSL-tdTomato*, in order to assess whether WT Npn-2 rescues the *Npn2*$^{-/-}$ spine phenotype. Deep layer *Npn2*$^{-/-}$ cortical neurons expressing WT Npn-2 had a spine density similar to that of *Npn2*$^{F/-}$ neurons expressing EGFP alone, showing that WT Npn-2 completely rescues the spine phenotype associated with *Npn2* deletion (**Figure 13**). To test the importance of the Npn-2 membrane-proximal cysteines, we assessed the rescue ability of the Npn-2 C878S/C885S/C887S mutant by electroporating embryos with *flag-Npn2 C878S/C885S/C887S-ires-EGFP + Cre + LSL-tdTomato*. Importantly, this mutant was not capable of rescuing the increased dendritic spine density phenotype. Taken together, these results reveal a requirement for the membrane-proximal Npn-2 cysteines in Sema3F-induced dendritic spine constraint in deep layer cortical neurons.

Npn-2 cysteines are not required for Npn-2/plexin-A3 interaction or Npn-2 homodimerization *in vitro*

The interaction between Npn-2/plexinA3 is critical for constraining spine density in response to Sema3F (Tran et al., 2009). We therefore wanted to know whether Npn-2 cysteines are required for Npn-2 interactions with plexinA3. To address this, we co-transfected 293T cells with myc-tagged plexinA3 and either WT or full CS Npn-2 and

then performed co-immunoprecipitation experiments. These biochemical assays revealed that full CS Npn-2 associates with plexinA3 as efficiently as does WT Npn-2 (**Figure 14, panel A**). This finding shows that the abolished rescue ability of the Npn-2 CS is not due to a lack of Npn-2 binding to plexinA3.

It is known that Npn-2 forms homodimers (Chen et al., 1998). Because cysteines can form disulfide bridges with adjacent cysteines, it is possible that Npn-2 cysteines mediate Npn-2 homodimerization via the formation of intermolecular disulfide bonds. To test whether membrane-proximal and/or cytoplasmic Npn-2 cysteines are required for Npn-2 homodimerization, we performed co-immunoprecipitation experiments involving Flag–Npn-2 and either WT or full CS pHluorin–Npn-2. This experiment showed a very strong association of full CS pHluorin-Npn-2 with WT Flag-Npn-2, similar to the association of WT pHluorin-Npn-2 with WT flag-Npn-2 (**Figure 14, panel B**). This finding suggests that these cysteine residues do not form disulfide bridges critical for intermolecular homophilic Npn-2/Npn-2 interactions.

Conclusions-discussion

My work identifies two guidance cue receptors broadly implicated in neural development, Npn-1 and Npn-2, as novel palmitoylated neuronal proteins. Npn-2 palmitoylation on transmembrane/membrane-proximal cysteines is essential for Npn-2 distribution, trafficking, and also most likely Sema3F/Npn-2–mediated spine constraint, whereas the Npn-2 C-terminal cysteines are apparently not required for either spine constraint or Npn-2 clustering.

Npn-1 and Npn-2 undergo trafficking through the Golgi apparatus. Npn-2 membrane-proximal cysteines are required for its stabilization and enrichment in Golgi membranes. This apparently renders the protein available to effectors of post-Golgi anterograde trafficking pathways that ensure its distribution into specialized plasma membrane domains, as revealed by the loss of clustering and segregation in cell surface subdomains following mutations in Npn-2 membrane-proximal cysteines. It is therefore likely that the defective cell surface Npn-2 C878S/C885S/C887S distribution results, at least in part, from aberrant Npn-2 Golgi localization. Importantly, the interesting correlation among the rescue ability of the various Npn-2 cysteine mutants, the cell surface distribution if these Npn-2 cysteine mutants in COS7 cells and cortical neurons, and the association patterns of these Npn-2 cysteine mutants with the Golgi apparatus in cortical neurons may very well provide a plausible explanation for the rescue ability of the C-terminal Npn2 (C922S/C923S) mutant and also the inability of the transmembrane and membrane-proximal CS Npn-2 (C878S/C885S/C887S) mutant to rescue the *Npn2*$^{-/-}$–associated spine density phenotype. We speculate that the C878S/C885S/C887S Npn-2 mutant cannot respond to Sema3F (although it is able to bind Sema3F) with spine constraint because it is not properly localized. On the other hand, the C-terminal C922S/C923S Npn-2 mutant rescues the *Npn2*$^{-/-}$-associated dendritic spine phenotype because it still is able to assume proper localization at the neuron cell membrane.

The role of palmitoylation in Npn-2 protein clustering suggested by our work presented thus far is consistent with previous studies showing that palmitoylation-deficient mutant proteins lose their clustering and become diffusely localized in the cell membrane (Noritake et al., 2009). However, Npn-1 and Npn-2 share the same

organization of cysteine residues in their transmembrane and membrane-proximal domains, yet they have completely different cell surface distribution patterns. We therefore speculated that these cysteines are necessary, but not sufficient, for Npn-2 clustering and then tried to identify additional Npn-2 sequences that might be required. We found that, for the most part, the Npn-2 transmembrane and juxtamembrane domains dictate Npn-2 clustering, however the smaller Npn-1/Npn-2 chimeras we generated and assessed for clustering did not reveal a requirement for a specific amino acid sequences adjacent the Npn-2 cysteines. We therefore have to consider the entire Npn-2 transmembrane/membrane-proximal domain of 28 amino acids as a determinant of Npn-2 cell surface clustered localization. This finding, in combination with the abolition of Npn-2 clustering observed when the three membrane-proximal cysteines are mutated to serine or upon 2-bromopalmitate treatment, show that palmitoylation of Npn-2 on membrane-proximal cysteines has features that must be distinct from the palmitoylation of Npn-1 membrane-proximal cysteines. Such a functional divergence could result from distinct interactions between Npn-1 and Npn-2 and with different palmitoyl acyltransferases, resulting in subsequent differences in palmitoylation of these two receptors. This issue is addressed below in Chapter 3.

Further, we have not yet determined the identity of the cell surface domains or compartments in which the Npn-2 clusters localize. It is well documented that palmitoylation targets proteins for insertion into lipid rafts (more precisely known as "detergent-resistant domains") (Levental et al., 2010). However, we have found that both Npn-1 and Npn-2 are enriched in the lipid raft fraction isolated from mouse brain lysates (**Figure 5**), as expected since they are both palmitoylated. This is consistent with

evidence that Sema3A-mediated axon guidance is dependent on the integrity of lipid rafts (Guirland et al., 2004). Therefore, the lipid raft hypothesis cannot on its own explain the differential cell surface distribution between Npn-1 and Npn-2.

The Npn-2 C-terminal cysteines C922 and C923 are dispensable for Npn-2 spine constraint. It is therefore likely that these residues play critical roles in other aspects of Npn-2 function, perhaps infrapyramidal tract pruning (Riccomagno MM. et al., 2012) or proper development of Npn-2–dependent axonal tracts (i.e. the anterior commissure). According to unpublished data generated in the Kolodkin laboratory by former postdoctoral fellow Martín Riccomagno (personal communication), the Rac GTPase activating protein (GAP) signaling protein β_2-chimaerin interacts more robustly with the C922S/C923S Npn-2 mutant protein than with the WT Npn-2 protein, whereas mutation of the membrane-proximal Npn-2 cysteines leaves this interaction unaltered. However, β_2-chimaerin exerts its effect on axon pruning upon its dissociation from Npn-2 (Riccomagno et al., 2012). So, the C-terminal cysteines might serve to downregulate β_2-chimaerin /Npn-2 interactions so that β_2-chimaerin can mediate pruning of the infrapyramidal tract. If this were true, the C922S/C923S Npn-2 mutant protein would prevent β_2-chimaerin from exerting its pruning effect. This interplay might result from prenylation of the Npn-2 C-terminal cysteine, which would lead to proteolytic cleavage and carboxy-methylation of the Npn-2 C-terminus and could, therefore, regulate this protein-protein interaction.

Experimental Procedures

Analysis of palmitoylation

***Acyl-Biotinyl Exchange (ABE) assay*:** performed according to (Wan et al., 2007), with slight modifications according to Hayashi et al. (2009). Briefly, on day 1, tissue is lysed in lysis buffer containing Methyl MethaneThioSulfonate (MMTS, Sigma, cat. no. 64306), which blocks free thiols. On day 2, inputs are taken from each sample and then samples are incubated with either a buffer containing Hydroxylamine (+HA buffer/sample) (Thermo Scientific, cat. no. 26103), which cleaves thioester-linked acyl modifications, or with a control buffer containing Tris (-HA buffer/sample). HPDP-biotin (Soltec Ventures, cat. no. B106) is used as a cysteine-specific biotinylation agent to biotinylate newly exposed cysteine thiols and is included in both +HA and -HA buffers. On day 3, all samples are incubated with low HPDP-Biotin buffer. On day 4, samples are incubated with Streptavidin agarose resin (Thermo Scientific, cat. no. 20349) in order to affinity purify biotinylated proteins, which represent the palmitoyl proteome. Finally, on day 5, resin is washed twice with no salt and twice with high salt (500mM NaCl) buffers and protein is dissociated from the resin by incubation with a 2-mercaptoethanol–containing buffer at 37ºC for 10 minutes with flick mixing. Supernatants are then transferred to clean Eppendorf tubes. Inputs and processed (+HA, -HA) samples are analyzed by SDS-polyacrylamide gel electrophoresis and immunoblotting with protein-specific antibodies.

Biochemical assays

SDS-PAGE and immunoblotting (Western blotting)*:* samples were mixed with 4x Laemmli buffer to a final concentration 1x (4x Laemmli: 10% 2-mercaptoethanol (Sigma,

cat. no. M6250), 90% 4x Laemmli sample buffer (Bio-rad, cat. no. 161-0747)), boiled for 5 minutes and stored at -20°C. Samples were run on 4-20% Mini-Protean TGX Precast gels (Bio-Rad, 10-well comb, cat. no. 456-1093; 15-well comb, cat. no. 456-1096), run under standard protein electrophoresis conditions and transferred on PVDF transfer membrane (Immobilon-P, Millipore, cat. no. IPVH00010). Membranes were blocked with 5% milk (Scientific, cat. no. M0841) diluted in TBS-T, for 1 hour at room temperature. Incubation with primary antibodies was performed in 5% milk at 4°C overnight, with rotation. The next day, membranes were washed 3x, 10 minutes each, with TBS-T. Secondary HRP-conjugated species-specific antibodies were diluted in 1% milk to a final concentration 1:10.000, and incubated with membranes for 1 hour at room temperature, with gentle shaking. Membranes were washed 4x, 10 minutes each, with TBS-T. The signal detection was performed with ECL (GE Healthcare) or ECL Prime (GE Healthcare) or Clarity (Biorad).

Primary antibodies: Neuropilin-2, 1:1000, rabbit, Cell Signaling cat. no. 3366S; Neuropilin-1, 1:1000, rabbit, AbCam cat. no. ab81321; Neuropilin-1, 1:1000, goat, R & D cat. no. AF566; PSD-95, 1:1000, mouse, NeuroMab, cat. no. 75-028; GM130, 1:1000, rabbit, AbCam; flotillin-1; actin; SAP102, NeuroMab, cat. no. 75-058.

Secondary antibodies: HRP-conjugated species-specific antibodies.

Co-immunoprecipitation: tissue was lysed in TNE buffer (NP-40, Tris, EDTA, NaCl, protease inhibitors). Samples were precleared with resin for 2 hours. After the preclear step, resin was discarded and supernatants were transferred to clean Eppendorf tubes. A small amount was kept and labeled as input and the rest of the samples were incubated

with antibody overnight at 4°C. Next day, protein A/G agarose resin (Thermo Scientific) was added to the samples and samples with resin were incubated at 4°C, for 2 hours, with end-over-end rotation. Resin was washed twice with high-salt buffer (500mM NaCl) and twice with low-salt buffer (150mM NaCl). Samples were mixed with Laemmli buffer, boiled and subjected to SDS-PAGE and immunoblotting.

Lipid raft isolation: detergent-resistant membranes (DRMs) or lipid rafts were isolated according to the "Isolation and Use of Rafts" protocol provided in the *Current Protocols in Immunology* textbook (Unit 11.10). In detail, wholebrains from WT CD1 mice were homogenized in TNE buffer (25mM Tris pH=7.4, 150 mM NaCl, 5mM EDTA, 1X Protease inhibitor cocktail, 1% Triton X-100) and debris was pelleted with centrifugation at 13.000 rpm. 2 ml supernatant (lysate) were mixed with 2 ml 80% sucrose and this 40% sucrose/lysate mix was placed at the bottom (bottom layer) of a Beckman ultracentrifuge tube (cat. no. 344059). This was overlayed with 4 ml 30% sucrose and this in turn was overlayed with 4 ml 5% sucrose. Ultracentrifugation was performed at 118,000g (26.200 rpm) with a SW41 rotor for 16 hours at 4ºC. The material centrifuged and distributed along the sucrose gradient was harvested by the collection of 12 1-ml fractions. The opaque layer representing DRMs was found at the 5%-30% sucrose interface (fraction 5: very solid white). Samples were mixed with Laemmli buffer and analyzed with SDS-PAGE followed by immunoblotting with protein-specific antibodies.

Golgi isolation: mouse whole brain was harvested and homogenized with a gentle pestle (Potter-Elvehjem homogenizer) to avoid Golgi stack fragmentation. Golgi stacks were

isolated by flotation through a discontinuous sucrose gradient according to the Basic Protocol 2 described in Unit 3.9 of the *Current Protocols in Cell Biology*. Briefly, light mitochondrial pellet was resuspended in 2 ml buffer and mixed with 8 ml 2.0 M sucrose so that final sucrose concentration is about 1.55 M. 5 ml of this mix was transferred to a 17-ml ultracentrifuge tube (Beckman) and overlayed with the following sucrose solutions: 4 ml 1.33 M sucrose, 2 ml 1.2 M sucrose, 2 ml 1.1 M sucrose, 2 ml 0.77 M sucrose, 0.25 M sucrose to fill the tube. Gradients were ultracentrifuged at 100,000 x g at 4˚C for one hour. Six fractions were collected in total: 1.55M, 1.55M/1.33M, 1.33M, 1.1M/1.2M, intervening material, 0.77M/1.1M. Samples were mixed with Laemmli buffer, boiled and analyzed with SDS-PAGE and immunoblotting with Npn-2, Npn-1 and GM130 antibodies.

2-bromopalmitate treatments

2-bromohexadecanoic acid (also known as 2-bromopalmitate) (Sigma-Aldrich, cat. no. 238422) was dissolved in Dimethyl Sulfoxide (DMSO, Sigma-Aldrich, cat. no. D2650) to make a stock. Stock solution was diluted in the appropriate culture medium to the indicated final concentrations (50μM or 10μM). Cells with 2-bromopalmitate–containing medium were incubated at 37^{o}C, 5% CO_2, for 6 hours or overnight.

Primary cortical cultures

Cortical cultures: timed-pregnant mice were either obtained from external mouse facilities (CD1 from Charles River; C57BL6 from Jackson Laboratories) or generated in-house by plug checks. Embryos were harvested at E14.5 (for deep cortical layer cultures)

and cerebral hemispheres were dissected out. The olfactory bulbs and the ganglionic eminences were removed and discarded and the cortices were kept on ice-cold L-15 medium (Leibovitz, Gibco). Tissue was trypsinized with 0.1% trypsin diluted in HBSS (Gibco) for 15 minutes in a 37^{o}C-water bath. Following trypsinization, cortices were washed twice with HBSS+10% FBS to inactivate trypsin and dissociated in neuron growth medium containing 10% FBS. Neurons in neuron growth medium were plated in 6-well plates for the performance of biochemical experiments or on 24-well plates containing round glass coverslips for immunofluorescence. Medium was partially changed every three days.

Plate/coverslip preparation*:* 12 mm round glass coverslips were treated with nitric acid overnight, washed with ddH_2O and ethanol and stored in 95% ethanol. The day of culture, coverslips were flamed, placed in 24-well plates and coated with 0.1mg/ml poly-D-lysine diluted in ddH_2O for at least two hours at 37ºC. Before plating of neurons, plates with coverslips were washed twice with DPBS.

Immunofluorescence

In vitro: cells were fixed with 4% PFA (prepared in 1x PBS from 16% EM-grade PFA (Electron Microscopy Sciences, cat. no. 15710)) for up to 10 minutes at room temperature, washed with PBS three times for 10 minutes each, and blocked with 10% goat or donkey serum and 0.1% Triton X-100 in PBS for one hour. Cells were incubated with primary antibodies overnight at 4ºC with gentle shaking. Next day, they were washed three times with PBS for 10 min each, and then incubated with secondary

antibodies for one hour at room temperature in the dark. Primary and secondary antibodies were diluted in 1% goat or donkey serum and 0.1% Triton X-100 in PBS. Following the incubation with secondary antibodies, cells were washed four times for 10 min. each with PBS and glass coverslips were placed upside-down on glass slides with mounting medium (Electron Microscopy Sciences, Fluoro-gel, cat. no. 17985). **Primary antibodies:** GFP (chicken, Avés, cat. no. GFP-1020), Npn-2 (rabbit, Cell Signaling, cat. no. 3366S), Npn-2 (goat, R & D), Npn-1 (goat, R & D), GM130 (rabbit, AbCam), dsRed (rabbit, Living Colors), flag (mouse M2, Sigma). **Secondary antibodies:** 488 donkey anti-chicken IgY (Biotium, cat. no. 20166), Alexa Fluor 647 donkey anti-rabbit IgG (Life technologies), Alexa Fluor 555 donkey anti-rabbit IgG (Life Technologies), Alexa Fluor 488 donkey anti-goat IgG (Life technologies), Alexa Fluor 555 goat anti-mouse IgG (Life Technologies), 647 donkey anti-rat IgG (Jackson).

Live staining:

Cells were incubated with primary antibody (Flag 1:50, GFP (chicken) 1:500) diluted in culture medium, for 10 min at room temperature. Then, they were washed three times with culture medium, and fixed with 4% PFA for ~10 min. Cells were washed with PBS, blocked and incubated with a fluorescent secondary antibody for one hour at room temperature. Finally, cells were washed and mounted.

Npn-2–Golgi association analysis

For the analysis of the Npn-2 and GM130 colocalization, I used Image J. The Npn-2 and Golgi (GM130) channels were split and thresholded (a different threshold was used for

each of the two channels), while thresholds were kept constant throughout the analysis. The area of the Npn-2 (A_{Npn2}) and the Golgi (A_{Golgi}) was selected and measured (μm^2). The colocalization plugin was used to find the colocalized area ($A_{Golgi\text{-}Npn2}$), which was then selected and measured. To assess the colocalization, the fraction of the Golgi associated with Npn-2 ($A_{Golgi\text{-}Npn2}/A_{Golgi}$) was calculated.

Fluorescence Recovery After Photobleaching (FRAP)

E14.5 WT CD1 primary cortical neurons were cultured as described above and plated on glass bottom dishes (MatTek, cat. no. P35G-0-14-C) precoated with poly-D-lysine. Between DIV 5 and DIV 8, neurons were transfected with the indicated pHluorin-Npn2-ires-dsRED expression plasmids using Lipofectamine (Lipofectamine 2000 Reagent, Invitrogen, cat. no.11668-019). Several days after transfection, transfected neurons, identified by the robust expression of pHluorin-tagged Npn-2 and dsRED, were imaged with an inverted LSM 700 microscope (Zeiss) with an incubation chamber (PeCon) (temperature: 37ºC, CO_2: 5%), using a 63X NA1.4 oil immersion lens. For the performance of fluorescence recovery after photobleaching (FRAP), we used the following protocol: a Region Of Interest (ROI) containing the main dendritic process was selected for FRAP analysis. Images were acquired every 30 seconds; 5 images were acquired prior to bleaching (prebleach time: 2.5 minutes) and 31 additional images were acquired post-bleaching (total post-bleach time: 15.5 minutes).

Analysis: Fluorescence intensity of time-lapse images was determined by measuring the fluorescence intensity within the ROI and correcting for fluorescence decay and for background fluorescence. Pooled data are presented for each plasmid (pHluorin-Npn2

WT: n=7; pHluorin-Npn2 C878S/C885S/C887S: n=8) as a percentage of recovery over time.

AP-fused ligands

HEK293T cells were transfected with the appropriate expression plasmids with the method of Lipofectamine (Invitrogen, Lipofectamine 2000 Reagent), and they were allowed to express and secrete the ligand for 2-5 days. The resulting culture supernatant was centrifuged at a low speed at 4ºC for 5 min. and supernatant was transferred to a clean filter tube for concentration. For AP concentration, a filter of 50K was used, whereas for Sema3A-AP or Sema3F-AP a filter of 100K was used (Millipore). The concentration of the ligands was determined by measuring the AP activity and was then converted in nM.

Dendritic spine analysis

For the assessment of dendritic spines *in vitro*, neurons were cultured on glass coverslips for 21 days in vitro (DIV) to allow robust spine formation. Between DIV6 and DIV8, neurons were transfected with pCIG2-ires-EGFP–expressing plasmids to visualize neuronal morphology. At DIV21, neurons were treated with 5nM AP-Sema3F or AP control for 6 hours at 37ºC. After treatment, neurons were processed for immunofluorescence according to the protocol described above.

Image acquisition and spine counting in vitro and in vivo: EGFP-expressing neurons were imaged with an upright confocal microscope (Zeiss, LSM 700) with the acquisition of Z-stacks. For spine analysis, the 3D projection of each neuron was calculated with

Image J. Upon setting the appropriate pixel-to-μm scale, the line tool was used to draw a segmented line starting and extending distally from the cell body, across the main dendrite *in vitro* and the apical dendrite *in vivo*. For spine analysis of cortical neurons *in vitro* and *in vivo*, all spines (stubby, mushroom, filopodia-like) were counted along the proximal 50 μm extending distally from the cell body.

Npn2*$^{-/-}$ rescue *in vitro: E14.5 *Npn2*$^{-/-}$ primary cortical neurons were cultured and, at DIV8, they were transfected with ires-EGFP plasmids expressing aminoterminally flag-tagged Npn-2. These included WT and various CS point mutants of Npn-2. Neurons were cultured for an additional 13 days (for a total of 21 DIV) to allow strong protein expression and complete spine formation. At DIV 21, neurons transfected with each of the indicated plasmids were treated for 6 hours with 5nM either Sema3F-AP or AP control. After treatment, neurons were fixed and subjected to immunofluorescence with antibodies specific to GFP for dendritic process and spine visualization and to Npn-2 to visualize and confirm Npn-2 expression.

Plasmids

Flag-tagged Npn-1 and Npn-2 were subcloned in a backbone vector containing the preprotrypsin signal peptide followed by the flag epitope. The Npn-1 or Npn-2 coding sequences were then cloned downstream and in frame with these elements. Cysteine-to serine point mutants were generated by amplification of the WT protein with various reverse primers, each containing the desired mutation. These plasmids were subcloned in a *pCIG2-ires-EGFP* backbone vector. pHluorin-tagged Npn-2 plasmids were generated

by cloning in frame and with a 5'→3' direction the endogenous signal peptide of Npn-2, the pHluorin coding sequence and the Npn-2 coding sequence downstream of its signal peptide. The PCR products were ligated using the EcoRV and SmaI sites in a *pCAGGS-dsRED* express backbone vector. All plasmids were fully sequenced and rigorously tested with respect to their expression in cell lines and neurons.

In utero electroporation

In utero electroporation of mouse embryos was performed on E13.5 embryos of timed-pregnant females according to (Saito, 2006). Briefly, a small vertical incision was made on the abdominal cavity and embryos were gently pulled out. DNA was microinjected in the lateral ventricle with a fine and polished glass capillary tube placed in a mouth-controlled pipette. DNA injection was followed by the administration of 5 electric pulses with forceps-type electrodes, according to the following scheme: 5 pulses of 33 mV, 50 ms each, inter-pulse interval of 950 ms. Occasionally, PBS containing 1x penicillin/streptomycin was poured onto the embryos to avoid drying of the embryos' tissue. Operated pregnant females were kept on a slide warmer until complete recovery and they were later placed back in their room.

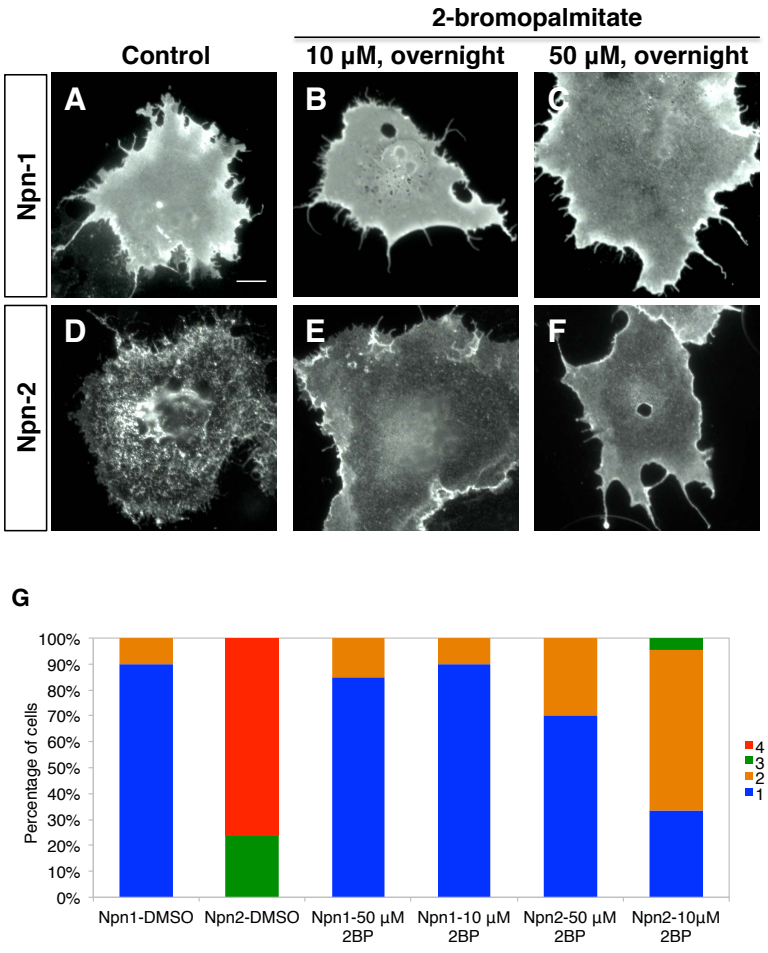

Figure 3. Npn-1 and Npn-2 exhibit distinct cell surface distribution that is abolished by a palmitoylation inhibitor.

COS7 cells were transfected with flag-tagged WT Npn-1 or WT Npn-2. Two days after transfection, cells were processed for live staining with a flag antibody to detect cell surface neuropilins. (A, D) Steady state Npn-1 and Npn-2 cell surface distributions. Notably, Npn-1 is diffuse (A), whereas Npn-2 is highly clustered (D). (B, C, E, F) COS7 cells expressing either Npn-1 or Npn-2 were treated with 10 µM or 50 µM 2-bromopalmitate, overnight. Npn-1 distribution remains diffuse regardless of the treatment

applied (B, C). On the contrary, 2-bromopalmitate treatments have a dramatic effect on Npn-2 surface protein, exhibiting a switch from clustering to diffusion (E, F). (G) Cells are assigned to four different categories according to whether protein is diffuse (1) (example: panel A), rather diffuse (2), rather clustered (3), clustered (4) (example: panel D). At least 20 cells were used for quantification for each condition depicted in the graph. Pooled data are presented as the fraction of cells (compared to the total number of cells quantified) exhibiting a specific type of protein distribution. Scale bar: 15 μm.

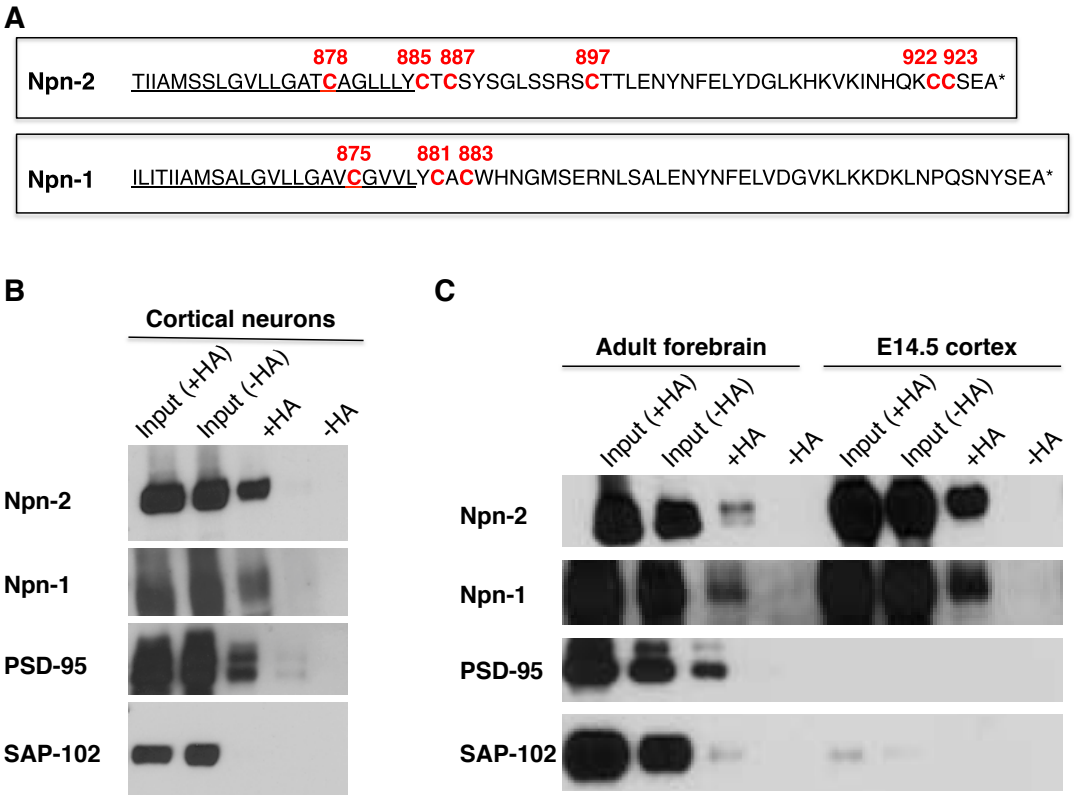

Figure 4. Neuropilins are S-palmitoylated *in vitro* and *in vivo*.

(A) Amino acid sequence of Npn-2 and Npn-1, including their transmembrane (underlined) and cytoplasmic domains. Cysteine residues are shown in bold red. (B, C) Palmitoylation was assessed with the ABE palmitoylation assay, in which samples were split in two halves and were treated either with hydroxylamine-containing buffer (+HA) or control buffer containing Tris (-HA). The latter serves as an internal negative control. These experiments showed that Npn-2 and Npn-1 are S-palmitoylated in E14.5 DIV 28 WT primary cortical neurons (B) and in the mouse brain, both in the embryonic cortex (E14.5) and in adulthood (C). PSD-95 is used as a positive palmitoylation control, whereas SAP -102 serves as a negative control for palmitoylation. Note the robust signal

in the +HA samples and the absence of signal in the –HA samples for neuropilins and PSD-95. This shows that neuropilins are indeed S-palmitoylated.

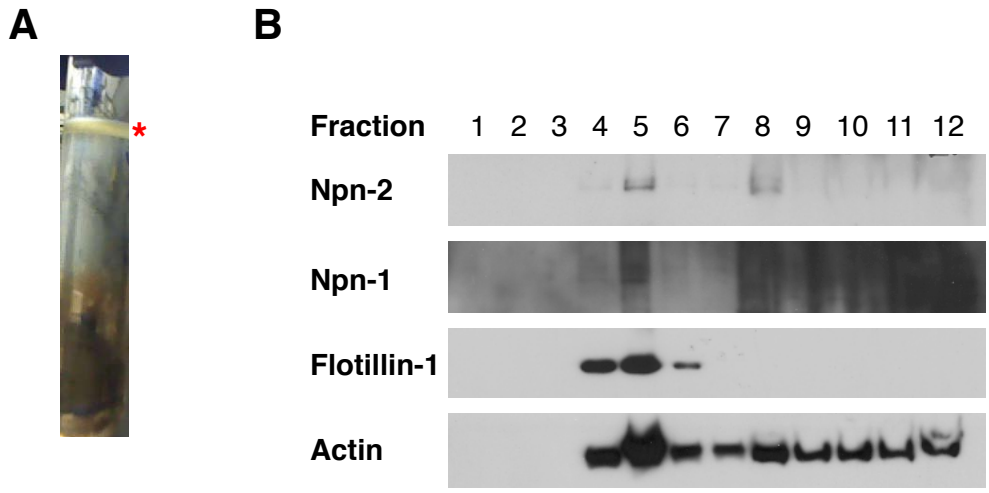

Figure 5. Npn-2 and Npn-1 are enriched in lipid rafts in the mouse brain.

(A, B) Lipid rafts (or detergent-resistant membranes) were isolated from adult mouse whole brain. The lipid raft fraction appears as a white opaque layer, marked with a red asterisk (A). Samples were analyzed by SDS-PAGE and immunoblotting with antibodies directed against Npn-2, Npn-1, the lipid raft marker flotillin-1 and actin (B). Flotillin-1 is particularly enriched in lipid rafts, confirming that the fraction 5 is the lipid raft fraction of the gradient.

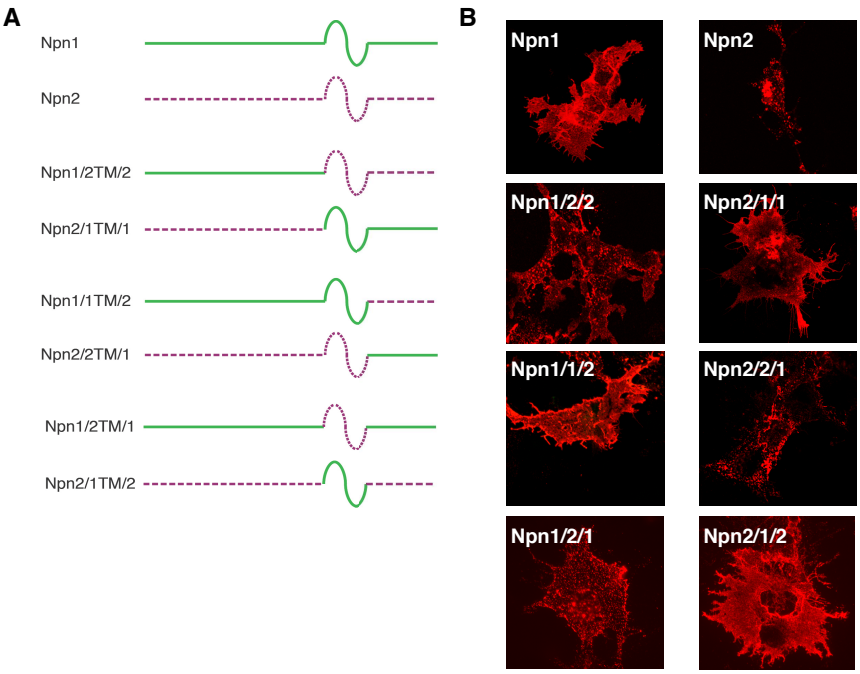

Figure 6. A structure-distribution analysis to identify determinants of Npn-2 clustering.

(A) Schematic of flag-tagged Npn1/Npn2 chimeric receptors that were generated. Each neuropilin consists of an ectodomain, a transmembrane domain and a cytoplasmic domain. The name of each chimeric neuropilin receptor is shown as a/b/c, where "a" is the ectodomain, "b" is the transmembrane domain and "c" is the cytoplasmic domain. (B) COS7 cells were transfected with these chimeras and then processed for live staining with a flag antibody that recognizes cell surface protein. Representative images are shown for each mutant protein. The top two panels show WT Npn-1 and Npn-2, which exhibit completely different distributions and as used as reference for the assessment of chimeras. The two panels at the second row show a swap of both the transmembrane and

the cytoplasmic domains. This reveals that the transmembrane and cytoplasmic domains dictate Npn-1 and Npn-2 distribution. To narrow down the domain that determines the divergent Npn-1 and Npn-2 distributions, two chimeras were tested in which only the transmembrane domain of each neuropilin was swapped with that of the other (bottom two panels). Npn-1 that harbors the transmembrane domain of Npn-2 becomes clustered, whereas Npn-2 that has the transmembrane domain of Npn-1 appears diffuse. These findings point toward a critical role of the transmembrane domain of each neuropilin in determining the pattern of protein distribution.

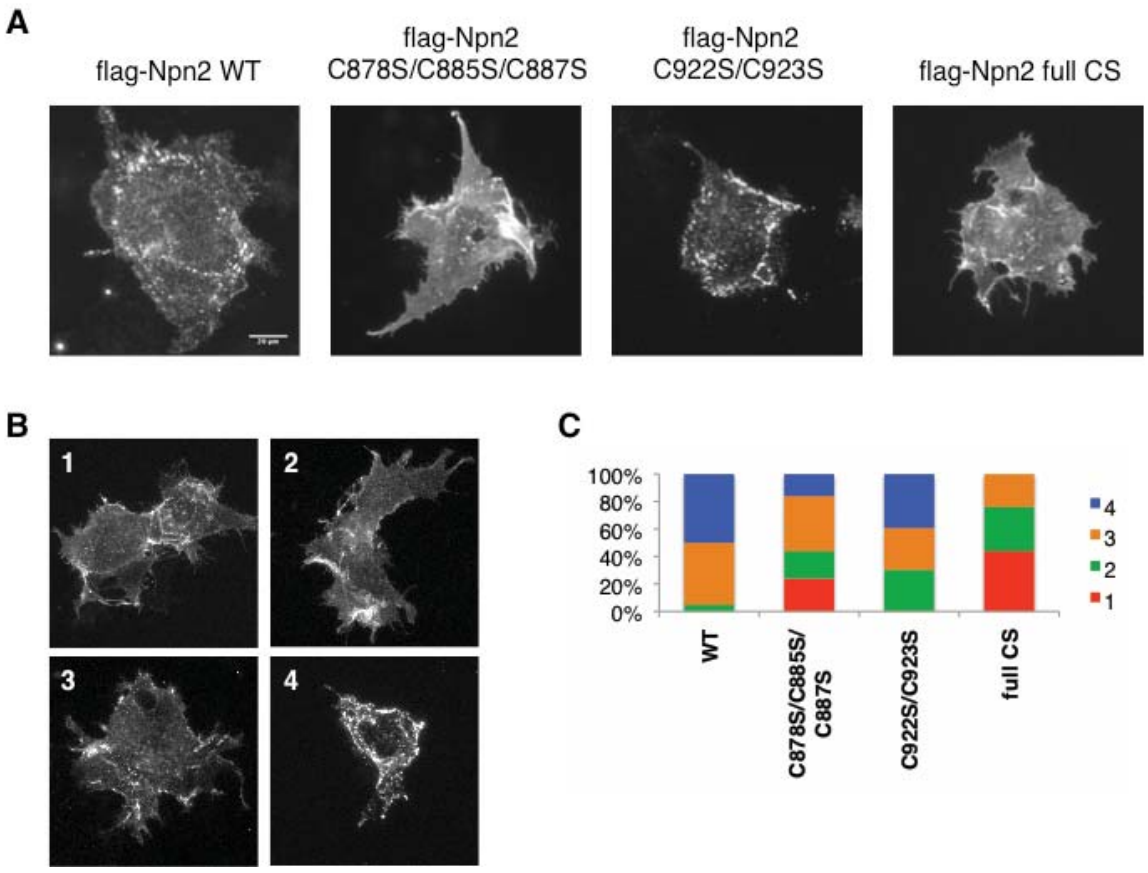

Figure 7. Select Npn-2 cysteines are required for surface Npn-2 clustering *in vitro*.

(A-D) COS7 cells were transfected with flag-tagged Npn2 plasmids and were then subjected to live staining with a flag antibody to visualize surface Npn-2. WT Npn-2 (A) and the C-terminal CS Npn-2 (C922S/C923S) (C) are distributed as multiple discrete puncta. In marked contrast, the mutation of the membrane-proximal cysteines abolishes Npn-2 clustering. (E) Cells are qualitatively assigned to four different categories according to the extent of Npn-2 clustering, according to the following scheme: 1 = diffuse, 4 = punctate, 2 = rather diffuse, 3 = rather punctate. Representative images for each of these categories are shown in E. (F) Cumulative data are presented as the fraction

of cells that has each of the four different types of surface protein distribution. Scale bar: 20 μm.

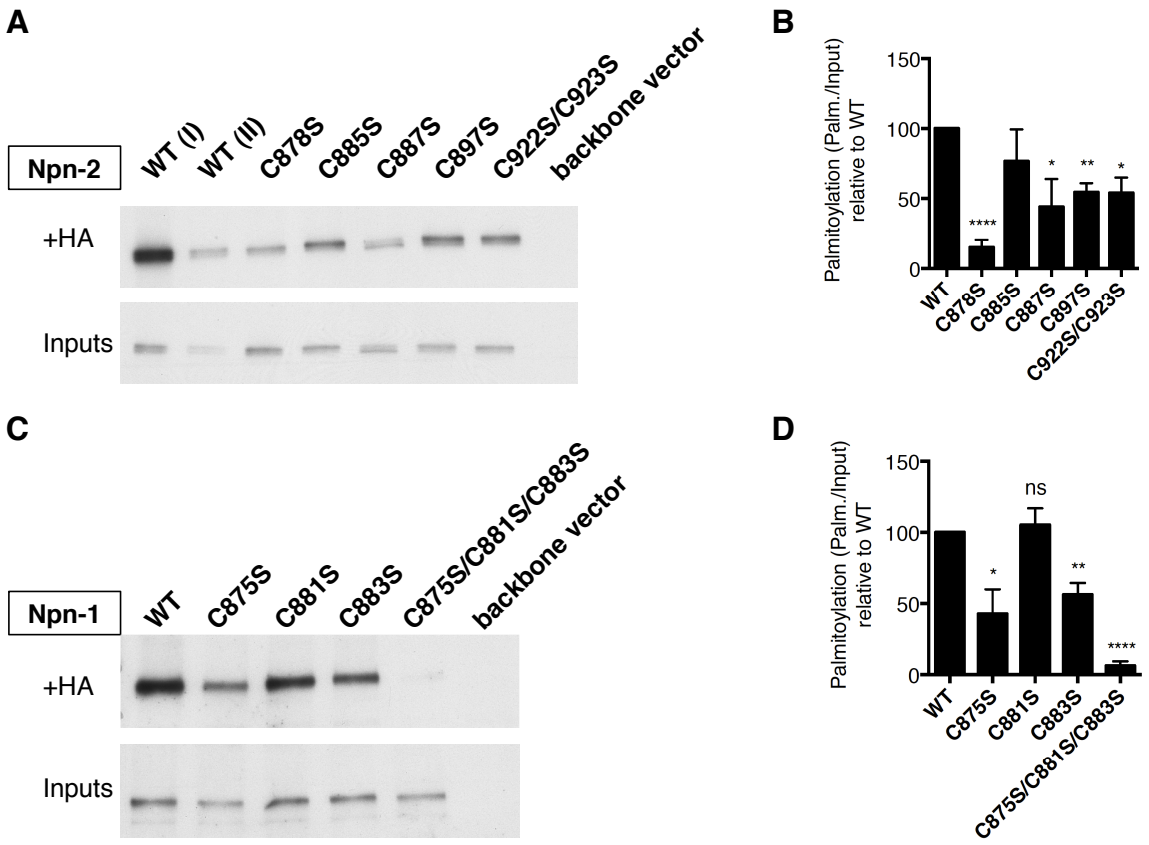

Figure 8. Npn-1 and Npn-2 exhibit distinct but overlapping palmitoylation patterns. N2A cells were transfected with various Npn-2 or Npn-1 plasmids and two days after transfection they were subjected to ABE for the assessment of palmitoylation. (A, B) Npn-2 mutants were assessed for their palmitoylation. The palmitoylation signal is equal to the ratio of the palmitoylated (+HA) to the total protein (Input). WT is considered as 1 (100%) and all the other Npn-2 plasmids are expressed as a percentage of the WT. (C, D) Npn-1 mutants are assessed for their palmitoylation relative to WT Npn-1.

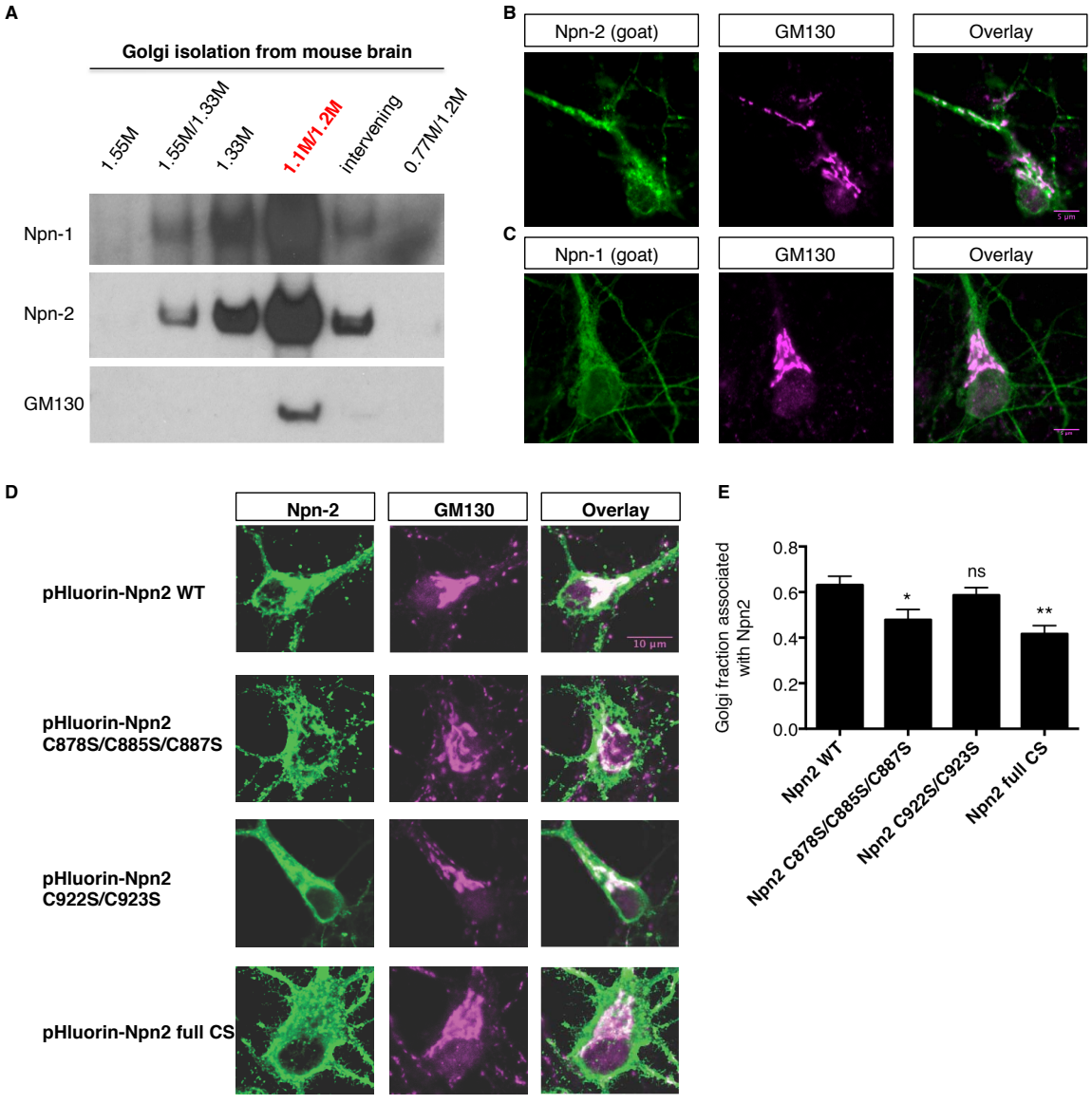

Figure 9. Neuropilins are enriched in the Golgi apparatus and the Npn-2 membrane-proximal cysteines are required for Npn-2–Golgi association.

(A) Golgi isolation was performed from adult mouse whole brain lysates. Six fractions were collected and samples were immunoblotted with Npn-2, Npn-1 or GM130 antibodies. The Golgi fraction is identified by the enrichment of the cis-Golgi marker

GM130, at the interface of the sucrose layers 1.1M and 1.2M. Both Npn-2 and Npn-1 are highly enriched in the cis-Golgi fraction. (B, C) E14.5 DIV13 WT primary cortical neurons were stained for endogenous Npn-2 (panel B, green, goat antibody) or Npn-1 (panel C, green, goat antibody) and GM130 (magenta, rabbit antibody). Npn-2 and Npn-1 display a strong association with the GM130-labeled Golgi apparatus in the perinuclear area (somatic Golgi) as well as in the dendritic shaft (Golgi outposts, prominent in panel B). (D, E) *Npn2*$^{-/-}$ primary cortical neurons were cultured at E14.5 for a total of 17 days in vitro. At DIV8 they were transfected with the indicated pHluorin-tagged Npn2–expressing plasmids. Immunofluorescence against GFP (chicken antibody, to detect exogenous Npn-2) and GM130 revealed that the C-terminal cysteines are dispensable for Npn-2–Golgi association, whereas the membrane-proximal Npn-2 cysteines are required for Npn-2 localization on Golgi membranes (D). (E) The association of Npn-2 with GM130 is shown as the fraction of the GM130-identified Golgi that is associated with Npn-2. This is equal to the ratio of the Npn-2/GM130 colocalization (calculated with the image J colocalization plugin) to the total Golgi detected with GM130. Scale bar: (B, C) 5 μm, (D) 10 μm. Statistics: t-test, * $p < 0.05$, ** $p < 0.01$, ns = not significant.

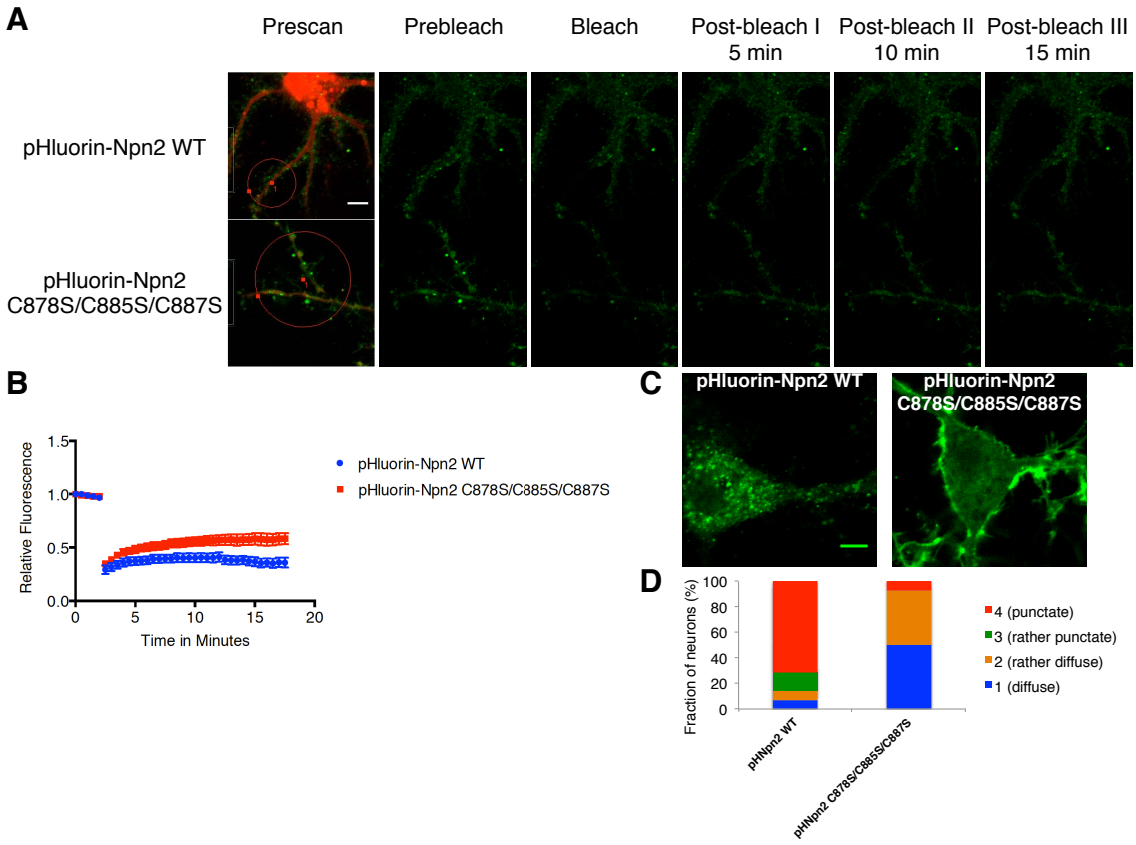

Figure 10. Effects of cysteine residues on cell surface Npn-2 distribution and trafficking in cortical neurons.

(A, B) Primary cortical neurons were transfected with pHluorin-tagged Npn-2 plasmids and subjected to FRAP analysis at an inverted LSM 700 microscope. (A) An image of a transfected neuron was taken before the FRAP image sequence (prescan) and a region-of-interest (ROI) was selected for bleach (delineated with a red circle). Then, the same neuronal area was imaged with the FRAP protocol, according to which images were taken before bleach (prebleach), immediately after bleach (bleach) and various time points after bleach (post-bleach) for monitoring fluorescence intensity over time for a total post-beach time of 15 minutes. Scale bar: 5 μm. (B) Pooled data from several

neurons (WT: n = 7, C878S/C885S/C887S: n = 8) are presented as relative fluorescence. This fluorescence has been corrected for background fluorescence as well as fluorescence decay resulting from time-lapse imaging. (C, D) Primary cortical neurons were transfected with pHluorin-tagged Npn-2 plasmids and imaged live with an inverted LSM 700 microscope (Zeiss) to visualize the distribution pattern of cell surface Npn-2. Npn-2 WT is clustered on the neuronal surface (multiple puncta). In marked contrast, the mutation of the three membrane-proximal Npn-2 cysteines dramatically changes this punctate distribution and renders Npn-2 diffusely distributed along the dendritic shaft and at the cell body (C). This is qualitatively quantified in panel D, where the neurons are classified as having diffuse (1), rather diffuse (2), rather punctate (3) or punctate (4) distribution. Scale bar: 5 μm.

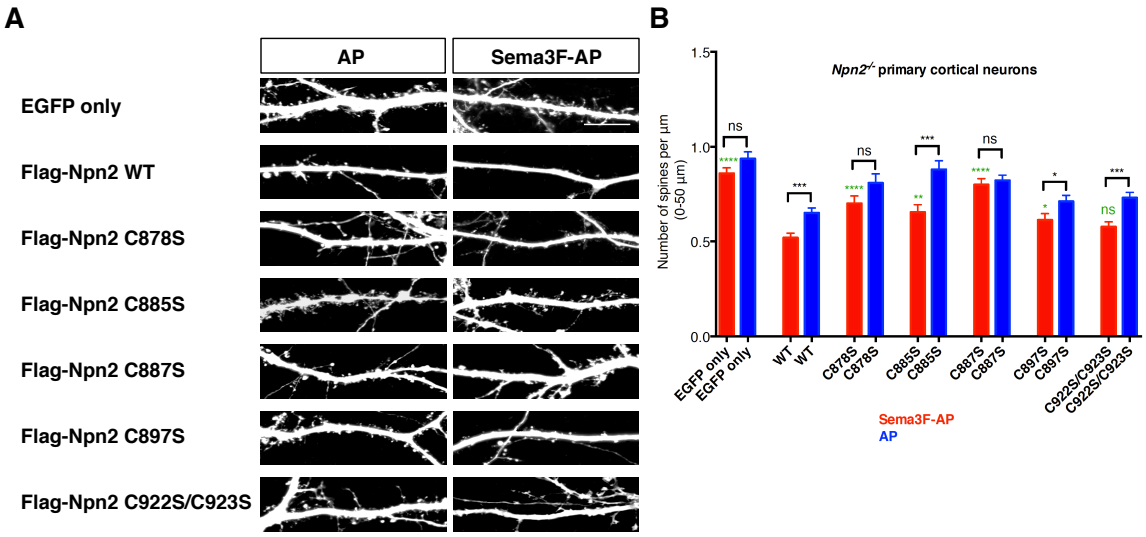

Figure 11. Select Npn-2 cysteine residues are required for Sema3F/Npn-2–mediated spine constraint in primary cortical neurons.

(A, B) *Npn2*$^{-/-}$ primary cortical neurons were cultured at E14.5 for a total of 21 days *in vitro*. At DIV 8, neurons were transfected with various plasmids including an EGFP-expressing plasmid and flag-tagged Npn-2-ires-EGFP–expressing plasmids. EGFP fills the neurons and delineates neuronal architecture including dendritic spines. The Npn-2 plasmids included WT Npn-2 and a number of CS point mutants for the membrane-proximal and cytoplasmic Npn-2 cysteines. At DIV 21, neurons were treated with 5 nM Sema3F-AP or AP for 6 hours. (A) Images of neurons expressing the indicated plasmids and treated with Sema3F-AP or AP. Neuronal morphology is visualized with EGFP immunofluorescence. Spines are counted along the proximal 50 µm of the main dendritic shaft, relative to the cell body. (B) Two different comparisons are shown for each of the tested plasmids: a. a comparison between Sema3F-AP and AP, indicated with the black brackets and asterisks, which shows whether neurons expressing the indicated plasmid

respond to Sema3F, and b. a comparison between the Sema3F-AP–treated neurons expressing WT Npn-2 and the Sema3F-AP–treated neurons expressing the indicated plasmid, shown with the green asterisks. The latter shows the rescue ability of each of the indicated mutant plasmids compared to WT Npn-2. Graph: mean ± s.e.m.; Statistics: unpaired t-test, * $p < 0.05$, ** $p < 0.01$, *** $p < 0.001$, **** $p < 0.0001$. Scale bar: 10 μm.

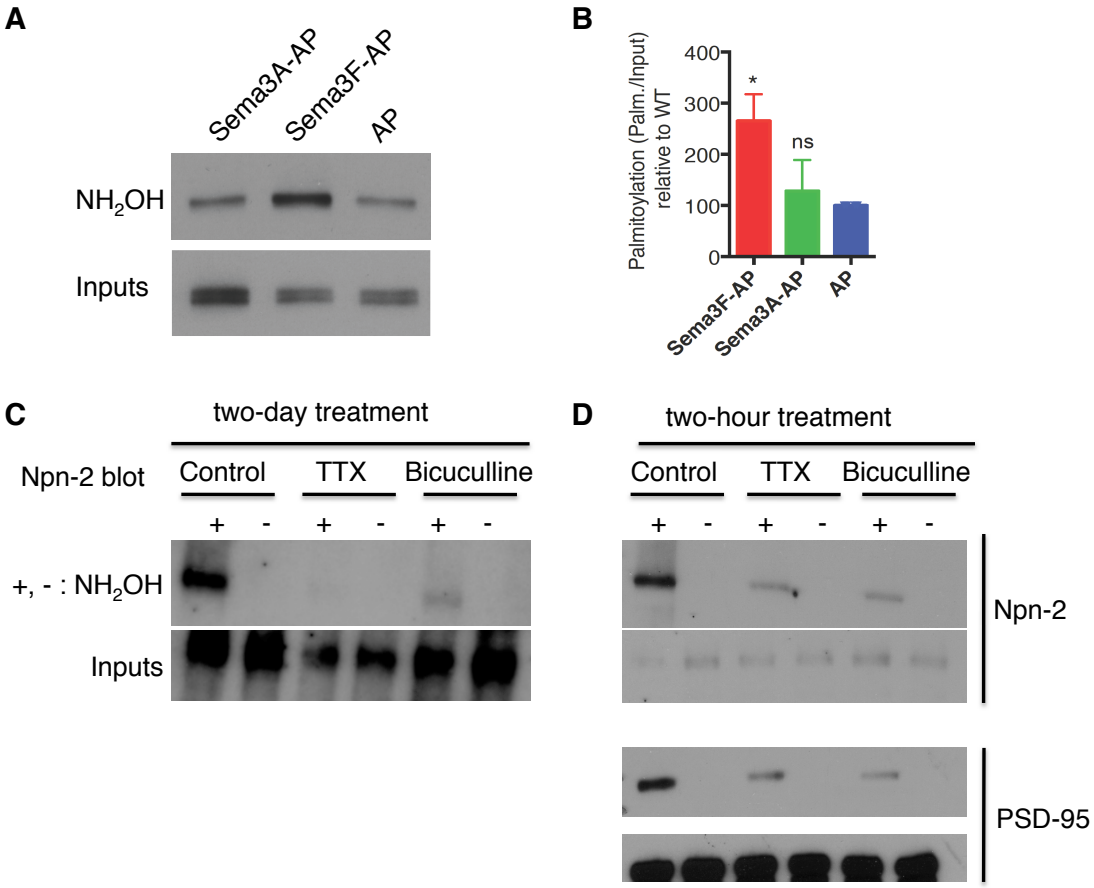

Figure 12. Npn-2 palmitoylation is regulated by Sema3F and neural activity.

(A, B) E14.5 WT primary cortical neurons (CD1 background) were cultured for 12 days *in vitro* (DIV). At DIV 12, they were treated with 5 nM Sema3A-AP, Sema3F-AP or AP for two hours and then subjected to palmitoylation analysis with the ABE assay. Endogenous Npn-2 was detected with immunoblotting with a Npn-2 antibody. (C, D) WT primary cortical neurons were treated with tetrodotoxin (TTX), bicuculline or control treatment for two days (C) or two hours (D). Following treatment, ABE was performed to assess palmitoylation and samples were analyzed with SDS-PAGE and immunoblotting.

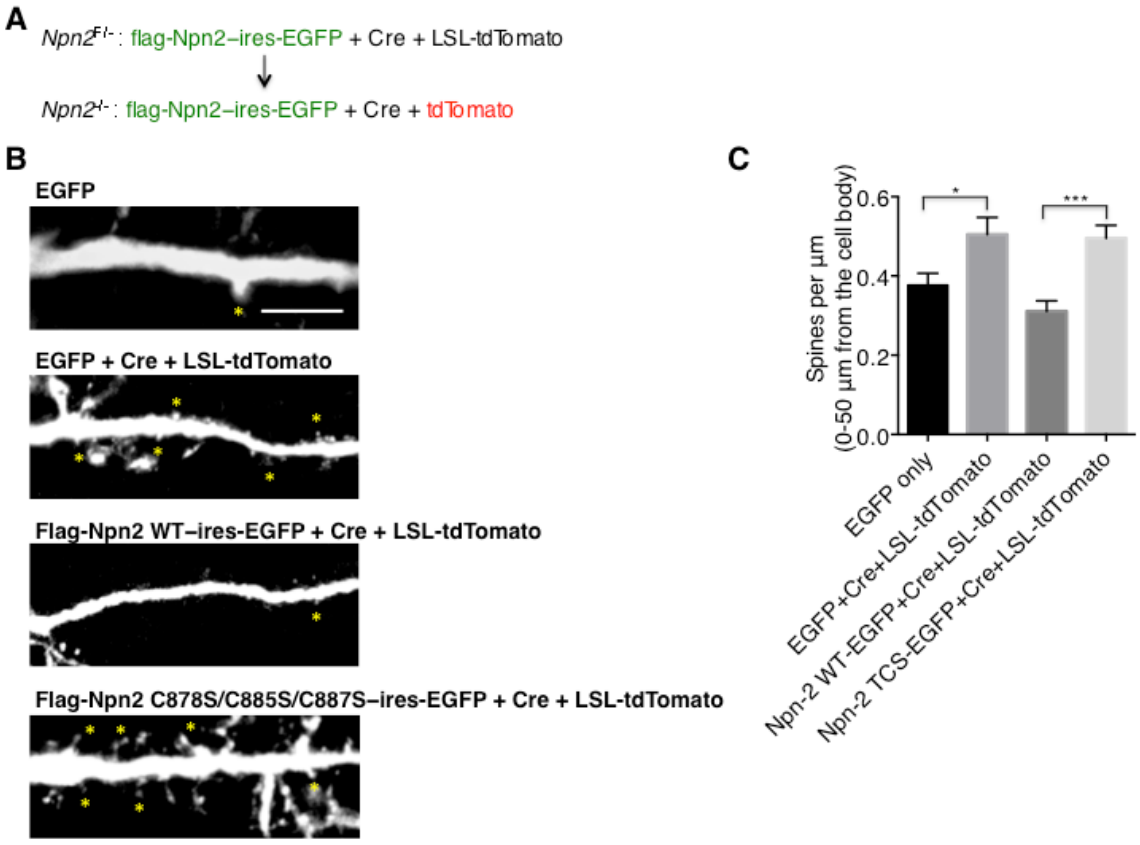

Figure 13. *In vivo* rescue of the *Npn-2*$^{-/-}$–associated dendritic spine phenotype.

(A-C) *Npn2*$^{F/-}$ embryos were electroporated *in utero* at E13.5 to target deep layer cortical pyramidal neurons. Different combinations of expression plasmids were used: *pCIG2-ires-EGFP* to label *Npn2*$^{F/-}$ cortical neurons, *pCIG2-ires-EGFP + Cre + LSL-tdTomato* to excise the floxed Npn-2 allele and render single neurons *Npn2*$^{-/-}$, *flag-Npn2 WT–ires-EGFP + Cre + LSL-tdTomato* in order to test the ability of WT Npn-2 in rescuing the *Npn2*$^{-/-}$–associated increased spine density phenotype, and *flag-Npn2 C878S/C885S/C887S (TCS)–ires-EGFP + Cre + LSL-tdTomato* in order to test the ability of this Npn-2 CS point mutant in rescuing the dendritic spine density phenotype. (B) Images of cortical pyramidal neurons expressing EGFP and/or tdTomato and/or flag-

tagged Npn-2 plasmids. The image of the *EGFP only*-expressing neuron shows EGFP immunofluorescence (grayscale), whereas the other images show *tdTomato* immunofluorescence (grayscale). Scale bar: 10 μm. (C) Dendritic spines are counted along the proximal 50 μm of the apical dendrite (relative to the cell body). Pooled data are presented in a column graph as a number of spines per μm; mean ± s.e.m. Statistics: t-test, * $p < 0.05$, ** $p < 0.01$, *** $p < 0.001$, **** $p < 0.0001$.

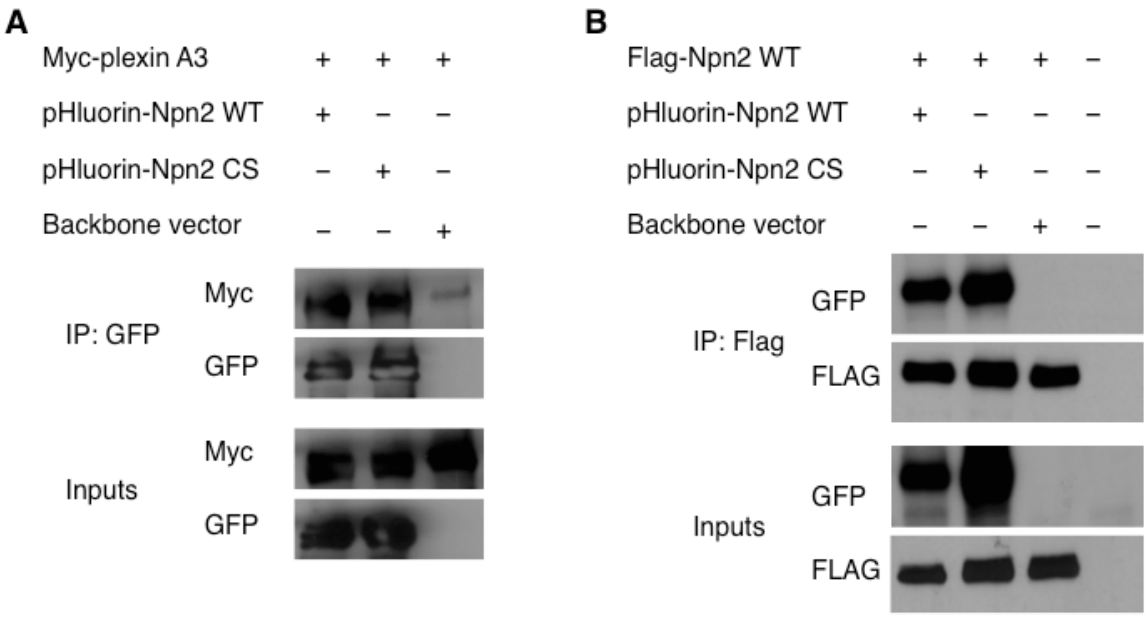

Figure 14. Npn-2 transmembrane and cytoplasmic cysteines are not required for Npn-2/plexin-A3 interactions or Npn-2 homodimerization.

(A) 293T cells were transfected with myc-tagged plexin-A3 and either pHluorin-tagged WT Npn-2, pHluorin-tagged CS Npn-2 or backbone vector. Immunoprecipitation of Npn-2 was performed with a GFP antibody. A myc immunoblot showed that plexin-A3 is co-immunoprecipitated with both WT and CS Npn-2. Thus, the transmembrane/membrane-proximal Npn-2 cysteines are not required for Npn-2/plexin-A3 association in 293T cells. (B) 293 T cells were transfected with flag-tagged WT Npn-2 and either pHluorin-tagged WT Npn-2 or pHluorin-tagged CS Npn-2 or backbone vector. Flag-tagged WT Npn-2 was immunoprecipitated with a flag antibody and samples were immunoblotted with a flag antibody to confirm the immunoprecipitation. An immunoblot with a GFP antibody, which detects pHluorin, showed that both WT and CS pHluorin-tagged Npn-2 proteins are co-immunoprecipitated with flag-tagged WT Npn-2.

Intended to be blank

CHAPTER 3

DISTINCT PALMITOYL ACYLTRANSFERASES CONVEY SPECIFICITY TO SEMAPHORIN SIGNALING

Introduction

Palmitoylation is the most common of the thioesterification reactions that occur on cysteine residues, and it leads to modification of the cysteine's thiol group (-SH) and is catalyzed by enzymes harboring the Asp-His-His-Cys (DHHC) cysteine-rich domain (CRD) known as palmitoyl acyltransferases (PATs, hereafter referred to as DHHCs). The DHHC signature sequence is conserved and catalytically required for palmitoylation performed by these enzymes. DHHCs were originally described in the yeast S. cerevisiae (Lobo et al., 2002; Roth et al., 2002, 2006). In the human and mouse genomes 23 distinct DHHCs encoded by separate genes have been identified thus far. Since there are many more palmitoylated proteins than DHHC enzymes, it is not surprising that DHHCs exhibit overlapping, yet distinct, substrate specificity (Huang et al., 2009; Roth et al., 2006). The investigation of the roles that DHHC enzymes play in vivo through the generation and assessment of knockout mice reveals essential roles for certain DHHCs in the proper development and function of select neuronal populations in the mouse brain. For example, there is increasing evidence showing that genetic deficits in select DHHC enzymes lead to improper function of proteins associated with neural diseases such as Huntington's disease (Yanai et al., 2006), aberrant neuronal phenotypes in a number of CNS structures (Mukai et al., 2008, 2015) and profound behavioral and cognitive deficits (Mansouri et al., 2005; Milnerwood et al., 2013; Mukai et al., 2004; Raymond et al.,

2007; Singaraja et al., 2011; Sutton et al., 2013). These studies, therefore, reveal novel major players in the largely unexplored processes of neuronal development and synaptic transmission, and they demonstrate the importance of DHHC-mediated protein palmitoylation for proper CNS function. However, in most cases the neuronal palmitoylated substrates that account for these structural and behavioral phenotypes have yet to be identified. Indeed, this is a major area of investigation.

Here, we identify certain DHHC enzymes, DHHC15 and DHHC8, as critical regulators of Npn-2 and Npn-1 palmitoylation and function, respectively. We show that, despite the known overlapping specificities of mammalian DHHCs for their substrates, there are unique patterns of DHHC-substrate specificity shown by these two PATs *in vitro* and *in vivo* that are critical for the functional diversification and specification of responses to neuronal cues. This DHHC enzyme-substrate pair specificity serves as a simple molecular code underlying, at least in part, the functional specificity imparted by Sema3A and Sema3F, and possibly additional molecular cues, in the regulation of CNS neuronal morphology.

Results

Npn-2 is a DHHC15 palmitoyl acyltransferase substrate

To identify palmitoyl acyltransferases that catalyze Npn-2 palmitoylation, we performed a screen for DHHCs with the capability of enhancing baseline Npn-2 palmitoylation in 293T cells following the co-expression of Npn-2 with each of the 23 mammalian DHHCs, extrapolating from the approach taken by M. Fukata and colleagues (Fukata et

al., 2004). This *in vitro* gain-of-function experiment suggested that a limited number of DHHCs might be involved in Npn-2 palmitoylation, one of which is DHHC15 (**Figure 15**). Moreover, two other transferases, DHHC11 and DHHC14, also enhanced Npn-2 palmitoylation to a significant extent. However, we decided to focus first on DHHC15 because mice harboring null mutations in *DHHC11* and *DHHC14* are not available and so would not accommodate loss-of-function studies in vivo. Moreover, DHHC15 also enhances the baseline palmitoylation of PSD-95 (Fukata et al., 2004), and this raises the possibility that it palmitoylates other synaptic proteins, too. Importantly, the *DHHC15* null mouse has been generated by Dr Tao Wang's laboratory (Johns Hopkins University) and was generously provided to our laboratory. This genetic tool has been of great importance to our study, and here we provide compelling evidence that Npn-2, but not Npn-1, is a palmitoyl substrate of DHHC15.

DHHC15 is strongly expressed in the cerebral cortex and in a number of other tissues, as demonstrated by immunoblotting of lysates derived from various mouse tissues using a DHHC15-specific antibody generated by Drs. Mejías-Estèvez and T. Wang (**Figure 16**).

To investigate whether Npn-2 is a palmitoyl substrate of DHHC15 in cortical neurons, we cultured E14.5 *DHHC15*$^{-/-}$ and WT C57BL6 primary cortical neurons for a total of 12 days in vitro and then performed ABE assays to assess palmitoylation levels of endogenous Npn-2. Importantly, the *DHHC15*$^{-/-}$ null mouse line has been crossed with *C57BL6* mice at least ten times, allowing us to use WT *C57BL6* mice/neurons as a control for our biochemical assays and phenotypic analyses. Interestingly, in the absence of DHHC15, Npn-2 palmitoylation is significantly reduced in cultured cortical neurons (by ~46%) (**Figure 17, panels A and B**). On the other hand, Npn-1 palmitoylation is not

affected (**Figure 17, panels C and D**). These data suggest that Npn-2 is a palmitoylation substrate of DHHC15 in cortical neurons, but apparently Npn-1 is not.

DHHC15 is required for proper Sema3F/Npn-2–mediated spine constraint, but not for Sema3A/Npn-1–induced dendritic elaboration in cortical neurons

To investigate whether DHHC15 plays a role in Sema3F/Npn-2–mediated dendritic spine constraint, we assessed *DHHC15*$^{-/-}$ primary cortical neurons for their response to Sema3F. Specifically, E14.5 *DHHC15*$^{-/-}$ primary cortical neurons were transfected at DIV8 with EGFP in order to visualize neuronal morphology, and they were then cultured for a total of 21 days in vitro to allow for the elaboration of mature and fully developed spine phenotypes. At DIV21 neurons were treated with 5nM Sema3F-AP or AP alone for 6 hours and then subjected to immunofluorescence to assess dendritic spine density. WT *C57BL6* cortical neurons responded to Sema3F with spine collapse responses comparable to those observed in the AP control (**Figure 18, panels A-C**). Interestingly, *DHHC15*$^{-/-}$ cortical neurons exhibited no spine constraint in response to Sema3F treatment (**Figure 18, panels D-F**). Importantly, neurons lacking another palmitoyltransferase, DHHC8, which were treated as a control, responded to Sema3F with a spine collapse (**Figure 18, panels G-I**), similar to the WT neurons. The lack of Sema3F-mediated spine constraint, in conjunction with the decreased Npn-2 palmitoylation in *DHHC15*$^{-/-}$ neurons, together strongly suggest that DHHC15-mediated Npn-2 palmitoylation is required for Npn-2 to function in response to Sema3F as a negative regulator of spine density in cortical neurons.

Since DHHC15 is critical for Sema3F/Npn-2 signaling in vitro, we sought to address whether DHHC15 is also required for Sema3A/Npn-1 signaling in cortical neurons. Sema3A/Npn-1 signaling promotes the elaboration of basal dendritic arbors in WT cortical neurons (Gu et al., 2003; Tran et al., 2009). Given this robust and highly penetrant phenotype, I developed an assay in which WT E14.5 primary cortical neurons at DIV12 are treated with 5nM Sema3A-AP or AP alone for 6 hours, and dendritic elaboration is assessed using immunofluorescence against the somatodendritic marker Microtubule-Associated Protein 2 (MAP2). WT cortical neurons robustly respond to Sema3A by enhanced elaborating their perisomatic dendrites (**Figure 22, panels A-C**), which corresponds to the basal dendritic domain of deep layer cortical neurons in vivo. Notably, *DHHC15*$^{-/-}$ neurons also respond to Sema3A to the same extent that WT neurons do (**Figure 22, panels G-I**), showing that DHHC15 is dispensable for Sema3A/Npn-1–mediated basal dendritic arbor complexity in cortical pyramidal neurons in culture. This is in accordance with the ABE assay showing that Npn-1 is not a major palmitoyl substrate of DHHC15 (**Figure 17, panels C and D**).

To test whether DHHC15 also plays a role in Sema signaling in vivo, we characterized the dendritic elaboration and spine density of *DHHC15*$^{-/-}$ deep layer cortical pyramidal neurons in the mouse brain. Given that *Sema3F*$^{-/-}$ and *Npn2*$^{-/-}$ mice also display an aberrant spine phenotype in the dentate gyrus granule cells, I also examined the spine density of *DHHC15*$^{-/-}$ dentate gyrus granule cells. To achieve this I used two strategies: 1) Thy1-GFP labeling of cortical neurons–*DHHC15*$^{-/-}$ mice were crossed with the *Thy1-GFP* (*Myp*) mouse line that robustly labels deep layers of the cerebral cortex, dentate gyrus granule cells and other cell populations; and 2) Golgi staining, which provides

strong but sparse labeling of neurons in vivo. As far as basal dendritic arbor elaboration is concerned, *DHHC15*$^{-/-}$ layer V cortical neurons labeled with Golgi staining exhibit no defect as compared to WT C57BL6 controls (**Figure 23**). This supports the idea that Npn-1 is unlikely to be a major substrate of DHHC15.

On the other hand, we analyzed the dendritic spines on deep layer cortical neurons in these mice with *Thy1-GFP* and Golgi staining. Interestingly, the dentate gyrus granule cells of the *DHHC15* null brains display a higher spine density compared to the WT dentate gyrus granule cells with both Thy1-GFP labeling (**Figure 19, panels C and D**) and Golgi staining (**Figure 19, panels E and F**). In the cerebral cortex, Thy1-GFP labeling has shown a modest difference in one out of two brains analyzed so far, and cumulative data are inconclusive (**Figure 19, panels A and B**, no significant difference thus far). However, more experiments are currently being performed in order to obtain definitive evidence about dendritic spines in layer V cortical neurons in vivo.

Taken together, these data demonstrate that DHHC15 is involved in the Sema3F signaling pathway, but not in the Sema3A pathway, with respect to regulating dendritic morphology and dendritic spine density, and therefore these experiments uncover functional differences between Sema3F and Sema3A by means of differential effects by DHHC enzymes on their co-receptors Npn-2 and Npn-1, respectively.

DHHC15 is not required for anterior commissure or cranial nerve development

Npn-2 is required for the proper formation of the anterior commissure (ac), as shown by the severely defective (largely absent) anterior commissure in the brains of *Npn-2* null

mice (Giger et al., 2000). This prompted us to assess the anterior commissure in the brains of DHHC15 homozygous mutant mice. Three *DHHC15*$^{-/-}$ and WT brains were sectioned and the sections were stained with neurofilament antibody (2H3) to visualize the ac. All *DHHC15*$^{-/-}$ brains examined have normally developed anterior commissures (**Figure 20**), ruling out the possibility that DHHC15-mediated Npn-2 palmitoylation is required for the development of this Npn-2–dependent axonal tract.

In addition, Npn-2 is also required for the development of a number of cranial nerves, including the trochlear nerve (IV) and the proper fasciculation of the oculomotor, trigeminal and facial nerves (Giger et al., 2000). To assess whether DHHC15-dependent Npn-2 function is required for this developmental process, I analyzed the cranial nerves of E11.5 embryos using whole-mount neurofilament (2H3) staining. Of note, all *DHHC15*$^{-/-}$ embryos had properly developed cranial nerves (**Figure 20**).

Taken together, DHHC15-mediated Npn-2 palmitoylation is not required for the development of the Npn-2–associated axonal tracts and therefore apparently plays no role in Sema3F-mediated axon guidance. Current experiments are addressing whether Sema3F pruning functions (Riccomagno and Kolodkin, 2015) are independent of DHHC15.

Npn-2 localization in *DHHC15*$^{-/-}$ primary cortical neurons

These data on the responsiveness of *DHHC15*$^{-/-}$ cortical neurons to the secreted semaphorin ligand Sema3F raise several questions about aspects of neuropilin trafficking are defective in these neurons and lead to the phenotypic defects. First, we assessed the

localization of Npn-2 in the Golgi apparatus with immunofluorescence, since WT Npn-2 is highly enriched in the Golgi. This experiment showed that endogenous Npn-2 is associated with the Golgi apparatus in *DHHC15*$^{-/-}$ mutants (**Figure 21, panel A**).

Second, we assessed the distribution of pHluorin-tagged WT Npn-2 transfected into *DHHC15*$^{-/-}$ cortical neurons with live imaging. However, Npn-2 is punctate in these neurons, similar to its distribution in WT neurons (data not shown).

Third, Sarah Mitchell isolated PSDs from wild type and *DHHC15*$^{-/-}$ primary cortical neurons to look for a potential redistribution of Npn-2 in different subcellular fractions. Two experiments performed thus far have shown a variable defect for Npn-2; specifically, in *DHHC15*$^{-/-}$ neurons Npn-2 exhibits variable increases in the S2 (soluble cytoplasmic fraction), which however is also observed for Npn-1. Importantly, one of the two experiments also revealed a complementary decrease of Npn-2 in the P2 (membrane) fraction, which was not observed for Npn-1 (**Figure 21, panels B-E**, one experiment shown). If this is true, and additional experiments are underway to investigate this issue, this is an important finding because it would show that DHHC15-mediated Npn-2 palmitoylation is essential for the proper distribution of Npn-2 in the membrane and soluble subcellular fractions, a basic property resulting from the proper palmitoylation status of palmitoyl substrates.

Differential Npn-2 cysteine requirements for selective palmitoyltransferase binding

Palmitoylated substrates associate with their respective enzymes and palmitoylated cysteine residues are required for such an association (Huang et al., 2009). Thus, we

sought to assess potential binding of Npn-2 to the palmitoyltransferase DHHC15. We performed co-immunoprecipitation experiments between Npn-2 and DHHC15, and also Npn-1 and DHHC15, and we found that both neuropilins associate with DHHC15 following their co-expression in 293T cells (data not shown). We also performed control co-immunoprecipitation experiments between Npn-2 and DHHC8 and between Npn-1 and DHHC8. These experiments also showed no specificity, since both Npn-1 and Npn-2 associated with DHHC8 (data not shown). These findings are consistent with data showing that the physical interactions between DHHC enzymes and palmitoyl substrates are promiscuous, in that they do not exhibit stereoselectivity and are not driven by a consensus sequence (Rocks et al., 2010). However, when substrates were tested for their palmitoylation by various co-expressed palmitoyltransferases, remarkable specificity was observed (Huang et al., 2009). These observations are consistent with our data showing that physical associations between neuropilins and DHHCs 15 and 8 are not specific but, with respect to the palmitoylation, Npn-2 (but not Npn-1) is a substrate of DHHC15.

To further investigate potential interaction specificity between neuropilins and DHHCs, in collaboration Sarah Mitchell we tested the association between DHHC15 or DHHC8 and various Npn-2 proteins, including WT, the C878S/C885S/C887S (TCS), the C922S/C923S (C-terminal) and the C878S/C885S/C887S/C897S/C922S/C923S (full CS mutants. All Npn-2 proteins associated with DHHC8 (data not shown). However, when DHHC15 was co-expressed with these Npn-2 proteins, WT Npn-2 associated robustly with the DHHC15, but the C878S/C885S/C887S and the full CS Npn-2 mutant proteins displayed little or no interaction with DHHC15, respectively. Importantly, the Npn-2 C-terminal cysteines are not required for the DHHC15–Npn-2 association (data not shown;

experiments in progress). This finding is potentially of great importance because it suggests a specific requirement for the Npn-2 membrane-proximal cysteines in DHHC15–Npn-2 association and subsequently in DHHC15-mediated Npn-2 palmitoylation. This observation is consistent with published observations which have shown that the palmitoylated cysteine residues are required for the interaction of a palmitoyl substrate with its palmitoyltransferases (Huang et al., 2009). We are now performing additional experiments to address whether there is a similar requirement for the association between Npn-1 and DHHC8, given that Npn-1 is a likely substrate of DHHC8 (see next section below).

DHHC8 is essential for Sema3A/Npn-1–induced dendritic elaboration but not for Sema3F/Npn-2–induced spine collapse

Another DHHC enzyme of critical importance for the development of the central nervous system is DHHC8 (also known as ZDHHC8). In particular, DHHC8 promotes the dendritic elaboration and spine formation of hippocampal pyramidal neurons in vitro and in vivo (Mukai et al., 2008). The dendritic hippocampal phenotype of *DHHC8*$^{-/-}$ neurons closely resembles the reduced dendritic elaboration phenotype resulting from the genetic abolition of the Sema3A/Npn-1 signaling in cortical neurons observed in the *Npn1*$^{Sema3A-}$ mouse (Gu et al., 2003). Given this striking similarity, I sought to investigate whether Npn-1 is a substrate of DHHC8 in the cortex. I first analyzed the dendritic arborization of *DHHC8*$^{-/-}$ or WT C57BL6 deep layer cortical pyramidal neurons with Golgi staining. This revealed a severe dendritic arborization defect of *DHHC8*$^{-/-}$ neurons, which exhibited significantly reduced basal dendritic arborization (perisomatic) compared to the

WT neurons (**Figure 23**). This shows that the *DHHC8* null mouse phenocopies the abolition of Sema3A/Npn-1 signaling in deep layer cortical neurons (Gu et al., 2003; Tran et al., 2009) and raises the possibility that Npn-1 is a substrate of DHHC8 in the cortex. To test this hypothesis, and to determine whether DHHC8 and Npn-1 function in the same or in parallel pathways, we tested the responsiveness of *DHHC8*$^{-/-}$ cortical neurons to Sema3A. Treatment of WT cortical neurons with Sema3A-AP results in a more elaborate dendritic arbor as compared to the AP treatment alone (**Figure 22, panels A-C**). If DHHC8 is not required for Sema3A/Npn-1 signaling, *DHHC8*$^{-/-}$ neurons should respond to Sema3A. On the contrary, if DHHC8-mediated Npn-1 palmitoylation is required for proper propagation of the Sema3A/Npn-1 signaling, then *DHHC8*$^{-/-}$ neurons are not expected to respond to Sema3A. We therefore treated *DHHC8*$^{-/-}$ with Sema3A-AP or AP alone and assessed basal dendritic elaboration in these neurons with MAP2 staining. Remarkably, *DHHC8*$^{-/-}$ neurons were unable to respond to Sema3A (**Figure 22, panels D-F**), suggesting that DHHC8 is required for Npn-1 function and that Npn-1 is a physiological substrate of DHHC8. To provide additional support for the hypothesis that Npn-1 is a substrate of DHHC8 in cortical neurons, I assessed Npn-1 palmitoylation in WT and *DHHC8*$^{-/-}$ neurons using ABE. Thus far, these experiments have been inconclusive, however additional ABE experiments are currently underway to assess DHHC8 activity, both in cell culture models and in the mouse brain.

Taken together, these findings suggest that Npn-1 is palmitoylated by DHHC8 in cortical neurons, and that this modification is required for Sema3A/Npn-1–induced dendritic arborization of these neurons.

To investigate whether this effect of DHHC8 is specific for Npn-1 as opposed to Npn-2, we assessed the responsiveness of *DHHC8*$^{-/-}$ cortical neurons to Sema3F by assessing their spine density after control AP or Sema3F-AP treatment. Importantly, *DHHC8*$^{-/-}$ neurons robustly respond to Sema3F with a decrease in their spine density. Furthermore, we assessed the spine density of deep layer cortical pyramidal *DHHC8*$^{-/-}$ neurons in vivo with Thy1-GFP. Interestingly, *DHHC8*$^{-/-}$ deep layer cortical pyramidal neurons exhibit significantly reduced spine density as compared to WT neurons, demonstrating that DHHC8 is required for spine formation or maintenance (**Figure 24**). This makes it unlikely that Npn-2 is a substrate of DHHC8, since the *Npn2*$^{-/-}$ mice display the opposite phenotype. This finding is in agreement with the role that DHHC8 plays in hippocampal pyramidal neurons (Mukai et al., 2008).

In summary, DHHC8 is palmitoyl acyltransferase that apparently acts on Npn-1, but not in Npn-2, to regulate palmitoylation and also select aspects of neuronal morphology. We can therefore speculate that DHHC8 recruits to the Sema3A/Npn-1 signaling pathway distinct effectors that cause dendrite growth-associated changes but not cytoskeletal rearrangements associated with spines. However, lack of knowledge regarding proteins that may interact with this transferase makes any speculations with respect to cytoskeleton rearrangements premature. Another possibility is that Npn-1 on its own interacts with cytoskeletal components related to dendritic growth, perhaps as a result of its subcellular distribution.

Conclusions-discussion

My work identifies palmitoylation as a post-translational modification critical for the functional specification and diversification of neuropilin receptors by means of palmitoyl acyltransferase-substrate specificity. These data are summarized in a schematic model (**Figure 25**). My study is one of the first, along with work from J. Gogos (Mukai et al., 2008, 2015), to demonstrate effects of palmitoyl acyltransferases on select aspects of neuronal morphology. Interestingly, I also identified specific neuronal protein substrates for these enzymes and I show that this specificity critically directs distinct aspects of neuronal morphology, ultimately contributing to the establishment of neuronal polarity. Of course, the phenotypes resulting from deletion of a palmitoyl acyltransferase constitute the net effect of the lack of palmitoylation of all substrates of this transferase. Therefore, if a DHHC knockout mouse phenocopies a specific mutant mouse, this raises the question as to whether these two proteins act in parallel or the same signaling pathway. Here, we provide two lines of evidence supporting the notion that Npn-1 functions in same pathway as DHHC8, and that Npn-2 functions in the same pathway as DHHC15. First, neuropilin palmitoylation is reduced in the respective *DHHC* loss-of-function neurons, showing that each neuropilin is a substrate of each specific DHHC enzyme. Second, *DHHC* KO cortical neurons do not respond to the respective Sema ligand, suggesting direct involvement of each DHHC enzyme in one of the two specific Sema signaling pathways.

Usually more than one palmitoyl acyltransferase will palmitoylate a protein, albeit to varying extents (Greaves and Chamberlain, 2011; Huang et al., 2004). The screens I performed suggest that baseline neuropilin palmitoylation is enhanced by a few different

palmitoyl acyltransferases. A challenging question to address is how deletion of a single palmitoyl acyltransferase, which causes a limited decrease in a specific protein's palmitoylation levels, leads to a specific inability to function properly. A plausible explanation would be that, upon loss of a palmitoyl acyltransferase, fewer protein molecules are palmitoylated and therefore there a severe imbalance develops in how that substrate protein is trafficked and functions. Another theory could be that of a "dominant" palmitoyl acyltransferase. Specifically, different palmitoyl acyltransferases might palmitoylate a protein on different cysteines and in distinct subcellular compartments. This could result in different palmitoylation events being important for distinct protein functions. For example, a palmitoylation event close to the plasma membrane might regulate the targeting of the protein to nearby dendritic spines, its insertion into a specific plasma membrane microdomain, or it might mediate activity-dependent protein targeting (Brigidi et al., 2014a; Fukata et al., 2013; Noritake et al., 2009). Such an event, even if it is quantitatively small and the bulk palmitoylation of the protein is not affected, could result in defects that affect proper distribution and function of a protein since at any one time only a small fraction of total protein might be functionally significant. However, in order to provide more insight into the trafficking and distribution of palmitoylated proteins in distinct subcellular compartments specific antibodies against palmitoylated proteins will have to be developed, with the goal of visualizing at a high resolution protein palmitoylation on specific residues, as has been previously shown for PSD-95 (Fukata et al., 2013). Specifically, Fukata and colleagues isolated an antibody that specifically recognized the conformation of palmitoylated PSD-95 by screening an

antibody phage display library, showing that they can specifically detect palmitoylated PSD-95 in neurons (Fukata et al., 2013).

Importantly, the implication of several palmitoyl acyltransferases in disease pathogenesis in the nervous system (Young et al., 2012) makes the identification of their substrates critical from a therapeutic standpoint. DHHC15 has been implicated in a case of a human X-linked mental retardation (Mansouri et al., 2005), whereas DHHC8 has been linked to the pathogenesis of schizophrenia (Mukai et al., 2004). The existence of specific substrates for these enzymes could provide a rationale for the development of targeted therapeutic approaches directed toward ameliorating the symptoms of mental and cognitive disorders associated with defects or loss in certain palmitoyl acyltransferases. However, this requires a much more extensive investigation of the complement of substrates that are palmitoylated by these enzymes coupled with thorough genetic analysis.

Experimental procedures

Dendritic elaboration analysis

Neuronal dendritic elaboration was assessed with Sholl analysis performed with Image J. In detail, confocal stacks of neurons were used to calculate the 3D projection, which was then thresholded. Any background fluorescence or neighboring neurons interfering with the analysis were erased with the paintbrush tool. The point-selection was placed at the center of the cell body and the Sholl analysis plugin was used to count the dendritic processes at various distances from the cell body, ranging from 0 μm to 100 μm.

Spine analysis

Described in detail in the experimental procedures of Chapter 2.

Immunofluorescence (in vivo)

Sections mounted on slides were left to dry at room temperature and then they were blocked with 10% goat or donkey serum + 0.1% Triton X-100 in PBS, for one hour at room temperature. Then tissue was incubated with primary antibodies diluted in 1% serum + 0.1% Triton X-100 in PBS, overnight at 4ºC. Tissue was washed three times 10 min. each with 1x PBS. Next, tissue was incubated with secondary antibodies diluted 1:500 for one hour at room temperature. Finally, tissue was washed four times 10 min. each with 1x PBS and a rectangular glass coverslip was placed with mounting medium on the slide with the sections. **Primary antibodies:** GFP, chicken IgY, 1:500 (Avés, cat. no. GFP-1020); MAP2, mouse, 1:1000 (Sigma, cat. no. M1406); GM-130 (AbCam, cat. no. ab52649); neurofilament (2H3), mouse monoclonal (Developmental Studies Hybridoma

Bank). **Secondary antibodies:** CF488A donkey anti-chicken IgY (Biotium, cat. no. 20166); Alexa Fluor 488 goat anti-mouse IgG (Life Technologies); Alexa Fluor 555 donkey anti-rabbit IgG (Life Technologies).

Neuron labeling *in vivo*

Thy1-GFP: the Thy1-GFP (m) line (MYP) was crossed to various knockout mice (*DHHC15*$^{-/-}$, *DHHC8*$^{-/-}$) for labeling of layer V cortical neurons and dentate gyrus granule cells. *DHHC15*$^{+/-}$*;Thy1-GFP* mice were crossed with each other to generate litter- and age-matched WT and *DHHC15*$^{-/-}$ mice expressing Thy1-GFP. Likewise, *DHHC8*$^{+/-}$*;Thy1-GFP* mice were crossed to generate WT and *DHHC8*$^{-/-}$ mice expressing Thy1-GFP.

Golgi staining: performed with the Rapid GolgiStain kit (FD Neurotechnologies, Cat. #: PK401) according to the protocol provided by the kit. Briefly, brains were dissected out and incubated with impregnation solution A+B for a total of twelve days in the dark at room temperature, while impregnation solution was changed on the second day of the incubation. After twelve days, impregnation solution was discarded and brains were incubated with solution C for a total of 4 days in the dark at 4^{o}C, while solution C was replaced by fresh solution C on the second day. Brains were embedded in NEG 50 following regular procedures and sectioned with a Leica cryostat (Z5470) at the coronal plane, at 100μm thickness. Sections were left to dry for 24 hours in the dark and next day they were subjected to staining according to the protocol. Stacks of neurons were acquired using a DIC at an inverted LSM 700 confocal microscope (Zeiss), with a 20X

lens for the visualization of dendrites and with a 63X oil lens for the assessment of dendritic spines.

Whole-mount neurofilament staining: E11.5 embryos were removed from the abdominal cavity of a timed-pregnant female and fixed overnight with 4% PFA at 4˚C. Next day, embryos were washed three times 10 min. each with PBS and gradually dehydrated with methanol diluted in PBS, according to the following scheme: 30% methanol for 1 hour, 50% methanol for 1 hour, 80% methanol for 2 hours, 100% methanol overnight. Endogenous peroxidase activity was quenched overnight. Incubation with 1x TNT, one hour each, five times. Incubation with the 2H3 neurofilament antibody (mouse monoclonal, Developmental Studies Hybridoma Bank) for 48 hours. Next, embryos were washed five times, 1 hour each, with TNT buffer and then incubated with a secondary antibody for 36 hours. Next, tissue was washed two times, 30 minutes each, overnight and two times 30 minutes each, with TBS. Signal was developed and then embryos were washed for 5-15 minutes with TBS. Next, tissue was fixed overnight, at 4˚C, with 4% PFA. Tissue was dehydrated with methanol diluted in PBS, according to the following scheme: 30% methanol for 1 hour, 50% methanol for 1 hour, 80% methanol for 2 hours, 100% methanol overnight. Finally, embryos were cleared with BABB solution and imaged with DIC.

Mice

Animal procedures were carried out in conformity with the policies and guidelines of the Animal Care and Use Committee of the Johns Hopkins University, which are established

according to the US National Research Council's Guide to the Care and Use of Laboratory Animals and in compliance with the Animal Welfare Act and Public Health Service Policy. WT C57BL6 mice were purchased from Jackson laboratories and WT CD1 mice were purchased from Charles River laboratories. The *DHHC15* (or *ZDHHC15*) null mouse line was generated and provided to our lab by Dr. Tao Wang's laboratory (Johns Hopkins University) and has been characterized by Rebeca Mejias-Estevez (Rebeca Mejias-Estevez et al., *unpublished*). The *DHHC8* (or *ZDHHC8*) null mouse was generated and provided to our lab by Dr. Joseph Gogos and colleagues (Columbia University) and has been previously characterized (Mukai et al., 2004, 2008).

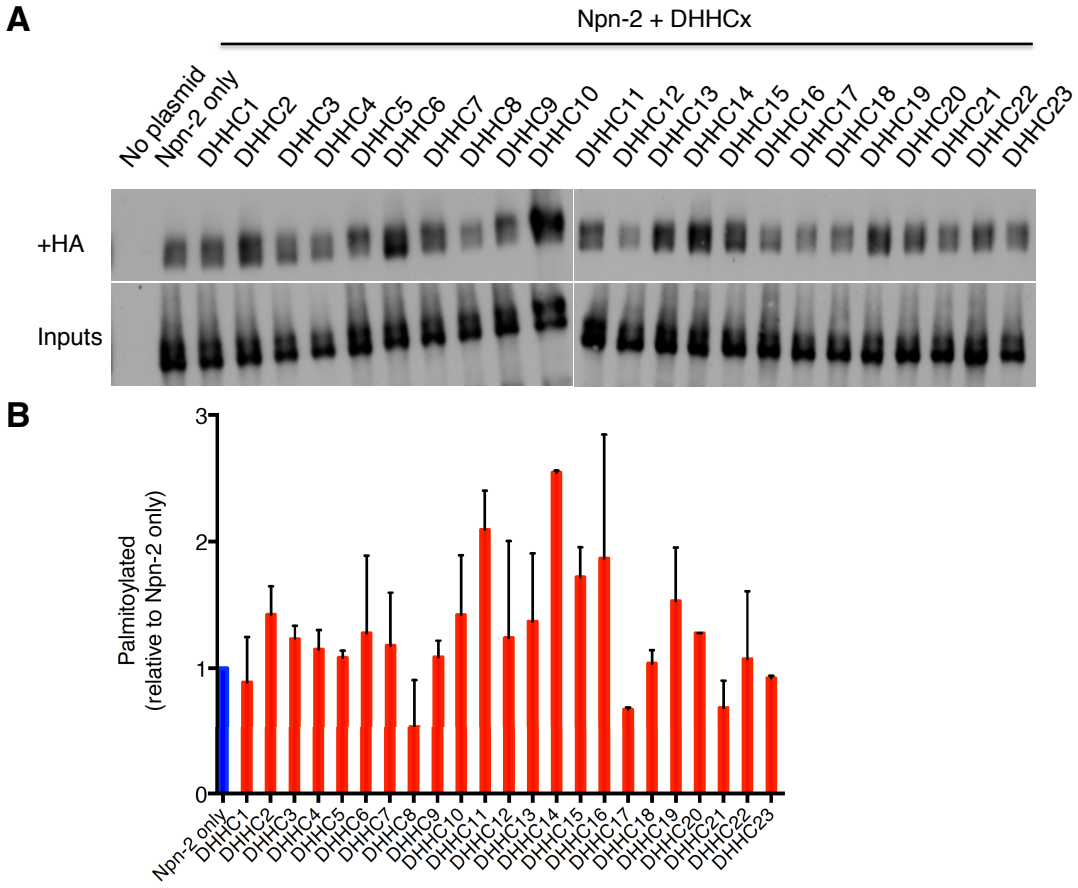

Figure 15. Npn-2 is a substrate for a subset of select palmitoyl acyltransferases.

(A, B) 293T cells were transfected with Npn-2 only or co-transfected with Npn-2 along with each of the 23 mammalian palmitoyl acyltransferases (DHHCs) (expression plasmids of DHHCs were provided by Masaki Fukata (Fukata et al., 2004). Following their expression, cells were subjected to the ABE assay for the assessment of Npn-2 palmitoylation. (A) Immunoblots with Npn-2 antibody (rabbit) showing the +HA (+ hydroxylamine) samples (top), which represent the palmitoylated protein, and the Npn-2 inputs (bottom). The no plasmid control sample (leftmost lane) confirms that the signal is specific to Npn-2 protein. (B) The average from two independent experiments is presented in a column graph and represents the ratio of palmitoylated protein (+HA) to

the total protein (Input). The ratio for each sample (Npn-2 along with each of the 23 DHHCs, red columns) is expressed as a percentage of the Npn-2 only sample (blue column, leftmost column in the graph). The Npn-2 only sample represents baseline Npn-2 palmitoylation and it's set at 100%. Graph: mean ± s.e.m.

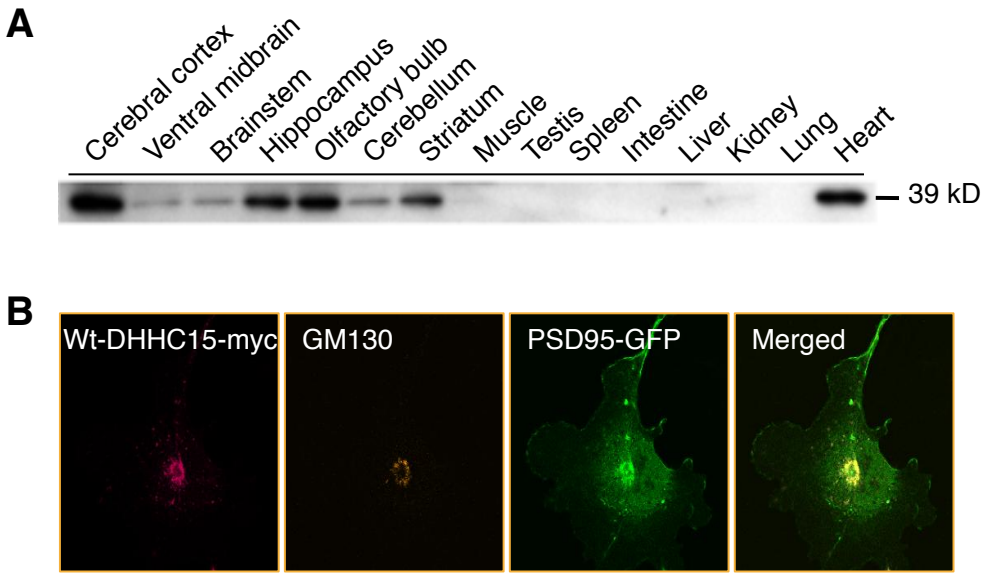

Figure 16. Tissue expression and localization of the palmitoyltransferase DHHC15.

(A) Tissue expression profile of DHHC15. Immunoblot using a custom rabbit antibody α-DHHC15 identified a 39 kD band corresponding to DHHC15 protein. The antibody was generated in Dr Tao Wang's lab (Johns Hopkins). (B) Subcellular distribution of DHHC15. COS cells were transfected with DHHC15-myc and psd95-GFP. Immunofluorescence was conducted using α-myc for DHHC15 (red), α-GM130 (Golgi marker, brown), α-GFP for psd-95 (green), merged image (yellow). Note co-localization of DHHC15 with GM130 in the Golgi apparatus. The figure is provided to us by courtesy of Rebeca Mejias-Estevez (*unpublished data*, Dr Tao Wang's lab, Johns Hopkins University).

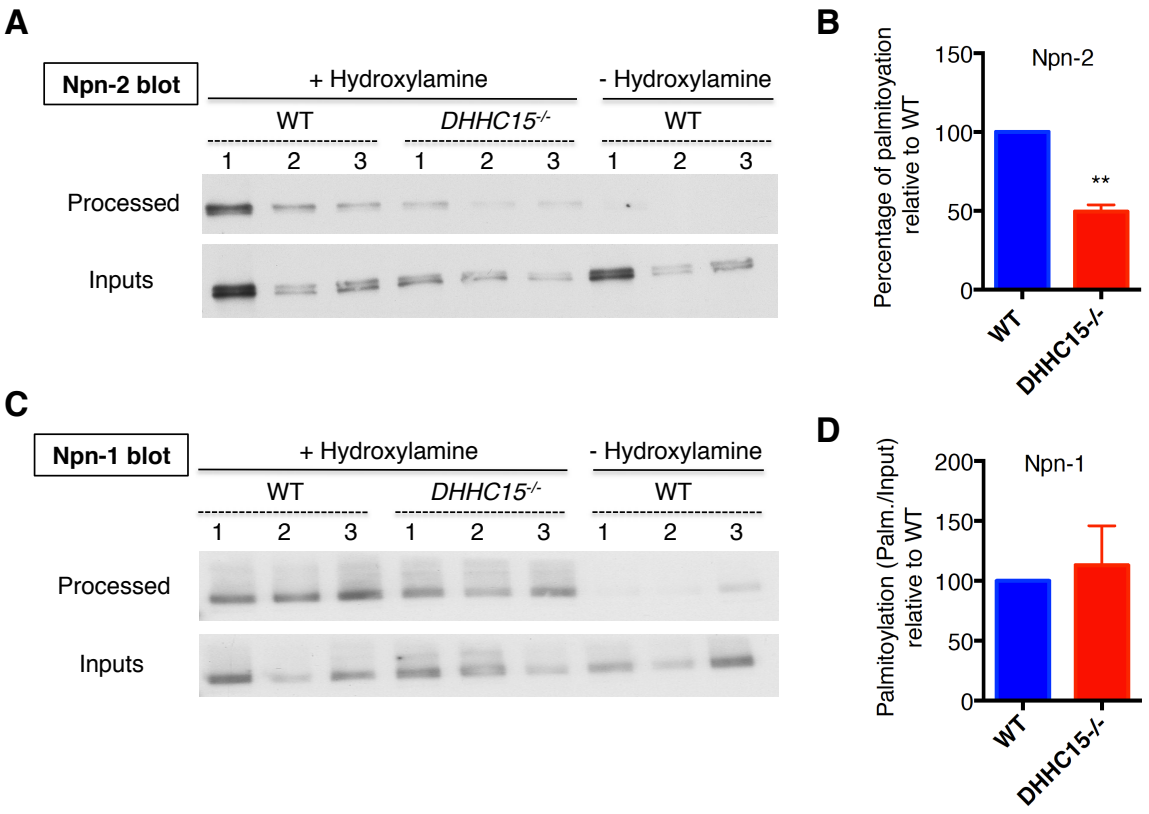

Figure 17. **Npn-2 is a palmitoyl substrate of DHHC15.**

(A-D) Wild-type C57BL6 and *DHHC15*$^{-/-}$ primary cortical neurons (DIV12) were subjected to the ABE assay for the assessment of palmitoylation of endogenous proteins. Samples were immunoblotted with a Npn-2 (A, B) or a Npn-1 (C, D) antibody to detect endogenous Npn-2 or Npn-1, respectively. Palmitoylated protein is presented as the ratio of +hydroxylamine sample (palmitoylated) to the corresponding input. In each experiment, an average is calculated for the WT and this is considered as being 100% (1). The palmitoylation of neuropilin in *DHHC15*$^{-/-}$ is shown as a percentage of the WT. Npn-2 palmitoylation in *DHHC15*$^{-/-}$ cortical neurons is reduced by ~ 46% (B), whereas Npn-1 palmitoylation is unaffected (D).

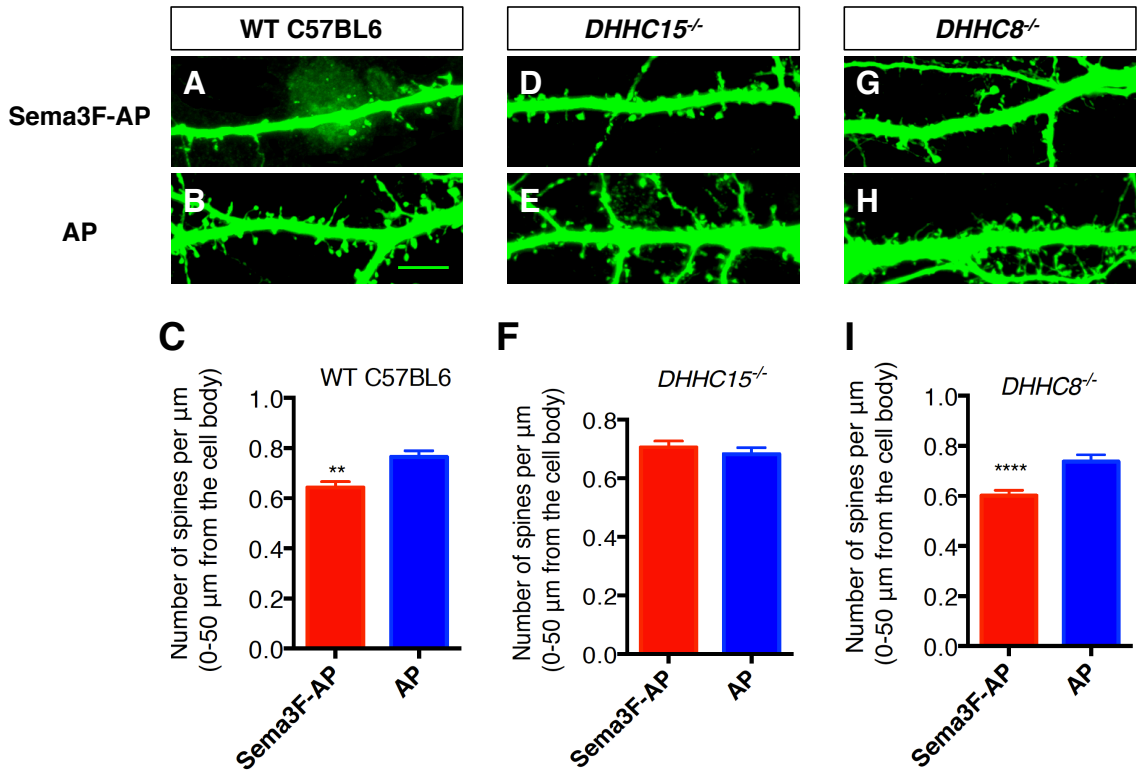

Figure 18. DHHC15 is required for Sema3F/Npn-2–mediated spine constraint *in vitro*.

(A-I) E14.5 WT C57BL6, *DHHC15*$^{-/-}$ or *DHHC8*$^{-/-}$ cortical neurons were transfected with an EGFP-expressing plasmid and cultured for a total of 21 days in vitro (DIV). At DIV 21, they were treated with 5 nM Sema3F-AP (A, D, G) or AP control (B, E, H) for 6 hours. EGFP immunofluorescence was performed in order to visualize neuronal morphology and neurons were imaged with a 63X oil immersion lens to visualize dendritic spines. All types of dendritic spines (mushroom, stubby, filopodia-like) were counted along the proximal 50 µm extending distally from the cell body. Pooled data are shown as a number of spines per µm (C, F, I).

(A-C) Wild-type C57BL6 cortical neurons responded to Sema3F-AP with a constraint of their dendritic spines. (D-F) *DHHC15*$^{-/-}$ primary cortical neurons were not responsive to

Sema3F. (G-I) *DHHC8*$^{-/-}$ primary cortical neurons were responsive to Sema3F, similar to WT neurons. Statistics: t-test, mean ± s.e.m. Statistical significance: * $p < 0.05$, ** $p < 0.01$, ** $p < 0.001$, *** $p < 0.0001$. Scale bar: 7 μm.

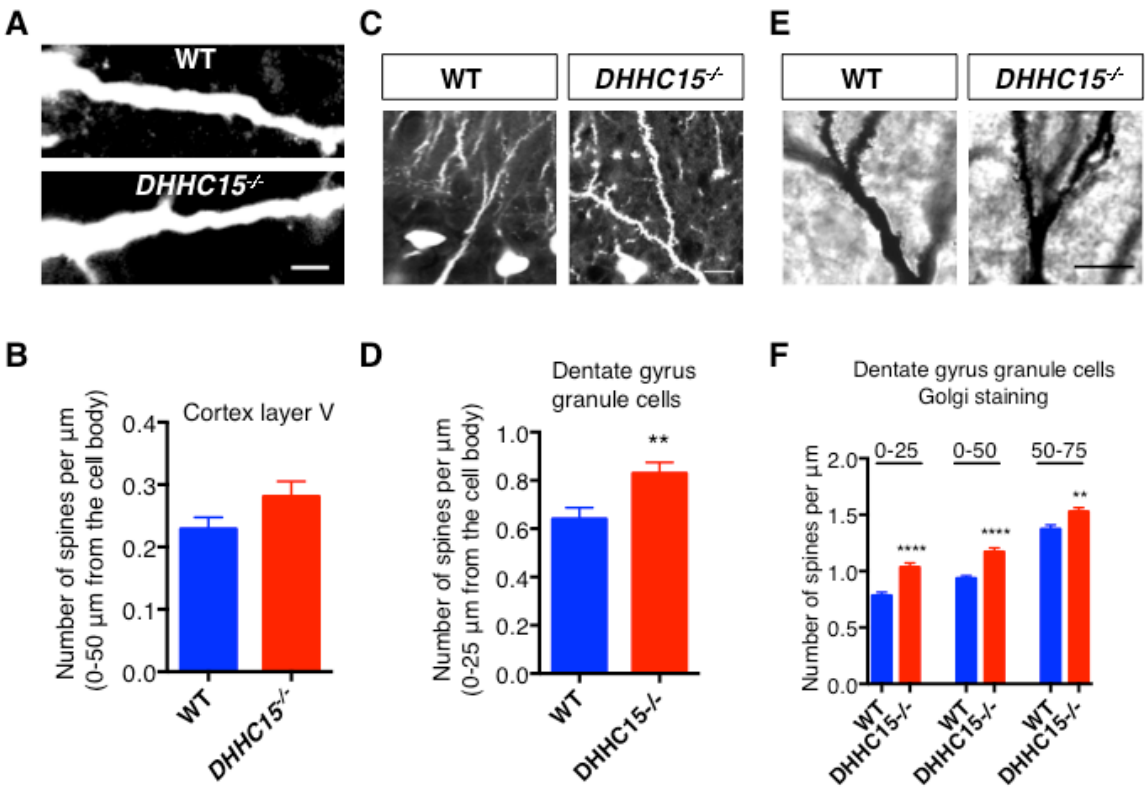

Figure 19. Effects of DHHC15 on dendritic spines of dentate gyrus granule cells and deep layer cortical neurons *in vivo*.

(A-D) Brains derived from WT or *DHHC15*$^{-/-}$ mice (4 weeks old) expressing Thy1-GFP (Thy1-GFP (m), myp), were analyzed with EGFP immunofluorescence to visualize neuronal morphology. Neurons, layer V cortical pyramidal neurons (A, B) and dentate gyrus granule cells (C, D), were imaged with the acquisition of confocal stacks and spines were counted along the indicated dendritic segments extending distally from the cell body. (A, B) Spine counts for layer V cortical pyramidal neurons labeled with EGFP (A) (two brains per genotype analyzed thus far; more experiments are ongoing) are shown in B (not significant difference). (C, D) Spine numbers for dentate gyrus granule

cells labeled with EGFP (C) are shown in D. (E, F) WT and *DHHC15*$^{-/-}$ brains were subjected to Golgi staining for sparse labeling of single neurons in vivo. Representative images of dentate gyrus granule cells are shown in E, and spine counts along various segments extending distally from the cell body are shown in F. Statistics: t-test, * $p < 0.05$, ** $p < 0.01$, *** $p < 0.001$, **** $p < 0.0001$. Scale bar: 5 μm in (A), 10 μm in (C), 10 μm in (E).

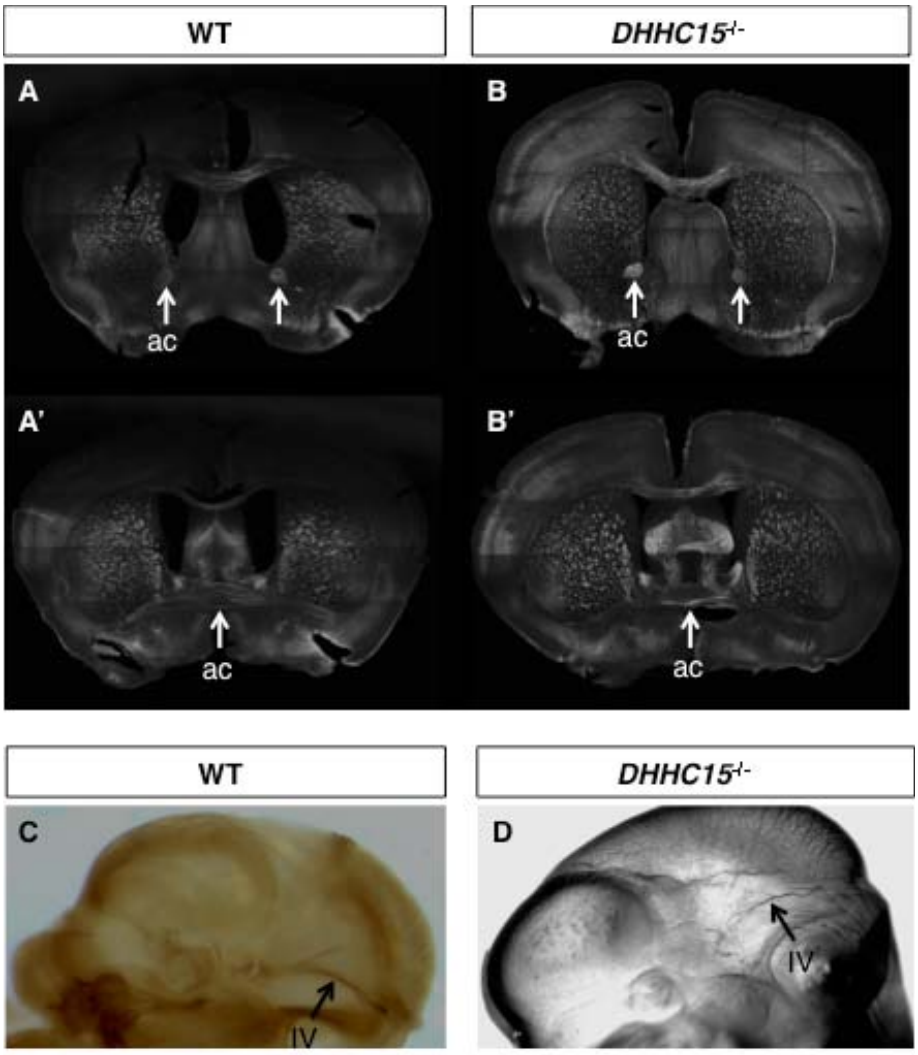

Figure 20. DHHC15 is not required for the development of the anterior commissure or cranial nerves that require Npn-2.

(A-A', B-B') Brains from WT (A, A') or *DHHC15*$^{-/-}$ (B, B') were sectioned (at 100 μm thickness) and sections were subjected to immunofluorescence with a neurofilament antibody (2H3) to visualize the axonal tracts. The anterior commissure, both the anterior branch (A, B; round structure marked with white arrows) and the midline-crossing fibers of the anterior commissure (A', B'; horizontal fibers in the midline marked with white

arrows) are intact in all *DHHC15*$^{-/-}$ brains examined thus far (3/3). (C, D) E11.5 embryos were subjected to whole-mount neurofilament staining for the visualization of cranial nerves. The trochlear nerve (IV; marked with a white arrow) is normally developed in *DHHC15*$^{-/-}$ mouse embryo brains (D), similar to the nerve in WT brains (C).

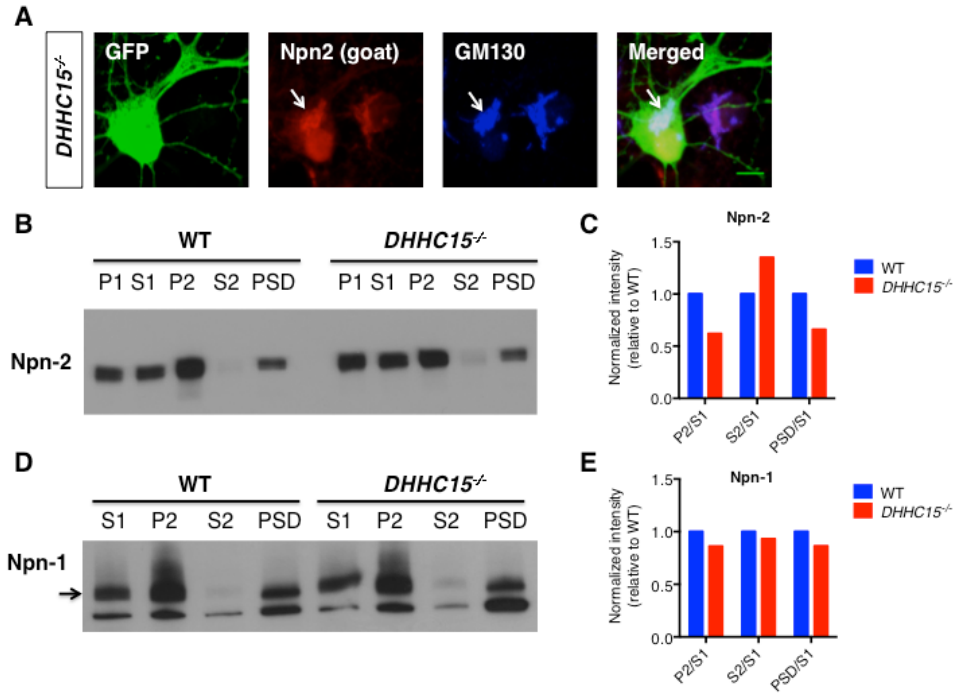

Figure 21. Npn-2 localization in *DHHC15*$^{-/-}$ cortical neurons.

(A) Immunofluorescence on E14.5, DIV15, *DHHC15*$^{-/-}$ primary cortical neurons, transfected with GFP (fills the neuron and delineates neuronal morphology), with antibodies directed against endogenous Npn-2 (goat), endogenous GM130 (rabbit) and GFP (chicken). White arrow points to the Npn-2 and GM130 signals and to their colocalization. (B-E) PSD prep performed on E14.5 DIV12 WT or *DHHC15*$^{-/-}$ primary cortical neurons (one experiment). A number of different fractions were collected and samples were analyzed with SDS-PAGE and immunoblotting with Npn-2 (rabbit) (B, C) or Npn-1 (rabbit) (D, E) antibodies. (C, E) Different fractions are normalized to S1, which represents the starting material, and WT values (ratios) are set to 1 (100%) whereas the *DHHC15*$^{-/-}$ values are expressed as a percentage of the WT. Scale bar in (A): 7 µm.

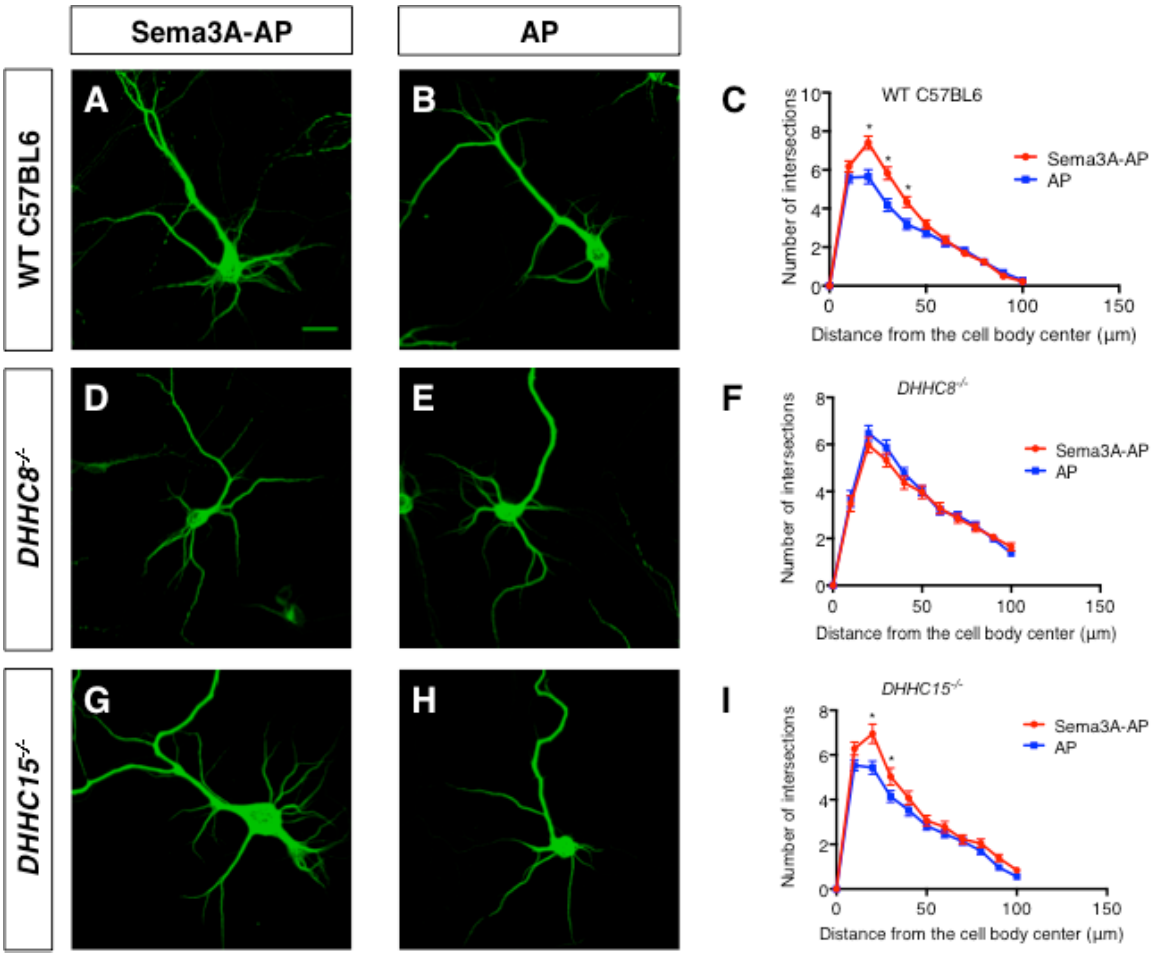

Figure 22. DHHC8 is required for Sema3A/Npn-1–induced basal dendritic elaboration in primary cortical neurons.

(A-I) E14.5 primary cortical neurons from WT (C57BL6) (A-C), *DHHC8*$^{-/-}$ (D-F) or *DHHC15*$^{-/-}$ (G-I) mouse embryos were cultured for a total of 12 days in vitro (DIV), and at DIV6, they were treated with 5nM Sema3A-AP or AP control for 6 hours. Dendritic elaboration was assessed with MAP2 immunofluorescence and quantified with Sholl analysis. Cumulative data from several independent experiments are presented as a number of intersections at various distances from the center of the cell body (C, F, I). (A-C) WT cortical neurons respond to Sema3A with an elaboration of their dendritic arbor.

(D-F) *DHHC8*$^{-/-}$ cortical neurons are not responsive to Sema3A (consistent across different experiments). (G-I) *DHHC15*$^{-/-}$ cortical neurons robustly respond to Sema3A, similar to the WT neurons. Statistics: t-test, significance: * $p < 0.05$. Scale bar: 16 μm.

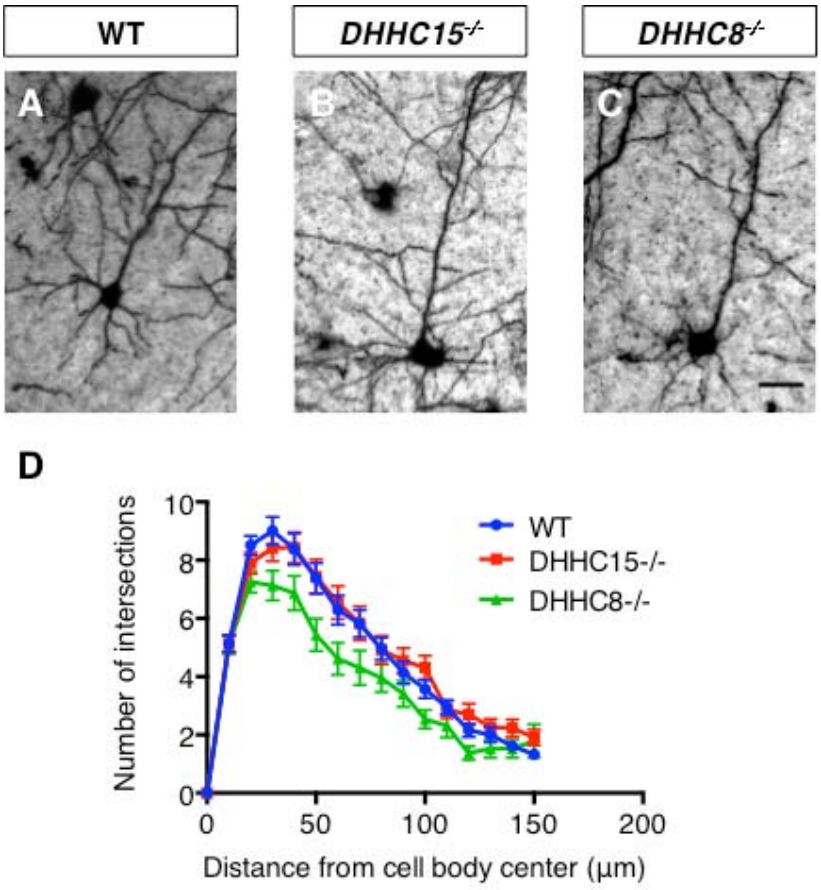

Figure 23. DHHC8 is required for proper dendritic elaboration of layer V cortical neurons in the mouse brain.

(A-D) WT C57BL6, *DHHC15*$^{-/-}$ or *DHHC8*$^{-/-}$ brains were subjected to Golgi staining for sparse labeling of neurons in vivo. Deep layer cortical neurons were imaged with the acquisition of stacks with a 20x lens using DIC. The Z-projection was calculated with image J and subsequently Sholl analysis was performed for the quantification of dendritic elaboration. (A-C) Representative images of WT (C57BL6), *DHHC15*$^{-/-}$ or *DHHC8*$^{-/-}$ deep layer cortical neurons. (D) Pooled data from different brains are presented as a number of intersections (between dendritic arbors and concentric circles drawn around

and at variable distances from the cell body) at the indicated distances from the cell body (μm). Scale bar in (A-C): 30 μm. Graph: mean ± s.e.m.

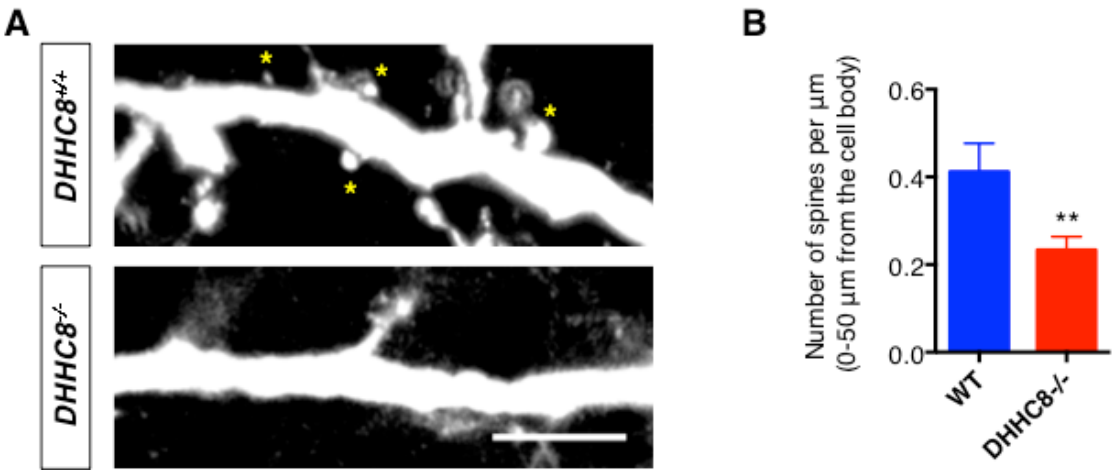

Figure 24. Effects of DHHC8 on dendritic spines of deep layer cortical neurons *in vivo*.

(A, B) *DHHC8*$^{+/+}$*;Thy1-GFP* and *DHHC8*$^{-/-}$*;Thy1-GFP* littermates were sacrificed and brains were processed for GFP immunofluorescence. GFP-expressing neurons were imaged by the acquisition of confocal stacks with a 63X oil immersion lens, for the visualization of the precise neuronal morphology including dendritic spines. (A) Panels show layer V cortical neurons and some spines are marked with yellow asterisks. Note the difference between WT and *DHHC8*$^{-/-}$. (B) Column graph shows the mean and error bars represent the standard error of the mean (s.e.m.). Spines were counted along the proximal 50 µm of the apical dendrite, relative to the cell body. Thus far, two brains in total (one per genotype) have been analyzed; analysis of more brains is ongoing. Scale bar in (A): 10 µm. Statistical significance is assessed with a paired t-test; ** $p < 0.01$.

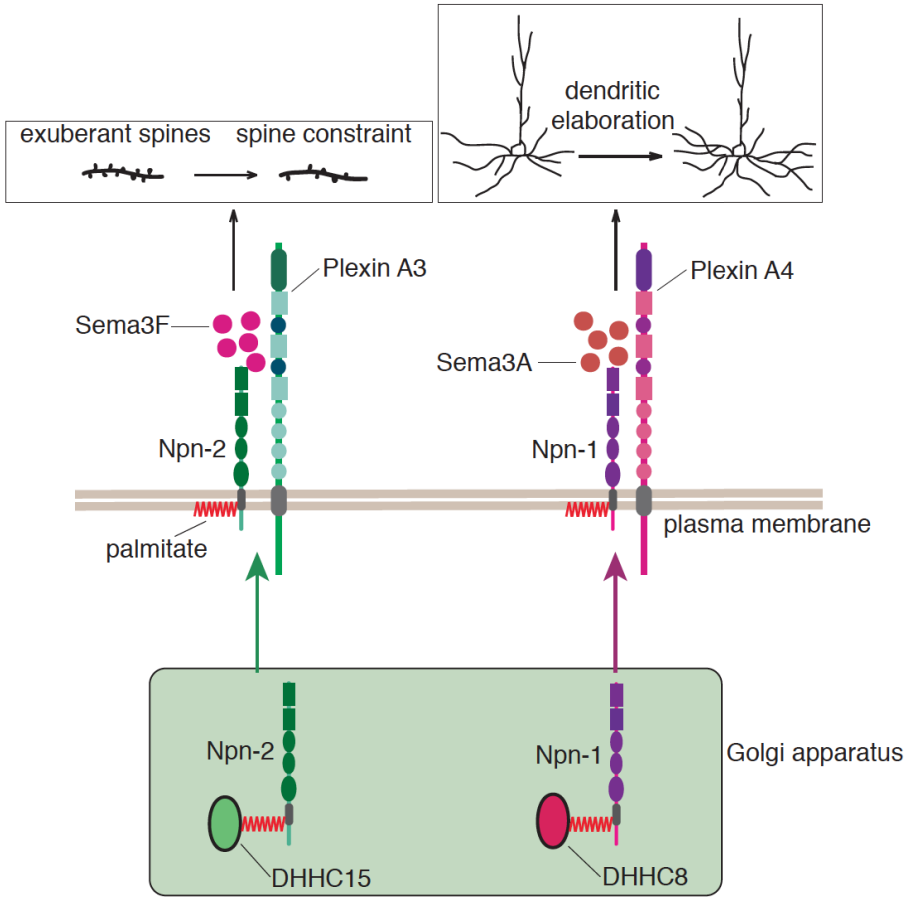

Figure 25. Schematic model.

Npn-2 and Npn-1 are S-palmitoylated in vitro and in vivo. This modification is essential for Npn-2 association with the Golgi apparatus as well as its proper distribution on the cell surface (clustering). Moreover, the membrane-proximal Npn-2 cysteines, which are palmitoylated, are required for Npn-2 response to Sema3F in order to cause a dendritic spine constraint. Interestingly, Npn-2 and Npn-1 are functionally associated with different palmitoyl acyltransferases; DHHC15 and DHHC8, respectively. This functional specificity between a palmitoyltransferase and different palmitoyl substrates reveals a molecular mechanism by which guidance cue receptors acquire and maintain their functional specification.

Intended to be blank

CHAPTER 4

SEMA3F IN CORTICAL CIRCUITS

Introduction

Sema3F plays an essential role in regulating the development of deep layer cortical pyramidal neurons, however the cell types that secrete Sema3F in the cerebral cortex have not been elucidated. Sema3F might be secreted by: 1) deep layer pyramidal neurons–in this case Sema3F would act cell autonomously (autocrine signaling); 2) subtypes of inhibitory neurons that lie in the vicinity of pyramidal neurons; 3) non-neuronal cells (including glial cells and endothelial cells); and 4) any combination of these different cell types. The identification of the cell types that secrete Sema3F requires the visualization of Sema3F-expressing and Sema3F-secreting cells with single cell resolution in vivo. The lack of optimal antibodies directed against Sema3F prompted us to generate an epitope-tagged knock-in *Sema3F* mouse in order to be able to perform high-resolution localization studies in vitro and in vivo. However, the visualization of Sema3F with high resolution in the cerebral cortex has not been sufficient to point toward a physiologically relevant source of Sema3F that accounts for the increased dendritic spine density phenotype observed in *Sema3F* mutants. To investigate this, we are currently using the floxed *Sema3F* mouse line made some time ago in the Kolodkin laboratory (Sahay et al., 2003) crossed to a number of different Cre lines, including: Rbp4-Cre (layer 5-specific), Emx1-Cre (pan-excitatory) and Dlx-5/6 Cre (pan-inhibitory), with the goal of assessing the spine density phenotype following these cell-type specific deletions of Sema3F to identify the role each of these cell types might play

in the *Sema3F*$^{-/-}$-associated phenotypes. Here, we describe the generation of the *Sema3F* knock-in mouse and our ongoing efforts to visualize Sema3F protein in the cortex and identify the relevant source of Sema3F.

Results

Generation and assessment of the *Sema3F-6xMYC* epitope-tagged knock-in mouse

To visualize Sema3F in vivo with high resolution, I generated an epitope-tagged knock-in *Sema3F* mouse in which a 6xMYC epitope tag has been inserted in exon 2 of the *Sema3F* coding sequence, downstream of its signal peptide. A floxed *NEO* cassette was cloned in the intron between exons 2 and 3 and serves as a positive control; this was excised after the line underwent germline transmission (**Figure 26, panels A and B**). The generation of this mouse line is described in greater detail in the Experimental Procedures. The *Sema3F*^{Myc} was germline transmitted and the genotype of this mouse line was assessed by two different PCR reactions (**Figure 26, panels C and D**).

To test this mouse for a potential disruption of Sema3F function because of the insertion of an epitope tag, we performed a number of experiments in which we assessed the integrity of axonal tracts that are dependent on Sema3F function in vivo. First, we assessed the embryonic cranial nerves with whole-mount neurofilament staining at E11.5. None of the *Sema3F*$^{myc/myc}$ embryos examined showed any *Sema3F*$^{-/-}$–associated defects (cranial nerves IV, V, VI, VII) (data not shown). Second, we performed neurofilament staining on coronal brain sections of postnatal mice to assess the anterior commissure. This showed that the anterior commissure is normally developed in *Sema3F*$^{myc/myc}$ mice,

with no defects in its anterior or posterior branches (data not shown). These experiments show that this mouse line does not display *Sema3F*$^{-/-}$-associated defects and it is therefore a valuable genetic tool for the investigation of Sema3F distribution and function.

Next, we wanted to test whether the 6xMYC-tagged Sema3F protein is secreted. To investigate this, we cultured E14.5 primary cortical neurons derived from either *Sema3F*$^{myc/myc}$ or *Sema3F*$^{+/+}$ embryos and let them grow in vitro for 12-15 days. Then, we collected the medium and concentrated it by centrifugation in a falcon tube carrying a 100K filter (Millipore). Samples were analyzed with SDS-PAGE and immunoblotting with two different antibodies that recognize the myc epitope (rabbit, clone 71D10 and mouse, clone 9E10) was performed. Both antibodies revealed a specific signal in the medium from *Sema3F*$^{myc/myc}$ neurons that was not present in the medium of *Sema3F*$^{+/+}$ neurons and that was of the molecular weight of Sema3F (**Figure 26, panel E**).

In summary, the 6xMyc-tagged knock-in mouse carries a tagged *Sema3F* allele that exhibits the properties of endogenous *Sema3F* and has no detectable mutant phenotypes. We can therefore use this tool to visualize Sema3F localization in vitro and in vivo.

Localization of Sema3F protein in the mouse brain

Next, we visualized the tagged Sema3F protein in mouse brain sections. Standard paraformaldehyde tissue processing and immunofluorescence did not give strong signal, perhaps because Sema3F is secreted, expressed at what we think are low levels, and perhaps folded in such a way that the epitope tag could be masked. To overcome these potential impediments, I used an alternative method for tissue processing and

immunofluorescence that has been previously used to visualize secreted guidance cue protein in vivo (Kennedy et al., 2006). This method included fixation with an organic solution (Carnoy's) and paraffin embedding and sectioning. The method followed here is described in detail in the experimental procedures. These experiments are preliminary and on going.

Immunofluorescence on brain sections revealed robust Sema3F immunoreactivity in the inferior colliculus and the olfactory bulb (**Figure 27, panels A-A', B-B'**). In the cerebral cortex, at early postnatal stages (P1), the signal is quite diffuse but seems to be neuron-specific (**Figure 27, panels C-C'**). However, at later developmental stages (P21), Sema3F immunoreactivity is specifically localized in deeper cortical layers, including the Ctip2-positive layer V (**Figure 27, panels D-D', E-E'**). Our endeavors to perform at the same time staining with cell type-specific markers were not particularly successful because of the organic fixation, which caused excessive background and non-specific labeling of several cell types. To get around this, we generated mice that harbored the *Sema3F-myc* allele, the *Dlx5/6-Cre* recombinase and *LSL-tdTomato* in order to unambiguously visualize inhibitory neurons labeled with tdTomato. These efforts are ongoing.

Preliminary experiments in primary cortical cultures have shown that Sema3F is detected in large CamKII+ neurons (**Figure 27, panel F**), which represent cortical pyramidal neurons, but also in smaller CamKII-neurons which we find in the vicinity of the large CamKII+ neurons and probably represent inhibitory neurons (data not shown). However, this remains to be confirmed with additional in vitro and also in vivo experiments.

The detection of Sema3F in a number of neuronal cell types makes it likely that there is a differential contribution of distinct neuron subtypes to the Sema3F-induced spine constraint. The investigation of this issue will require functional experiments in which Sema3F is deleted in a subset of neurons and the spine density of cortical pyramidal neurons in assessed in vivo.

Sema3F secretion is regulated by neuronal activity

This *Sema3F*^{Myc} mouse line has also been used in our laboratory for the investigation of the mechanism by which Sema3F/Npn-2 signaling affects the synaptic scaling in neural networks. Qiang Wang has shown that Sema3F/Npn-2 is required for proper downscaling of cell surface AMPA receptors following an excessive increase in network activity. In more detail, following bicuculline treatment, which inhibits GABAergic transmission and causes increased neuronal activity, WT neurons display a downregulation of synaptic GluA1 in order to compensate for the aberrant activity. However, *Npn2*$^{-/-}$ neurons are not capable of downscaling network activity (Wang et al., *unpublished observations*). To investigate the role of Sema3F in downscaling, Dr. Wang cultured *Sema3F*$^{myc/myc}$ neurons, treated them with bicuculline and assessed the amount of secreted Sema3F in the culture media compared to the control treatment. Remarkably, bicuculline treatment caused a marked increase in secreted Sema3F, suggesting that Sema3F secretion may play an important role in downregulating excitatory activity, perhaps by means of its known role in regulating dendritic spine and excitatory synapse constraint (Wang et al., *unpublished observations*).

Summary

We have generated and characterized an epitope-tagged *Sema3F*^{6xMyc} knock-in mouse, and our analysis shows that this mouse is an excellent genetic tool that allows for the detection and visualization of endogenous Sema3F in vivo with single cell resolution. Moreover, we have been performing functional experiments to identify the physiologically important cellular source of Sema3F in the cerebral cortex, taking advantage of our conditional *Sema3F* mouse line and available *Cre* driver lines. Finally, we have strong preliminary data showing that Sema3F is regulated in response to activity and that this is important for network activity scaling. Given the increase in Sema3F secretion following bicuculline treatment, which was detected using my *Sema3F*^{6xMyc} mouse line, we can use this mouse to investigate potential increases or decreases in Sema3F secretion following manipulations of the neural network, including aberrant neural activity in genetic mouse models of epileptic activity, cognitive disorders and degenerative diseases of the CNS.

Experimental procedures

Generation of the 6xMyc-tagged Sema3F knock-in mouse

The targeting vector was made using a homologous recombination-mediated gene targeting strategy, as described (Liu et al., 2003). Briefly, a *Sema3F* BAC clone was used for the retrieval of a *Sema3F* genomic DNA sequence that included exon 2 and genomic sequences upstream and downstream of exon 2, which made up the long and short homology arms, respectively; these were cloned into the PBS-DTA vector, resulting in the gap-repaired plasmid. DTA encodes for diphtheria toxin A, which served as a negative selection marker during ES cell screening. The long homology arm consisted of ~9,580 base pairs and extended upstream of exon 2, whereas the short arm consisted of 1,720 base pairs and extended downstream of exon 2. Next, the 6xMYC nucleotide sequence was subcloned into the second exon of Sema3F, between DNA sequences encoding the amino acids L26 and P27, eight amino acids downstream of the predicted signal sequence cleavage site, which lies between P18 and A19. Subsequently, short genomic fragments flanking the tag insertion site were subcloned on either side of the epitope tag and a *LoxP-NEO-LoxP* (LNL) cassette was inserted 510 base pairs downstream of the exon 2 coding sequence. *NEO*, encoding for neomycin, serves as a positive selection marker. This constructed *Sema3F* genomic sequence was subcloned in the PL451 vector and this plasmid, known as the mini-targeting vector, carried all the desired modifications to be inserted in the Sema3F locus (epitope tag and *NEO* cassette). This modified genomic fragment was introduced in the *Sema3F* gap repaired plasmid by homologous recombination and led to the generation of the targeting vector. The targeting vector was sequenced, linearized and given to the Johns Hopkins Transgenic

Mouse Core for electroporation into embryonic stem cells. Plated clones were positively selected with neomycin, whereas diphtheria toxin A expression served as a negative selection for incorrect clones. The clones that were able to grow were screened using PCR and positive clones were further tested with karyotyping and Southern blots. Finally, the correct clones were injected into 129S6/SvEvTac mouse blastocysts for the generation of chimeric mice, and chimeras were crossed with wild type mice to obtain germline transmission. Progeny harboring the ^{Myc}*Sema3F* allele were crossed with CMV-cre line (a germline Cre) for excision of the floxed NEO cassette. Mice were screened for ^{myc}Sema3F protein expression by SDS-PAGE and Western blot analysis using cortical lysates and culture medium collected from ^{myc}*Sema3F* primary cortical cultures, and in addition immunofluorescence on ^{myc}*Sema3F* brain sections was performed. The genotype of this mouse line was assessed and confirmed by two pairs of primers; the forward and reverse primers of the first pair anneal upstream and downstream of the epitope tag insertion site, respectively, and they detect both the wild-type and the ^{myc}*Sema3F* alleles. Thus, this PCR reaction distinguishes among ^{myc}*Sema3F* homozygous ($^{myc/myc}$*Sema3F*), heterozygous ($^{myc/+}$*Sema3F*) and wild type (*Sema3F*$^{+/+}$) mice. The PCR product size for the wild type Sema3F allele is 457 base pairs and the size for the ^{myc}*Sema3F* allele is 730 base pairs. The sequences of these primers are: forward primer (anneals upstream of exon 2): 5' – tgagccgagggctatgagcatgg – 3', reverse primer (anneals downstream of exon 2): 5' – tgcagggaaaccagcactgtgagg -3'. The primers of the second pair were used to detect the ^{Myc}*Sema3F* allele only since the forward primer anneals on the epitope tag sequence; therefore this PCR distinguishes mice harboring the ^{myc}*Sema3F* allele (heterozygous and homozygous mice) from wild type mice. The size of this PCR product is 607 base pairs.

The sequences of these primers are: forward primer: 5' – gagagcttgggcgacctcaccatg -3' and reverse primer: 5'-cgatgaattcggcactgggttattaaagtactccgtgg - 3'.

Immunofluorescence

Tissue processing: brains were dissected out and incubated with Carnoy's fixative (50ml: 30ml ethanol, 15ml chloroform, 5ml glacial acetic acid) for 30min until they sink and stay at the bottom of the tubes. Fixative was changed and tissue was incubated with 100% methanol three times, 30 min. each. Tissue was incubated with Toluene two times, 30 min. each and at 56ºC for 30min. Tissue was incubated with paraffin two times 30 min. each at at 56ºC and then overnight. Tissue was placed in a cassette and embedded in molds with paraffin. Embedded brains were stored at room temperature and sectioned with a microtome at the sagittal plane, at 10µm thickness.

Staining: *Removal of paraffin and rehydration of the tissue:* Xylene 3x 5min. each, 100% ethanol 3x 3min. each, 95% ethanol 2x 3min. each, 80% ethanol 2x 3min. each, ddH_2O 5x 1min. each. 0.3% Triton X-100 in PBS, 3x 5min. each. *Antigen retrieval:* 10mM sodium citrate, 0.05% Tween-20, pH: 6, boiling for 10min. Then cooling on ice for 20min. *Blocking:* 10% goat serum, 0.1% Triton X-100 in PBS for 1 hour at room temperature. **Primary antibodies:** Myc (rabbit, Cell Signaling, 71D10) 1:500; Ctip2 (rat, AbCam) 1:500; CaMKII (mouse, AbCam, cat. no. ab22609). **Secondary antibodies:** Alexa Fluor 488 goat anti-rabbit IgG (Life Technologies), Alexa Fluor 647 goat anti-rat IgG (Jackson), Alexa Fluor 546 goat anti-mouse IgG. PBS washes 5x 5min. each. Dehydration: 80% ethanol 2x 1min. each, 95% ethanol 2x 1min. each, 100% ethanol 3x 1min. each.

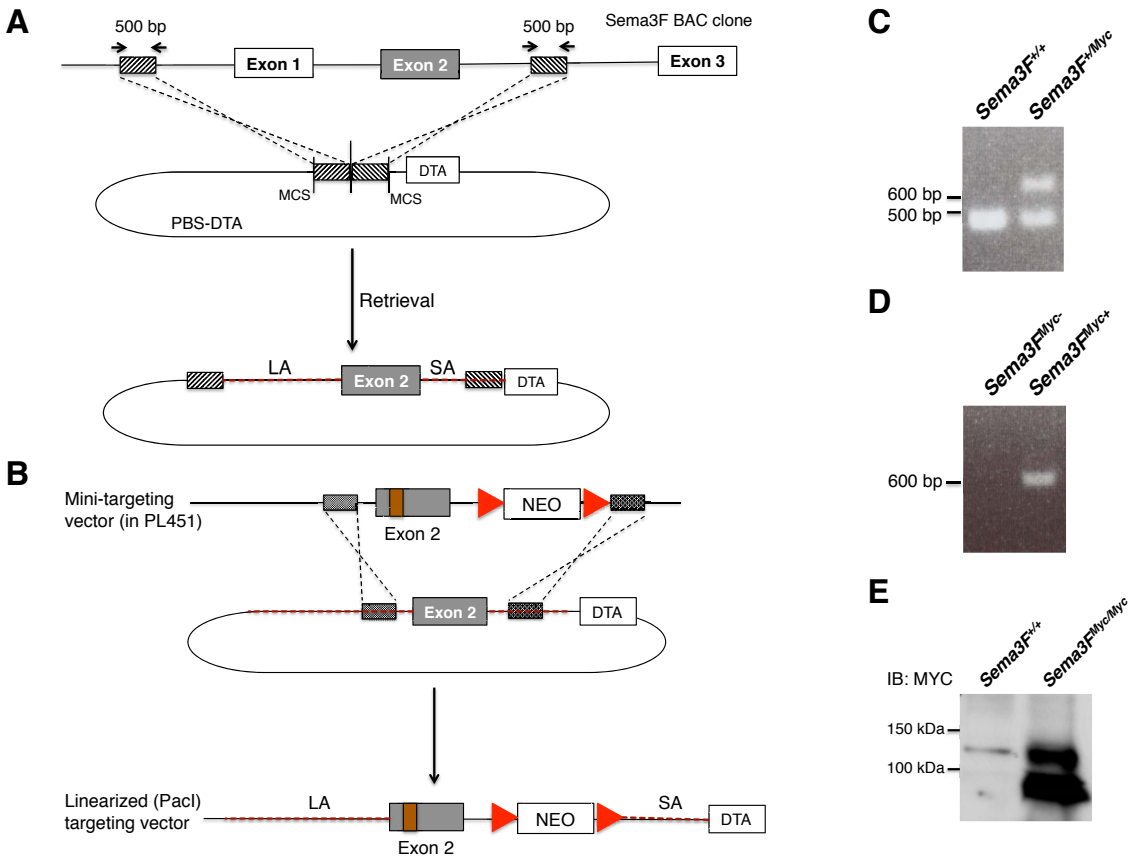

Figure 26. Generation and assessment of the *6xMyc-Sema3F* knock-in mouse.

(A, B) The *6xMyc Sema3F* knock-in mouse line was generated by the insertion of a 6xMyc epitope tag in exon 2 of Sema3F with a two-step recombineering. (A) At the first step, which is known as gap repair, the long and short arms were retrieved into the backbone vector PBS-DTA, in which short fragments of 500 bp that flanked the locus to be retrieved were previously directionally cloned. This retrieval was achieved by transforming competent cells containing the Sema3F BAC clone with the linearized PBS-DTA carrying these 500 bp DNA fragments. This led to the retrieval of the long and short arms into the PBS-DTA vector. (B) The mini-targeting vector was constructed with regular cloning and included the insertion of a 6xMyc epitope tag in exon 2 of Sema3F,

downstream of its signal peptide, and the cloning of floxed NEO cassette about 500 bp downstream of exon 2 (intron 2-3: intron between exons 2 and 3). For the 2nd step of recombineering, the mini-targeting vector was linearized and then transformed into bacterial cells containing the retrieval plasmid obtained from the first step. This second recombination led to the generation of the final targeting vector. The latter was linearized with Pac I and properly prepared for transformation into embryonic stem (ES) cells. *Abbreviations and drawings:* orange rectangle: 6xMYC epitope tag; LA: long arm, SA: short arm, red triangle: loxP site, black vertical lines: restriction sites, MCS: multiple cloning site, red horizontal dashed line: long and short arms of the targeting vector. (C, D) Testing for germline transmission and genotyping of progeny was performed with two different pairs of primers. The forward and reverse primer of the first pair anneal upstream and downstream of exon 2, respectively and PCR with this pair gives a WT band for the WT allele (457 bp) and the MYC band for the *Sema3F*^{myc} allele (730 bp). WT mice should give only the WT band, *Sema3F*^{myc} homozygous mutant mice should give only the MYC band, and heterozygous mice give both bands (C). The forward primer of the other pair of primers used to genotype this mutant mouse line, anneals on the MYC epitope tag while the reverse primer anneals downstream of exon 2. Thus, this pair gives a MYC band when the *Sema3F*^{myc} allele id present, regardless of whether the mouse is heterozygous or homozygous for the *Sema3F*^{myc} allele, whereas the absence of this band shows that this mouse is *Sema3F*$^{+/+}$ (D). (E) To test whether the 6xMyc-tagged Sema3F protein is expressed and secreted, E14.5 primary cortical neurons were cultured from *Sema3F*$^{+/+}$ or *Sema3F*$^{myc/myc}$ embryos and incubated in culture for several days. Culture medium was collected and concentrated. The concentrated mediums were mixed

with Laemmli buffer and samples were analyzed with SDS-PAGE and immunoblotting for Sema3F protein using a Myc antibody (clone 9E10, mouse, Sigma). Another Myc antibody (rabbit monoclonal, Cell Signaling) gave similar results (data not shown). More than one specific bands are seen in the *Sema3F*$^{myc/myc}$ medium, which are not present in the *Sema3F*$^{+/+}$ medium. Some of these bands might represent cleaved Sema3F (bands with a size lower than the predicted).

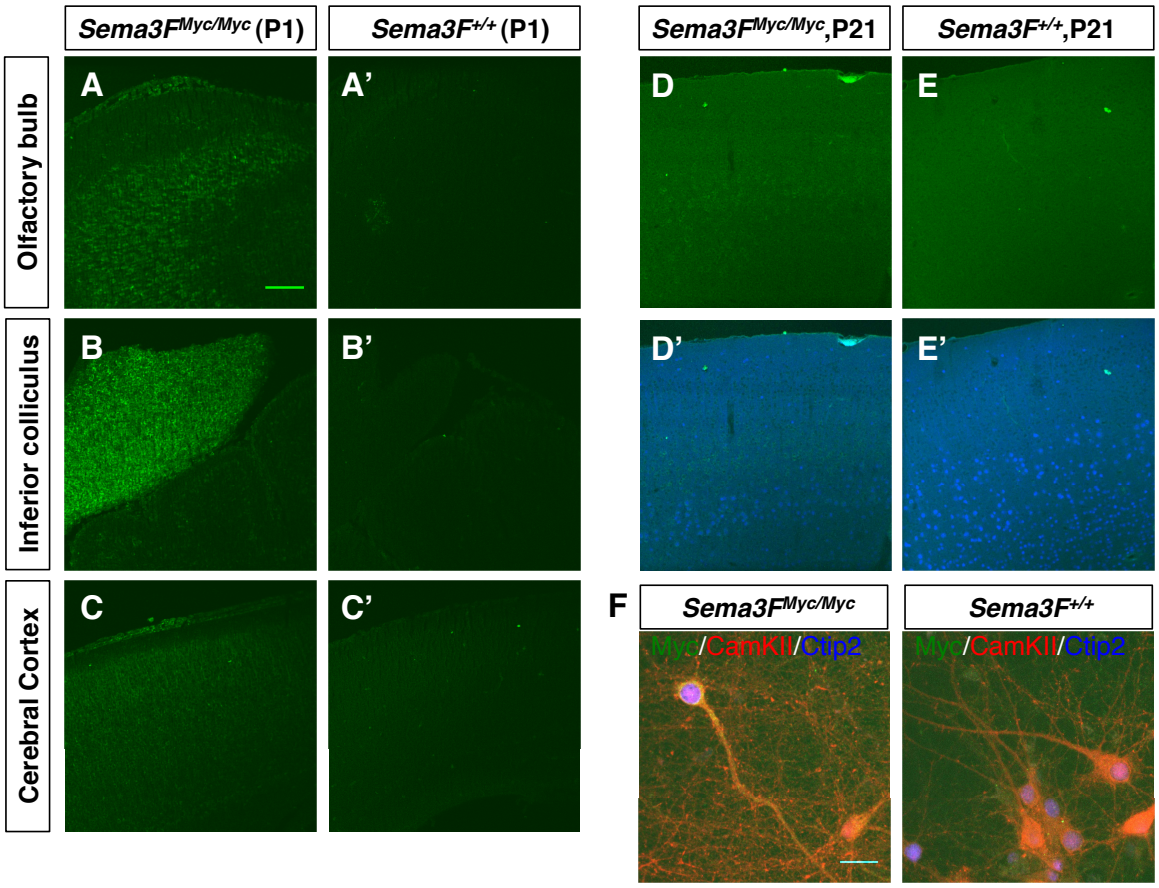

Figure 27. Sema3F protein localization in the mouse brain.

(A-E') Sema3F protein expression and localization in the mouse brain was tested on brain sections of *Sema3F*$^{Myc/Myc}$ and *Sema3F*$^{+/+}$ mice sacrificed at different developmental time points. Brains were processed with organic fixation (Carnoy's), paraffin embedding and staining of microtome-cut brain sections, as described in the experimental procedures of this Chapter. Antigen retrieval was also performed to enhance immunoreactivity. At P1, strong Sema3F protein expression is detected in the olfactory bulbs (central part) (A), the inferior colliculus and a small subset of cerebellar cells (B) and the cerebral cortex (C). This signal is specific because it is not detected in the *Sema3F*$^{+/+}$ brain (A', B', C'). At P21, sema3F immunoreactivity in the cerebral cortex is

more segregated, compared to P1, in the deeper cortical layers, including Ctip2-positive layer V neurons (D, D'). This signal is not detected in the WT brain (E, E') confirming that it is indeed 6xMyc-tagged Sema3F protein. (F) E14.5 primary cortical neurons were cultured from *Sema3F*$^{Myc/Myc}$ and *Sema3F*$^{+/+}$ embryos and stained with Myc, Ctip2 and CamKII antibodies. *Sema3F*$^{Myc/Myc}$ cortical neurons display specific Myc immunoreactivity, which represents Sema3F protein, in Ctip2−positive and CamKII−positive neurons. Moreover, in some instances, CamKII−positive large pyramidal-like neurons in culture are negative for Sema3F, but they are surrounded by smaller neurons with strong Sema3F immunoreactivity. These are likely to be inhibitory interneurons (data not shown). Scale bar in A-E': 100 μm; scale bar in F: 22 μm.

Intended to be blank

CHAPTER 5

DISCUSSION

The regulation of distinct aspects of cortical neuron architecture by the Sema3F/Npn-2/plexinA3 and Sema3A/Npn-1/plexinA4 signaling pathways is a challenging problem to elucidate. There are a number of possible mechanisms that mediate the functional diversification of these signaling pathways and allow them to affect distinct aspects of neuronal morphology and function. First, distinct protein-protein interactions specifically involved in either Sema3A or Sema3F signaling, including other transmembrane receptors, cytoskeleton regulators, enzymes and cytoplasmic proteins, could generate distinct responses to Sema3F and Sema3A. Second, post-translational modifications including palmitoylation, differentially affecting Sema3A and Sema3F signaling components, could regulate, at least in part, the functional outcome. Third, plexinA3 and plexinA4 might propagate the signal by recruiting distinct signaling cascades, therefore giving rise to different responses. The same is formally a possibility for Npn-1 and Npn-2; indeed, a specific signaling component is known to selectively associate with only one of the Npns and thereby mediate axon pruning (Riccomagno et al., 2012). Fourth, the dendritic localization and local translation of RNA transcripts has emerged as a robust mechanism by which proteins achieve their local compartmentalized effects. Further, local translation and availability of a protein could make the protein accessible to different modifying enzymes or signaling molecules. This possibility is particularly tempting for neuropilins, since we have found that both Npn-1 and Npn-2 transcripts are localized in the dendrites of primary cortical neurons in vitro by utilizing fluorescent in

situ hybridization techniques (FISH) (data not shown). Finally, two or more of the aforementioned mechanisms could simultaneously act to convey distinct function to the Sema3A and Sema3F signaling pathways.

Does neuropilin palmitoylation convey specificity to semaphorin signaling?

My work shows that both Npn-1 and Npn-2 are robustly palmitoylated in vitro and in vivo. Moreover, both neuropilins are palmitoylated in their membrane-proximal sequences in a similar pattern. Yet, this modification can be a source of functional difference between Npn-1 and Npn-2 by means of the distinct protein interactions Npn-1 and Npn-2 might have with different palmitoyl acyltransferases (see Chapter 3). Palmitoyltransferase substrate specificity has been shown to account for several cases of a protein's functional specificity (Greaves et al., 2010; Mukai et al., 2015; Yanai et al., 2006) . However, the current work is the first to directly compare two palmitoyl substrates that exert distinct functions in the same cell type and to show in *DHHC* knockout neurons, and not in gain-of-function paradigms, that there is strict functional segregation within the family of palmitoyl acyltransferases related to their corresponding palmitoyl substrates. The mechanism by which DHHC enzymes convey specificity is probably the functional interaction among different members of the DHHC protein family with distinct cytoskeleton regulators, transmembrane proteins (DHHC enzymes are transmembrane proteins) and subsequently with distinct signaling effectors.

Another mechanism by which palmitoylation can convey signaling specificity is the subcellular location of local palmitoylation events, resulting in a protein being targeted to

a particular subcellular compartment (for example, dendritic spines). This requires the detection of the palmitoylated fraction of the protein as compared to the localization of the total protein. To achieve this, we will need to generate antibodies directed against specific palmitoylated forms of palmitoyl substrates (Fukata Y. et al., 2013).

In addition, palmitoylation can be regulated by external stimuli (i.e. ligands, neural activity). This provides an ideal mechanism for conveying specificity, given that particular stimuli can enhance the palmitoylation of a protein at specific subcellular compartments and on specific cysteine residues. This stimulus-induced palmitoylation specificity is illustrated in the case of Sema3F-induced Npn-2 palmitoylation. In particular, Sema3F leads to an increase in Npn-2 palmitoylation but, notably, Sema3A does not enhance Npn-2palmitoylation. This selective ligand-induced neuropilin palmitoylation is one of the mechanisms by which palmitoylation can convey specificity to the neuronal semaphorin signaling, most likely in a two-step process: 1) activation of DHHCs specific to one of the two neuropilins and 2) engagement of distinct signaling effectors associated with these palmitoyl acyltransferases. Then, two or more mechanisms could collaborate to convey functional specificity. However, the mechanisms that activate these enzymes have not been elucidated and it is therefore hard to provide insight into this question at the present time.

A dilemma for palmitoylated proteins: are cysteines important as palmitate-carrying residues or as structural determinants?

My work provides both correlative and causal data supporting the fact that palmitoylation of the Npn-2 cysteines is essential for Npn-2 function and that the cysteines themselves do not serve as structural determinants of protein dimerization.

These data that demonstrate a causal relationship between Npn-2 palmitoylation and Npn-2 trafficking and function are:

1. Inhibition of palmitoylation with 2-bromopalmitate disperses the clusters of Npn-2, rendering surface Npn-2 protein diffusely distributed, though all cysteines are still intact.
2. Cortical neurons lacking specific palmitoyl acyltransferases are incapable of responding to secreted Semas and neuropilin palmitoylation in those neurons is significantly reduced.

The experimental evidence that reveals a strong correlation between Npn-2 palmitoylation and function is:

1. Strong correlation between the extent to which a protein is palmitoylated and its rescue ability. Specifically, Npn-2 mutants that have severely disrupted palmitoylation have completely lost or severely compromised rescue ability, whereas mutants that are still quite well palmitoylated rescue the phenotype at least partially.
2. Sema3F enhances Npn-2 palmitoylation and it is therefore likely that this effect is required for sema3F-induced spine constraint.

Of note, these data supporting the notion that the cysteine residues are functionally important because of their palmitoylation does not rule out the possibility that these cysteines are also engaged in other intramolecular or intermolecular interactions, for instance by forming disulfide bridges. Furthermore, given that palmitoylation is a reversible and highly dynamic protein modification, there could be an intricate interplay between the palmitoylation of a cysteine residue and its engagement in the formation of disulfide bridges. There might be baseline equilibrium between these two processes and upon the presence of external stimuli (i.e. Sema3F, electrical activity), and this balance could be shifted towards palmitoylation or towards the formation of disulfide bonds.

A potential interplay between neuronal activity and semaphorin signaling by means of palmitoylation

In neural networks there are at least two main mechanisms that affect circuit assembly: chemotropic signaling and neural activity. As stated in the introduction (Chapter 1) during neural circuit formation neurons respond to both guidance cues and neuronal activity (Greer and Greenberg, 2008; Shen and Cowan, 2010). Therefore, there might be a bidirectional interplay between these two processes: on one hand, signaling pathways regulate neural development, circuit assembly and synaptic transmission, and on the other hand, emerging neuronal activity modulates the response of neurons (by means of the receptors expressed on them) to guidance cues. The mechanisms by which neuronal activity affects responses to guidance cues are largely unknown. Interestingly, there is compelling evidence to show that protein palmitoylation is regulated by activity (Hayashi et al., 2009; Kang et al., 2008).

Sema3F/Npn-2 signaling is essential for proper formation of excitatory synapses and balanced neuronal activity in cortical circuits (Tran et al., 2009). Moreover, the present work strongly suggests that palmitoylation of Npn-2 on specific cysteine residues is required for the spine constraint caused by Sema3F. It then becomes clear that palmitoylation is a post-translational modification critical for regulating synapse formation and function in neural circuits. Here, I also show that DHHC15 is involved in Npn-2 palmitoylation in cortical neurons. Of note, the *DHHC15* homozygous null mutant mice are hyperactive (Rebeca Mejias-Estevez, Tao Wang, *personal communication*), which raises the possibility that their neural circuits are hyperexcitable. Although a rigorous assessment of the neural activity in the brains of these mice is not available, it is

tempting to speculate that these mice exhibit defects similar to the *Npn-2*$^{-/-}$ mice. This is also a striking resemblance to the *Sema3F*$^{-/-}$ mice, which also display hyperexcitability and are prone to seizures (Sahay et al., 2005). This is a behavioral and functional similarity that increases the possibility that some of the behavioral deficits of *DHHC15* homozygous mutant mice result in part from the lack of DHHC15-induced Npn-2 palmitoylation.

Thus far, I have described how neuronal protein palmitoylation regulates the development of neurons, synapses and neural activity within CNS circuits. What about the other side of the coin, namely, that neural activity regulates protein palmitoylation? A number of studies have demonstrated that activity regulates the extent to which certain proteins are palmitoylated; these proteins include GluR1 and GluR2 (Hayashi et al., 2005), NR2A and NR2B (Hayashi et al., 2009) and δ-catenin (Brigidi et al., 2014a). In the case of δ-catenin, increased synaptic activity upregulates δ-catenin palmitoylation mediated by DHHC5, and this leads to an increase in δ-catenin– cadherin association. This in turn causes increases in dendritic spine size, synaptic GluA1 and GluA2 and postsynaptic currents. (Brigidi et al., 2014a). In other words, activity alters protein palmitoylation, which in turn modulates synaptic function.

I have previously shown that activity alters Npn-2 palmitoylation levels. Moreover, treatment of neurons with bicuculline (which increases neural activity) leads to a significant increase in Sema3F secretion (Qiang Wang, Chapter 4). Here, I show that Sema3F enhances Npn-2 palmitoylation and therefore leads to a more robust Npn-2 function. This suggests the existence of a negative feedback loop whereby excessive or unnecessary increases in network activity enhances Sema3F secretion, and this in turn

upregulates Npn-2 palmitoylation, thereby enhancing Npn-2's excitatory synapse-restricting function in order to compensate for the increased activity and to maintain the balance between excitation and inhibition.

Concluding remarks

In summary, we have discovered that the post-translational modification palmitoylation occurs on neuropilins and that this modification is critical for neuropilin protein subcellular distribution and function in cortical neurons. This is particularly important since palmitoylation is reversible and it therefore has the potential to dynamically regulate protein trafficking and function. This raises the intriguing possibility that external stimuli (i.e. Sema3F, Sema3A, neural activity, neurotransmitters) modulate neuropilin function by altering its palmitoylation status. Given that some of these stimuli are directly related to the external environment where a living organism is exposed (for instance neural activity), neuropilin palmitoylation could mediate some of the molecular responses (structural rearrangements of dendritic spines and arbors) of context-related stimuli. Furthermore, we have found that palmitoylation conveys specificity to the class 3 secreted semaphorin signaling pathways by means of palmitoyltransferase substrate specificity. This modification can therefore explain, at least to some extent, the functional divergence and specification of Npn-1 and Npn-2, and by extension, Sema3A and Sema3F. This finding has broader implications for all palmitoyl substrates, which by means of palmitoylation can achieve a great degree of functional specificity in time (during development), space (subcellular compartment) and distinct neurodevelopmental

processes (axon pathfinding, dendritic arborization, dendritic spine formation and/or maintenance, synaptic plasticity, embryonic and adult neurogenesis). Moreover, the implication of protein palmitoylation in a multitude of neuronal physiological processes makes it likely that is also plays essential roles in the pathogenesis of diseases of the CNS, including neurodegenerative and cognitive disorders. This is supported by the discovery of genetic defects of various palmitoyltransferases in humans with cognitive impairment.

REFERENCES

Adamson, P., Marshall, C.J., Hall, A., and Tilbrooks, P.A. (1992). Post-translational Modifications of p2 lrho Proteins *. *267*.

Allen, J.A., Halverson-Tamboli, R.A., and Rasenick, M.M. (2007). Lipid raft microdomains and neurotransmitter signalling. Nat. Rev. Neurosci. *8*, 128–140.

Arstikaitis, P., Gauthier-campbell, C., Carolina, R., Herrera, G., Huang, K., Levinson, J.N., Murphy, T.H., Kilimann, M.W., Sala, C., Colicos, M.A., et al. (2008). Paralemmin-1 , a Modulator of Filopodia Induction Is Required for Spine Maturation. *19*, 2026–2038.

Ayoob, J.C., Terman, J.R., and Kolodkin, A.L. (2006). Drosophila Plexin B is a Sema-2a receptor required for axon guidance. Development *133*, 2125–2135.

Bagri, A., Cheng, H.J., Yaron, A., Pleasure, S.J., and Tessier-Lavigne, M. (2003). Stereotyped pruning of long hippocampal axon branches triggered by retraction inducers of the semaphorin family. Cell *113*, 285–299.

Baudet, M.L., Bellon, A., and Holt, C.E. (2013). Role of microRNAs in Semaphorin function and neural circuit formation. Semin. Cell Dev. Biol. *24*, 146–155.

Bouzioukh, F., Daoudal, G., Falk, J., Debanne, D., Rougon, G., and Castellani, V. (2006). Semaphorin3A regulates synaptic function of differentiated hippocampal neurons. Eur. J. Neurosci. *23*, 2247–2254.

Brigidi, G.S., Sun, Y., Beccano-Kelly, D., Pitman, K., Mobasser, M., Borgland, S.L., Milnerwood, A.J., and Bamji, S.X. (2014a). Palmitoylation of δ-catenin by DHHC5 mediates activity-induced synapse plasticity. Nat. Neurosci. *17*, 522–532.

Brigidi, G.S., Sun, Y., Beccano-Kelly, D., Pitman, K., Mobasser, M., Borgland, S.L., Milnerwood, A.J., and Bamji, S.X. (2014b). Palmitoylation of δ-catenin by DHHC5 mediates activity-induced synapse plasticity. Nat. Neurosci. *17*, 522–532.

Burkhardt, C., Müller, M., Badde, A., Garner, C.C., Gundelfinger, E.D., and Püschel, A.W. (2005). Semaphorin 4B interacts with the post-synaptic density protein PSD-95/SAP90 and is recruited to synapses through a C-terminal PDZ-binding motif. FEBS Lett. *579*, 3821–3828.

Carrillo, R. a., Olsen, D.P., Yoon, K.S., and Keshishian, H. (2010). Presynaptic activity and CaMKII modulate retrograde semaphorin signaling and synaptic refinement. Neuron *68*, 32–44.

Chen, H., Chédotal, A., He, Z., Goodman, C.S., and Tessier-Lavigne, M. (1997). Neuropilin-2, a novel member of the neuropilin family, is a high affinity receptor for the semaphorins Sema E and Sema IV but not Sema III. Neuron *19*, 547–559.

Chen, H., He, Z., Bagri, A., Tessier-lavigne, M., and Francisco, S. (1998). Semaphorin – Neuropilin Interactions Underlying Sympathetic Axon Responses to Class III Semaphorins. *21*, 1283–1290.

Dalva, M.B., McClelland, A.C., and Kayser, M.S. (2007). Cell adhesion molecules: signalling functions at the synapse. Nat. Rev. Neurosci. *8*, 206–220.

Ding, J.B., Oh, W.-J., Sabatini, B.L., and Gu, C. (2012). Semaphorin 3E-Plexin-D1 signaling controls pathway-specific synapse formation in the striatum. Nat. Neurosci. *15*, 215–223.

Drisdel, R.C., and Green, W.N. (2004). Labeling and quantifying sites of protein palmitoylation. *36*.

Drisdel, R.C., Alexander, J.K., Sayeed, A., and Green, W.N. (2006). Assays of protein palmitoylation. Methods *40*, 127–134.

Duan, Y., Wang, S.H., Song, J., Mironova, Y., Ming, G. li, Kolodkin, A.L., and Giger, R.J. (2014). Semaphorin 5A inhibits synaptogenesis in early postnatal- and adult-born hippocampal dentate granule cells. Elife *3*, 1–24.

El-Husseini, A.E.D., Schnell, E., Dakoji, S., Sweeney, N., Zhou, Q., Prange, O., Gauthier-Campbell, C., Aguilera-Moreno, A., Nicoll, R. a., and Bredt, D.S. (2002). Synaptic strength regulated by palmitate cycling on PSD-95. Cell *108*, 849–863.

Eroglu, C., and Barres, B.A. rEvIEW Regulation of synaptic connectivity by glia. 2–10.

Fukata, Y., and Fukata, M. (2010). Protein palmitoylation in neuronal development and synaptic plasticity. Nat. Rev. Neurosci. *11*, 161–175.

Fukata, Fukata, Adesnik, Nicoll, and Bredt (2004). Identification of PSD-95 palmitoylating enzymes. Neuron *44*, 987–996.

Fukata, Y., Dimitrov, A., Boncompain, G., Vielemeyer, O., Perez, F., and Fukata, M. (2013). Local palmitoylation cycles define activity-regulated postsynaptic subdomains. J. Cell Biol. *202*, 145–161.

Fukuhara, K., Imai, F., Ladle, D.R., Katayama, K., Leslie, J.R., Arber, S., Jessell, T.M., and Yoshida, Y. (2013). Specificity of monosynaptic sensory-motor connections imposed by repellent Sema3E-PlexinD1 signaling. Cell Rep. *5*, 748–758.

George, J., Soares, C., Montersino, A., Beique, J.-C., and Thomas, G.M. (2015). Palmitoylation of LIM Kinase-1 ensures spine-specific actin polymerization and morphological plasticity. Elife *4*, 1–25.

Giger, R.J., Urquhart, E.R., Gillespie, S.K.H., Levengood, D. V., Ginty, D.D., and Kolodkin, A.L. (1998). Neuropilin-2 is a receptor for semaphorin IV: Insight into the

structural basis of receptor function and specificity. Neuron *21*, 1079–1092.

Giger, R.J., Cloutier, J.-F., Sahay, A., Prinjha, R.K., Levengood, D. V, Moore, S.E., Pickering, S., Simmons, D., Rastan, S., Walsh, F.S., et al. (2000). Neuropilin-2 Is Required In Vivo for Selective Axon Guidance Responses to Secreted Semaphorins. Neuron *25*, 29–41.

Godenschwege, T. a, Hu, H., Shan-Crofts, X., Goodman, C.S., and Murphey, R.K. (2002). Bi-directional signaling by Semaphorin 1a during central synapse formation in Drosophila. Nat. Neurosci. *5*, 1294–1301.

Greaves, J., and Chamberlain, L.H. (2011). DHHC palmitoyl transferases: Substrate interactions and (patho)physiology. Trends Biochem. Sci. *36*, 245–253.

Greaves, J., Gorleku, O.A., Salaun, C., and Chamberlain, L.H. (2010). Palmitoylation of the SNAP25 Protein Family: SPECIFICITY AND REGULATION BY DHHC PALMITOYL TRANSFERASES. J. Biol. Chem. *285*, 24629–24638.

Greer, P.L., and Greenberg, M.E. (2008). From Synapse to Nucleus: Calcium-Dependent Gene Transcription in the Control of Synapse Development and Function. Neuron *59*, 846–860.

Gu, C., Rodriguez, E.R., Reimert, D. V., Shu, T., Fritzsch, B., Richards, L.J., Kolodkin, A.L., and Ginty, D.D. (2003). Neuropilin-1 conveys semaphorin and VEGF signaling during neural and cardiovascular development. Dev. Cell *5*, 45–57.

Guirland, C., Suzuki, S., Kojima, M., Lu, B., and Zheng, J.Q. (2004). Lipid Rafts Mediate Chemotropic Guidance of Nerve Growth Cones. *42*, 51–62.

Hayashi, T., Rumbaugh, G., and Huganir, R.L. (2005). Differential Regulation of AMPA Receptor Subunit Trafficking by Palmitoylation of Two Distinct Sites. Neuron *47*, 709–723.

Hayashi, T., Thomas, G.M., and Huganir, R.L. (2009). Dual Palmitoylation of NR2 Subunits Regulates NMDA Receptor Trafficking. Neuron *64*, 213–226.

Horton, A.C., Rácz, B., Monson, E.E., Lin, A.L., Weinberg, R.J., and Ehlers, M.D. (2005). Polarized Secretory Trafficking Directs Cargo for Asymmetric Dendrite Growth and Morphogenesis. Neuron *48*, 757–771.

Huang, K., Yanai, A., Kang, R., Arstikaitis, P., Singaraja, R.R., Metzler, M., Mullard, A., Haigh, B., Gauthier-Campbell, C., Gutekunst, C.A., et al. (2004). Huntingtin-interacting protein HIP14 is a palmitoyl transferase involved in palmitoylation and trafficking of multiple neuronal proteins. Neuron *44*, 977–986.

Huang, K., Sanders, S., Singaraja, R., Orban, P., Cijsouw, T., Arstikaitis, P., Yanai, A., Hayden, M.R., and El-Husseini, A. (2009). Neuronal palmitoyl acyl transferases exhibit

distinct substrate specificity. FASEB J. *23*, 2605–2615.

Inagaki, S., Ohoka, Y., Sugimoto, H., Fujioka, S., Amazaki, M., Kurinami, H., Miyazaki, N., Tohyama, M., and Furuyama, T. (2001). Sema4C, a Transmembrane Semaphorin, Interacts with a Post-synaptic Density Protein, PSD-95. J. Biol. Chem. *276*, 9174–9181.

Innocenti, G.M., and Price, D.J. (2005). Exuberance in the development of cortical networks. Nat. Rev. Neurosci. *6*, 955–965.

Jennings, B.C., Nadolski, M.J., Ling, Y., Baker, M.B., Harrison, M.L., Deschenes, R.J., and Linder, M.E. (2009). 2-Bromopalmitate and 2-(2-hydroxy-5-nitro-benzylidene)-benzo[b]thiophen-3-one inhibit DHHC-mediated palmitoylation in vitro. J. Lipid Res. *50*, 233–242.

Kang, R., Wan, J., Arstikaitis, P., Takahashi, H., Huang, K., Bailey, A.O., Thompson, J.X., Roth, A.F., Drisdel, R.C., Mastro, R., et al. (2008). Neural palmitoyl-proteomics reveals dynamic synaptic palmitoylation. Nature *456*, 904–909.

Kennedy, T.E., Wang, H., Marshall, W., and Tessier-lavigne, M. (2006). Axon Guidance by Diffusible Chemoattractants : A Gradient of Netrin Protein in the Developing Spinal Cord. *26*, 8866–8874.

Kita, E.M., Bertolesi, G.E., Hehr, C.L., Johnston, J., and McFarlane, S. (2013). Neuropilin-1 biases dendrite polarization in the retina. Development *140*, 2933–2941.

Komiyama, T., Sweeney, L.B., Schuldiner, O., Garcia, K.C., and Luo, L. (2007). Graded expression of semaphorin-1a cell-autonomously directs dendritic targeting of olfactory projection neurons. Cell *128*, 399–410.

Koropouli, E., and Kolodkin, A.L. (2014). Semaphorins and the dynamic regulation of synapse assembly, refinement, and function. Curr. Opin. Neurobiol. *27*, 1–7.

Kutzleb, C., Sanders, G., Yamamoto, R., Wang, X., Lichte, B., Petrasch-Parwez, E., and Kilimann, M.W. (1998). Paralemmin, a prenyl-palmitoyl-anchored phosphoprotein abundant in neurons and implicated in plasma membrane dynamics and cell process formation. J. Cell Biol. *143*, 795–813.

Kuzirian, M.S., Moore, A.R., Staudenmaier, E.K., Friedel, R.H., and Paradis, S. (2013). The class 4 semaphorin Sema4D promotes the rapid assembly of GABAergic synapses in rodent hippocampus. J. Neurosci. *33*, 8961–8973.

Lee, K., Kim, J.-H.J.-H., Kwon, O.-B., An, K., Ryu, J., Cho, K., Suh, Y.-H.Y.-H., and Kim, H.-S.H.-S. (2012). An activity-regulated microRNA, miR-188, controls dendritic plasticity and synaptic transmission by downregulating neuropilin-2. J. Neurosci. *32*, 5678–5687.

Levental, I., Lingwood, D., Grzybek, M., Coskun, U., and Simons, K. (2010).

Palmitoylation regulates raft affinity for the majority of integral raft proteins. Proc. Natl. Acad. Sci. U. S. A. *107*, 22050–22054.

Liu, X.-B., Low, L.K., Jones, E.G., and Cheng, H.-J. (2005). Stereotyped axon pruning via plexin signaling is associated with synaptic complex elimination in the hippocampus. J. Neurosci. *25*, 9124–9134.

Lobo, S., Greentree, W.K., Linder, M.E., and Deschenes, R.J. (2002). Identification of a Ras Palmitoyltransferase in Saccharomyces cerevisiae *. *277*, 41268–41273.

Low, L.K., Liu, X.-B., Faulkner, R.L., Coble, J., and Cheng, H.-J. (2008). Plexin signaling selectively regulates the stereotyped pruning of corticospinal axons from visual cortex. Proc. Natl. Acad. Sci. U. S. A. *105*, 8136–8141.

Mansouri, M.R., Marklund, L., Gustavsson, P., Davey, E., Carlsson, B., Larsson, C., White, I., Gustavson, K.-H., and Dahl, N. (2005). Loss of ZDHHC15 expression in a woman with a balanced translocation t(X;15)(q13.3;cen) and severe mental retardation. Eur. J. Hum. Genet. *13*, 970–977.

Martin, B.R., Wang, C., Adibekian, A., Tully, S.E., and Cravatt, B.F. (2011). Global profiling of dynamic protein palmitoylation. Nat. Methods *9*, 84–89.

Matsuoka, R.L., Chivatakarn, O., Badea, T.C., Samuels, I.S., Cahill, H., Katayama, K.-I., Kumar, S.R., Suto, F., Chédotal, A., Peachey, N.S., et al. (2011a). Class 5 transmembrane semaphorins control selective Mammalian retinal lamination and function. Neuron *71*, 460–473.

Matsuoka, R.L., Nguyen-Ba-Charvet, K.T., Parray, A., Badea, T.C., Chédotal, A., and Kolodkin, A.L. (2011b). Transmembrane semaphorin signalling controls laminar stratification in the mammalian retina. Nature *470*, 259–263.

Mcallister, A.K. (2007). Dynamic Aspects of CNS Synapse Formation.

Milnerwood, A.J., Parsons, M.P., Young, F.B., Singaraja, R.R., Franciosi, S., Volta, M., Bergeron, S., Hayden, M.R., and Raymond, L.A. (2013). Memory and synaptic deficits in Hip14/DHHC17 knockout mice. Proc. Natl. Acad. Sci. U. S. A. *110*, 20296–20301.

Ming, G.L., Henley, J., Tessier-Lavigne, M., Song, H.J., and Poo, M.M. (2001). Electrical activity modulates growth cone guidance by diffusible factors. Neuron *29*, 441–452.

Mizumoto, K., and Shen, K. (2013). Interaxonal Interaction Defines Tiled Presynaptic Innervation in C. elegans. Neuron *77*, 655–666.

Mukai, J., Liu, H., Burt, R.A., Swor, D.E., Lai, W.-S., Karayiorgou, M., and Gogos, J.A. (2004). Evidence that the gene encoding ZDHHC8 contributes to the risk of schizophrenia. Nat. Genet. *36*, 725–731.

Mukai, J., Dhilla, A., Drew, L.J., Stark, K.L., Cao, L., MacDermott, A.B., Karayiorgou, M., and Gogos, J. a (2008). Palmitoylation-dependent neurodevelopmental deficits in a mouse model of 22q11 microdeletion. Nat. Neurosci. *11*, 1302–1310.

Mukai, J., Tamura, M., Fénelon, K., Rosen, A.M., Spellman, T.J., Kang, R., MacDermott, A.B., Karayiorgou, M., Gordon, J.A., and Gogos, J.A. (2015). Molecular Substrates of Altered Axonal Growth and Brain Connectivity in a Mouse Model of Schizophrenia. Neuron *86*, 680–695.

Ng, T., Ryu, J.R., Sohn, J.H., Tan, T., Song, H., Ming, G.L., and Goh, E.L.K. (2013). Class 3 Semaphorin Mediates Dendrite Growth in Adult Newborn Neurons through Cdk5/FAK Pathway. PLoS One *8*, 1–15.

Nicol, X., Voyatzis, S., Muzerelle, A., Narboux-Nême, N., Südhof, T.C., Miles, R., and Gaspar, P. (2007). cAMP oscillations and retinal activity are permissive for ephrin signaling during the establishment of the retinotopic map. Nat. Neurosci. *10*, 340–347.

Nishiyama, M., Togashi, K., von Schimmelmann, M.J., Lim, C.-S., Maeda, S., Yamashita, N., Goshima, Y., Ishii, S., and Hong, K. (2011). Semaphorin 3A induces CaV2.3 channel-dependent conversion of axons to dendrites. Nat. Cell Biol. *13*, 676–685.

Nl, D. (1998). letters to nature. *394*, 192–195.

Noritake, J., Fukata, Y., Iwanaga, T., Hosomi, N., Tsutsumi, R., Matsuda, N., Tani, H., Iwanari, H., Mochizuki, Y., Kodama, T., et al. (2009). Mobile DHHC palmitoylating enzyme mediates activity-sensitive synaptic targeting of PSD-95. J. Cell Biol. *186*, 147–160.

O'Connor, T.P., Cockburn, K., Wang, W., Tapia, L., Currie, E., and Bamji, S.X. (2009). Semaphorin 5B mediates synapse elimination in hippocampal neurons. Neural Dev. *4*, 18.

Paradis, S., Harrar, D.B., Lin, Y., Koon, A.C., Hauser, J.L., Griffith, E.C., Zhu, L., Brass, L.F., Chen, C., and Greenberg, M.E. (2007). An RNAi-Based Approach Identifies Molecules Required for Glutamatergic and GABAergic Synapse Development. Neuron *53*, 217–232.

Pecho-Vrieseling, E., Sigrist, M., Yoshida, Y., Jessell, T.M., and Arber, S. (2009). Specificity of sensory-motor connections encoded by Sema3e-Plxnd1 recognition. Nature *459*, 842–846.

Pecot, M.Y., Tadros, W., Nern, A., Bader, M., Chen, Y., and Zipursky, S.L. (2013). Multiple Interactions Control Synaptic Layer Specificity in the Drosophila Visual System. Neuron *77*, 299–310.

Penzes, P., Cahill, M.E., Jones, K.A., VanLeeuwen, J.-E., and Woolfrey, K.M. (2011). Dendritic spine pathology in neuropsychiatric disorders. Nat. Neurosci. *14*, 285–293.

Raissi, A.J., Staudenmaier, E.K., David, S., Hu, L., and Paradis, S. (2013). Sema4D localizes to synapses and regulates GABAergic synapse development as a membrane-bound molecule in the mammalian hippocampus. Mol. Cell. Neurosci. *57*, 23–32.

Raymond, F.L., Tarpey, P.S., Edkins, S., Tofts, C., O'Meara, S., Teague, J., Butler, A., Stevens, C., Barthorpe, S., Buck, G., et al. (2007). Mutations in ZDHHC9, Which Encodes a Palmitoyltransferase of NRAS and HRAS, Cause X-Linked Mental Retardation Associated with a Marfanoid Habitus. Am. J. Hum. Genet. *80*, 982–987.

Resh, M.D. (2006). Use of analogs and inhibitors to study the functional significance of protein palmitoylation. Methods *40*, 191–197.

Riccomagno, M.M., and Kolodkin, A.L. (2015). Sculpting Neural Circuits by Axon and Dendrite Pruning. Annu. Rev. Cell Dev. Biol. *31*, annurev – cellbio – 100913–013038.

Riccomagno, M.M., Hurtado, A., Wang, H., MacOpson, J.G.J., Griner, E.M., Betz, A., Brose, N., Kazanietz, M.G., and Kolodkin, A.L. (2012). The RacGAP β2-chimaerin selectively mediates axonal pruning in the hippocampus. Cell *149*, 1594–1606.

Rocks, O. (2005). An Acylation Cycle Regulates Localization and Activity of Palmitoylated Ras Isoforms. Science (80-.). *307*, 1746–1752.

Rocks, O., Gerauer, M., Vartak, N., Koch, S., Huang, Z.-P., Pechlivanis, M., Kuhlmann, J., Brunsveld, L., Chandra, A., Ellinger, B., et al. (2010). The Palmitoylation Machinery Is a Spatially Organizing System for Peripheral Membrane Proteins. Cell *141*, 458–471.

Roth, A.F., Feng, Y., Chen, L., and Davis, N.G. (2002). The yeast DHHC cysteine-rich domain protein Akr1p is a palmitoyl transferase. J. Cell Biol. *159*, 23–28.

Roth, A.F., Wan, J., Bailey, A.O., Sun, B., Kuchar, J.A., Green, W.N., Phinney, B.S., Yates, J.R., and Davis, N.G. (2006). Global Analysis of Protein Palmitoylation in Yeast. Cell *125*, 1003–1013.

Sahay, A., Molliver, M.E., Ginty, D.D., and Kolodkin, A.L. (2003). Semaphorin 3F Is Critical for Development of Limbic System Circuitry and Is Required in Neurons for Selective CNS Axon Guidance Events. *23*, 6671–6680.

Sahay, A., Kim, C.-H., Sepkuty, J.P., Cho, E., Huganir, R.L., Ginty, D.D., and Kolodkin, A.L. (2005). Secreted Semaphorins Modulate Synaptic Transmission in the Adult Hippocampus. J. Neurosci. *25* , 3613–3620.

Saito, T. (2006). In vivo electroporation in the embryonic mouse central nervous system. Nat. Protoc. *1*, 1552–1558.

Salaun, C., Greaves, J., and Chamberlain, L.H. (2010). The intracellular dynamic of protein palmitoylation. J. Cell Biol. *191*, 1229–1238.

Sankaranarayanan, S., Angelis, D. De, Rothman, J.E., and Ryan, T.A. (2000). The Use of pHluorins for Optical Measurements of Presynaptic Activity. Biophys. J. *79*, 2199–2208.

Schultze, W., Eulenburg, V., Lessmann, V., Herrmann, L., Dittmar, T., Gundelfinger, E.D., Heumann, R., and Erdmann, K.S. (2001). Semaphorin4F interacts with the synapse-associated protein SAP90/PSD-95. J. Neurochem. *78*, 482–489.

Shahinian, S., and Silvius, J.R. (1995). Doubly-lipid-modified protein sequence motifs exhibit long-lived anchorage to lipid bilayer membranes. Biochemistry *34*, 3813–3822.

Shelly, M., Cancedda, L., Lim, B.K., Popescu, A.T., Cheng, P.L., Gao, H., and Poo, M.M. (2011). Semaphorin3A regulates neuronal polarization by suppressing axon formation and promoting dendrite growth. Neuron *71*, 433–446.

Shen, K., and Cowan, C.W. (2010). Plasticity. 1–18.

Singaraja, R.R., Huang, K., Sanders, S.S., Milnerwood, A.J., Hines, R., Lerch, J.P., Franciosi, S., Drisdel, R.C., Vaid, K., Young, F.B., et al. (2011). Altered palmitoylation and neuropathological deficits in mice lacking HIP14. Hum. Mol. Genet. *20*, 3899–3909.

Spruston, N. (2008). Pyramidal neurons: dendritic structure and synaptic integration. Nat. Rev. Neurosci. *9*, 206–221.

Sun, L.O., Jiang, Z., Rivlin-Etzion, M., Hand, R., Brady, C.M., Matsuoka, R.L., Yau, K.-W., Feller, M.B., and Kolodkin, A.L. (2013). On and off retinal circuit assembly by divergent molecular mechanisms. Science *342*, 1241974.

Sutton, L.M., Sanders, S.S., Butland, S.L., Singaraja, R.R., Franciosi, S., Southwell, A.L., Doty, C.N., Schmidt, M.E., Mui, K.K.N., Kovalik, V., et al. (2013). Hip14l-deficient mice develop neuropathological and behavioural features of Huntington disease. Hum. Mol. Genet. *22*, 452–465.

Sweeney, L.B., Chou, Y.-H., Wu, Z., Joo, W., Komiyama, T., Potter, C.J., Kolodkin, A.L., Garcia, K.C., and Luo, L. (2011). Secreted Semaphorins from Degenerating Larval ORN Axons Direct Adult Projection Neuron Dendrite Targeting. Neuron *72*, 734–747.

Takemoto-Kimura, S., Ageta-Ishihara, N., Nonaka, M., Adachi-Morishima, A., Mano, T., Okamura, M., Fujii, H., Fuse, T., Hoshino, M., Suzuki, S., et al. (2007). Regulation of Dendritogenesis via a Lipid-Raft-Associated Ca2+/Calmodulin-Dependent Protein Kinase CLICK-III/CaMKI?? Neuron *54*, 755–770.

Thomas, G.M., Hayashi, T., Chiu, S.-L., Chen, C.-M., and Huganir, R.L. (2012). Palmitoylation by DHHC5/8 Targets GRIP1 to Dendritic Endosomes to Regulate AMPA-R Trafficking. Neuron *73*, 482–496.

Tran, T.S., Rubio, M.E., Clem, R.L., Johnson, D., Case, L., Tessier-Lavigne, M., Huganir, R.L., Ginty, D.D., and Kolodkin, A.L. (2009). Secreted semaphorins control

spine distribution and morphogenesis in the postnatal CNS. Nature *462*, 1065–1069.

Wan, J., Roth, A.F., Bailey, A.O., and Davis, N.G. (2007). Palmitoylated proteins: purification and identification. Nat. Protoc. *2*, 1573–1584.

Webb, Y., Hermida-Matsumoto, L., and Resh, M.D. (2000). Inhibition of protein palmitoylation, raft localization, and T cell signaling by 2-bromopalmitate and polyunsaturated fatty acids. J. Biol. Chem. *275*, 261–270.

Winberg, M.L., Mitchell, K.J., and Goodman, C.S. (1998). Genetic analysis of the mechanisms controlling target selection: Complementary and combinatorial functions of netrins, semaphorins, and IgCAMs. Cell *93*, 581–591.

Yanai, A., Huang, K., Kang, R., Singaraja, R.R., Arstikaitis, P., Gan, L., Orban, P.C., Mullard, A., Cowan, C.M., Raymond, L.A., et al. (2006). Palmitoylation of huntingtin by HIP14 is essential for its trafficking and function. Nat. Neurosci. *9*, 824–831.

Young, F.B., Butland, S.L., Sanders, S.S., Sutton, L.M., and Hayden, M.R. (2012). Putting proteins in their place: Palmitoylation in Huntington disease and other neuropsychiatric diseases. Prog. Neurobiol. *97*, 220–238.

Zhang, F.L., and Casey, P.J. (1996). Protein prenylation: molecular mechanisms and functional consequences. Annu. Rev. Biochem. *65*, 241–269.

CURRICULUM VITAE

ELEFTHERIA KOROPOULI March 24th, 2016

PERSONAL INFORMATION

Date of birth: May 22nd, 1983
Place of birth: Marousi, Attica, Greece
Citizenship: Greek

Educational History

Ph.D. expected	2016	Neuroscience	Johns Hopkins School of Medicine Mentor: Alex L. Kolodkin, Ph.D.
M.D.	2007	Medicine	National and Kapodistrian University of Athens School of Medicine, Greece

Research rotations

Research rotation 2008 Lab of Dr Frederick Lenz, Johns Hopkins Hospital

Research rotation 2008 Lab of Dr Jay Baraban, Johns Hopkins University

Postgraduate clinical training

2007-2008	Oncology Unit, Sotiria General Hospital, University of Athens School of Medicine
2006	1st Hellenic Summer School of Oncology for medical students, Patra, Greece

Scholarships-Grants

2008-2011	Scholarship by the Greek State Scholarships Foundation
2011-2012	Scholarship by the A.G. Leventis Foundation
2008-2009	Fulbright Grant (Fulbright Foundation in Greece)

Academic Awards - Honors

2008	Nikolaos Kepetzis Award by the Academy of Athens
2007	Prestigious Distinction, University of Athens School of Medicine
2006	Second Prize at the 1st Hellenic Summer School of Oncology for medical students, Patra (Rio), Greece

Scientific presentations-Posters

1.**Eleftheria Koropouli**, Qiang Wang, David D. Ginty, Alex L. Kolodkin. The Function of Class III Secreted Semaphorins in Cortical Neuron Development, 2014 Cold Spring Harbor Laboratory Meeting in Axon Guidance, Synapse Formation and Regeneration. 16-20 September 2014.
2.Qiang Wang, **Eleftheria Koropouli**, Sarah Mitchell, David D. Ginty, Alex L. Kolodkin. Secreted Semaphorins Regulate Cortical Neuron Synaptic Plasticity, 2014 Cold Spring Harbor Laboratory Meeting in Axon Guidance, Synapse Formation and Regeneration. 16-20 September 2014.
3.**Eleftheria Koropouli**, Qiang Wang, Dorothy V. Reimert, David D. Ginty, Alex L. Kolodkin. Neuropilin and Class III Secreted Semaphorin Control of Neuronal Morphology, EMBO Workshop: Semaphorin function and mechanism of action, 29-31 October 2013, Cernay-la-Ville, France.
4.**Eleftheria Koropouli**, Qiang Wang, Dorothy V. Reimert, David D. Ginty, Alex L. Kolodkin. Neuropilin and Class III Secreted Semaphorin Control of Neuronal Morphology, Howard Hughes Medical Institute Scientific Meeting, October 8-10, 2013, Janelia Farm Research Campus, 19700 Helix Drive, Ashburn, VA 20147, USA.
5.Tracy S. Tran, Qiang Wang, **Eleftheria Koropouli**, David D. Ginty, Alex L. Kolodkin. Secreted Semaphorin Control Of Dendrite and Spine Morphology During Development and in The Adult Mouse CNS, 2010 Cold Spring Harbor Laboratory Meeting in Axon Guidance, Synaptic Plasticity and Regeneration.

Review Articles

1. **Eleftheria Koropouli**, Alex L Kolodkin, Semaphorins and the dynamic regulation of synapse assembly, refinement, and function. *Current Opinion in Neurobiology*, 2014, 27:1-7.
2. **Eleftheria Koropouli**; Leonidas Manolopoulos; Hardev Pandha; Konstantinos N. Syrigos, The Biological Role of mTOR in the Pathogenesis of Solid Tumors: An Overview. *Current Enzyme Inhibition*, 2009, 5:51-65.

Peer-reviewed research papers

Submitted:

Qiang Wang, **Eleftheria Koropouli**, Shu-Ling Chiu, Ingie Hong, Sarah Mitchell, Ahleah S. Gustina, David D. Ginty, Richard L. Huganir, Alex L. Kolodkin. Neuropilin-2/PlexinA3 Receptors Associate with GluA1 and Mediate Sema3F-dependent Homeostatic Scaling in Cortical Neurons.

In preparation:

Eleftheria Koropouli, Qiang Wang, Sarah Mitchell, David Ginty, Alex L. Kolodkin. Palmitoyltransferase substrate specificity: a molecular code that regulates neuronal morphology mediated by semaphorin signaling.

Teaching

2009-2010 (one semester)	teaching assistant in Neuroscience & Cognition I, Neuroscience Graduate Program, Johns Hopkins University
2015 (summer)	EXROP program of HHMI